Transmission Fiber Nonlinearity Mitigation in Optical Communication Links Using Phase-Sensitive Parametric Amplifiers

EGON ASTRA

TAL
TECH
PRESS

TALLINN UNIVERSITY OF TECHNOLOGY
School of Information Technologies
Thomas Johann Seebeck Department of Electronics
The dissertation was accepted for the defence of the degree of Doctor of Philosophy in Electronics and Telecommunication on 5 November 2019

Supervisor: Prof. Peter Avo Andrekson,
Department of Microtechnology and Nanoscience, Photonics Laboratory,
Chalmers University of Technology,
Gothenburg, Sweden

Co-supervisor: Prof. Toomas Ruuben,
Thomas Johann Seebeck Department of Electronics,
Tallinn University of Technology,
Tallinn, Estonia

Opponents: Associate Prof. Michael Galili,
Department of Photonics Engineering,
Technical University of Denmark,
Kgs. Lyngby, Denmark

Associate Prof. Pierpaolo Boffi,
Department of Electronics and Information,
Politecnico di Milano,
Milan, Italy

Defence of the thesis: 13 December 2019, Tallinn

Declaration:
Hereby I declare that this doctoral thesis, my original investigation and achievement, submitted for the doctoral degree at Tallinn University of Technology, has not been submitted for any academic degree elsewhere.

Egon Astra

_____
                                                        signature

European Union
European Regional
Development Fund

Investing
in your future

Edastusfiibri mittelineaarsete mõjutuste vähendamine optilistes sidesüsteemides faasitundlike parameetriliste võimendite abil

EGON ASTRA

To my family.

TABLE OF CONTENTS

LIST OF PUBLICATIONS

The work of this thesis is based on the following publications:

A   S. L. I. Olsson, H. Eliasson, **E. Astra**, M. Karlsson and P. A. Andrekson, "Long-haul optical transmission link using low-noise phase-sensitive amplifiers," *Nature Communications*, no. 9 (2018): 2513. [ETIS 1.1]

B   **E. Astra**, S. L. I. Olsson, H. Eliasson and P. A. Andrekson, "Dispersion management for nonlinearity mitigation in two-span 28 GBaud QPSK phase-sensitive amplifier links," *Optics Express*, 25, no. 12 (2017): 13163–13173. [ETIS 1.1]

C   **E. Astra**, H. Eliasson and P. A. Andrekson, "Four-span dispersion map optimization for improved nonlinearity mitigation in phase-sensitive amplifier links," in Proc. *European Conference on Optical Communication (ECOC)*, Gothenburg, Sweden (2017): paper P2.SC6.14. [ETIS 3.1]

D   **E. Astra**, H. Eliasson, T. Ruuben and P. A. Andrekson, "Improved mitigation of self-phase modulation induced impairments in 28 GBaud phase-sensitive amplified links," *Optics Express*, 27, no. 4 (2019): 4304–4316. [ETIS 1.1]

E   H. Eliasson, K. Vijayan, B.Foo, S.L.I. Olsson, **E. Astra**, M. Karlsson and P. A. Andrekson, "Phase-sensitive amplifier link with distributed Raman amplification," *Optics Express*, 26, no. 16 (2018): 19854–19863. [ETIS 1.1]

ABBREVIATIONS

ADC	Analog-to-digital converter
AQN	Amplified quantum noise
BER	Bit error ratio
BL	Bit rate-distance product
CMA	Constant modulus algorithm
DAC	Digital to analog converter
DBP	Digital back-propagation
DCF	Dispersion compensating fiber
DCM	Dispersion compensation module
DD-LMS	Decision-directed least mean square
DFF	Dispersion-flattened fiber
DSF	Dispersion-shifted fiber
DSP	Digital signal processing
EDFA	Erbium-doped fiber amplifier
EVM	Error vector magnitude
FBG	Fiber Bragg grating
FIR	Finite-impulse response
FLAG	Fiber-optic link around the Globe
FOPA	Fiber-optical parametric amplifier
FSO	Free-space optical
GDR	Group delay ripple
GVD	Group-velocity dispersion
HNLF	Highly nonlinear fiber
IIR	Infinite-impulse response
ISI	Intersymbol interference
LAN	Local area network
Li-Fi	Light fidelity
MLSI	Mid-link spectral inversion
MMF	Multi-mode fiber
MZM	Mach-Zender modulator
NFT	Nonlinear Fourier transform
NLPN	Nonlinear phase noise
NLSE	Nonlinear Schrödinger equation

OPC	Optical phase conjugation
OSNR	Optical signal-to-noise ratio
PBS	Polarization beam splitter
PC	Polarization controller
PCTW	Phase-conjugated twin-waves
PIA	Phase-insensitive amplifier
PLL	Phase-locked loop
PM-QPSK	Polarization multiplexed quadrature phase shift keying
PMD	Polarization-mode dispersion
PSA	Phase-sensitive amplifier
PS-QPSK	polarization switched quadrature phase shift keying
QAM	Quadrature amplitude modulation
QPSK	Quadrature phase shift keying
RF	Radio frequency
Rx	Receiver
SBS	Stimulated Brillouin scattering
SDM	Space-division multiplexing
SE	Spectral efficiency
SNR	Signal-to-noise ratio
SOA	Semiconductor optical amplifier
SPM	Self-phase modulation
SRS	Stimulated Raman scattering
SSFM	Split-step Fourier method
SSMF	Standard single-mode fiber
TOD	Third-order dispersion
Tx	Transmitter
WDM	Wavelength-division multiplexing
XPM	Cross-phase modulation

Part I

Introduction

1. BACKGROUND

The need for an information transmission over long distances has always been an important issue and optical communications in a broad sense are known to be used from antiquity [1]. For example smoke signals, fire beacons, signaling lamps, flags and mirrors can be used to convey a single piece of information. However, more sophisticated systems started to evolve quite lately and the first idea about the "optical telegraph," that could transmit mechanically coded messages over long distances, was suggested in 1792 by Claude Chappe [2]. After the advent of the electrical telegraphy in the 1830s [3] and the invention of the telephone in 1876 [4], optical communication systems were replaced by electrical communication systems for almost a century.

The history of fiber-optic communication systems starts in the second half of the twentieth century, when it was realized that optical waves as a carrier would provide an increase of several orders of magnitude in the bit rate-distance product (BL) [5]. After the laser was invented and demonstrated by Maiman in 1960 [6] together with the invention of the optical fiber in 1966 [7], the most important building blocks for a fiber-optic communication system were established. Yet an another important milestone was the demonstration of compact semiconductor lasers in 1970 [8] together with the considerable optical fiber loss reduction demonstration from 1000 dB/km to 20 dB/km in 1970 [9] that led to a worldwide development of fiber-optic communication links. The evolution of a fiber-optic transmission capacity over the past decades and the biggest technological steps, that have enabled such an increase, are shown in Fig. 1.1.

The next breakthrough in fiber-optic communications was enabled by the invention of the erbium-doped fiber amplifier (EDFA) in 1987 [10, 11]. EDFAs replaced repeaters and later allowed the use of the wavelength-division multiplexing (WDM) through broadband amplification capability, which enabled the transmission of multiple channels through a single fiber at different wavelengths. More lately, an adaption of coherent receivers has allowed an increase of the spectral efficiency by the use of advanced multilevel modulation formats [12]. Recently, the limitations of a bandwidth scaling of fiber-optic communication links, the so called "capacity crunch", are foreseen to overcome by a parallelism in the space domain [13]. A significant capacity scaling will be enabled by the integration of WDM spectral superchannels with space-division multiplexed (SDM) spatial superchannels (parallel spatial paths) in order to create

hybrid superchannels. The total number of resulting available channels would be $WDM_{\text{channels}} \times SDM_{\text{channels}}$. Alternative options to increase fiber-optic transmission channel capacity limits are to reduce an optical amplifier noise and/or mitigate transmission fiber nonlinear distortions of a transmitted useful signal [14].
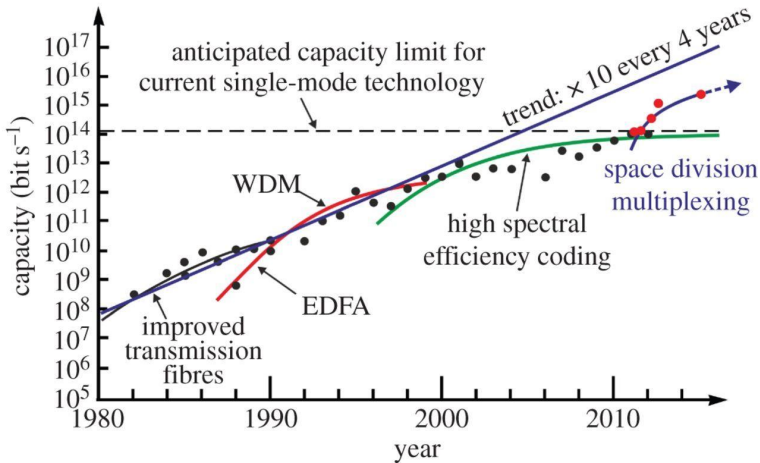

Figure 1.1 The transmission capacity evolution of fiber-optic transmission systems over the past decades from reference [15]. The data points represent the state-of-the-art laboratory transmission demonstrations.

The optical communication systems could be classified into two large categories by the medium, where an optical signal propagates or three large categories, based on their application differences: the short-haul and the long-haul fiber-optic communication systems and the free-space optical communication systems. The short-haul and long-haul fiber-optic systems differ mainly by the transmission reach, the operating wavelength and the transmission fiber type. The short-haul transmission extends up to few km-s, uses a multi-mode fiber (MMF) and is usually operated at 850 nm wavelength, while the long-haul links extend up to ten thousands of km-s, use a standard single-mode fiber (SSMF) and are operated at 1310 nm (older systems) or at 1550 nm wavelengths. Short-haul links are usually deployed in data center interconnects, super-computers, ultra high-speed local area network (LAN) connections, etc., where transmission distances are short. On the other hand, long-haul fiber-optic links are used all over the globe in communication systems for intra- and intercity, also intra- and intercontinental connections, covering the Internet critical transmission backbone for all possible services. The free-space or optical wireless communication systems are usually free-space optical (FSO) point to point links or light fidelity (Li-Fi) networks. FSO links are under special interest, while in the near future a deep space optical communication would be needed for high-speed connections between Earth, the Moon and Mars [16]. Also, there has been an ambitious idea proposed of a non-geostationary satellite system by SpaceX to build a FSO

network, consisting of a constellation of low-Earth orbit satellites, that provide a low latency and a high-speed optical connection all over the globe [17].

This thesis focuses only on a specific aspect in the optical communication society, which is the transmission fiber nonlinearity mitigation in long-haul fiber-optic communication links that are making use of the phase-sensitive amplifiers.

1.1.   Motivation

It is no secret that the number of internet users, connected devices and services are increasing on a daily basis. The emergence of 5G networks, the adoption of cloud based infrastructures with online audio-, video-streaming and gaming services, artificial intelligence controlled autonomous systems and smart devices, sensor networks, virtual reality and the rapid growth of users and connected devices (Internet of things) are driving an ever-increasing demand on a transmission system throughput and a transmission medium capacity. However, all that enormous data traffic needs to be serviced by the core network. The real "internet backbone" transmission systems are based on fiber-optic networks that provide ultra-fast and reliable connection for connecting long distances over intra- and intercity connections, intra- and intercontinental connections and even very short connections inside data centers or supercomputers [13]. The most critical intercontinental network backbone consists of submarine fiber-optic cables shown in Fig. 1.2. All of the real-time and therefore time-critical applications, but also all of the enormous amount of data traffic between different continents would not be possible without fast and high-bandwidth optical submarine connections. The optical fiber deployment has exceeded 4 billion kilometers to date, meaning that the globe could be wrapped around approximately 100 000 times with an optical fiber [18, 13].

There are five physical dimensions in fiber-optic communication systems that are available for the modulation and multiplexing of optical waves: time, frequency, polarization, quadrature and space. It means that a fiber channel capacity increase can rely only on those five dimensions that can be described with the modified Shannon capacity theorem [13]

$$C = M \times B \times 2 \times log_2(1 + SNR), \qquad (1.1)$$

where C is the total channel capacity, M is the number of parallel spatial paths, B is the bandwidth of used WDM channels, a factor of two accounts for the polarization multiplexing into two orthogonal polarizations (if used) and the SNR stands for the signal-to-noise ratio of a single-polarization, complex (quadrature) optical signal. The logarithmic term expresses the maximum possible spectral efficiency (SE). The current "capacity crunch," that can be seen in Fig. 1.1, is planned to overcome by the formation of hybrid superchannels by integrating
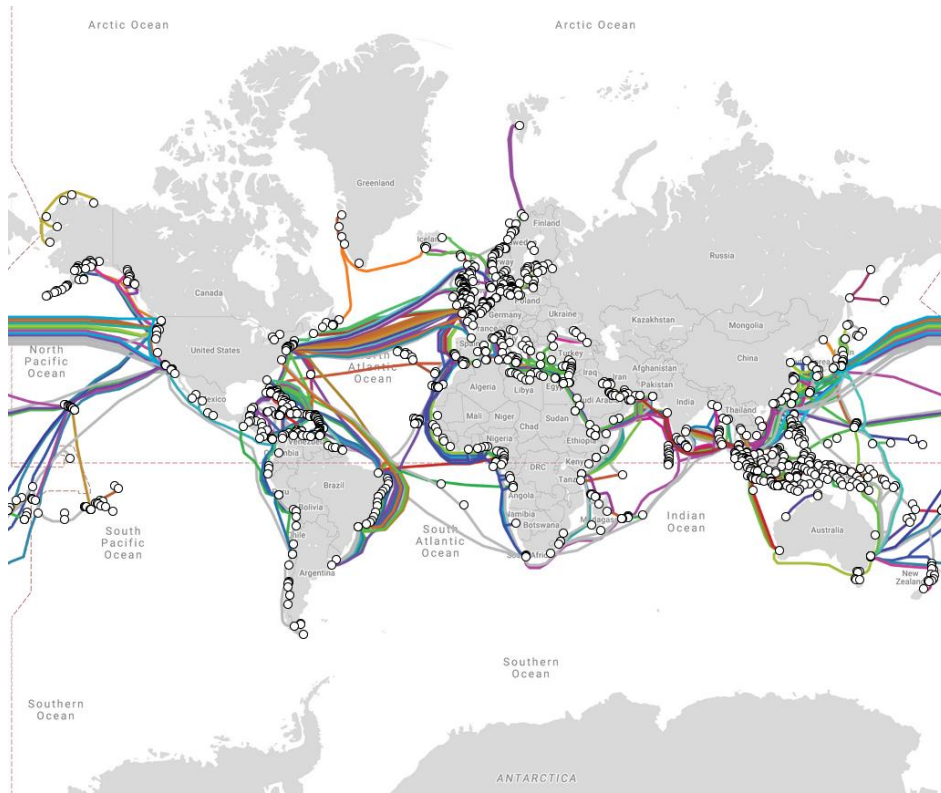
Figure 1.2 The submarine cable map showing submarine fiber-optic cables from reference [19]

WDM (frequency domain) and SDM (space domain) superchannels [20]. The spatial multiplexing can be implemented by using fiber bundles, multi-core fibers, few-mode fibers or a combination of them [15]. Other optical fiber dimensions are almost utilized, while in the time domain spectrally efficient Nyquist shaped pulses are already used, the two orthogonal polarizations of a light are also in use and the adoption of coherent transmission systems allowed the use of more spectrally efficient quadrature modulation formats [13].

Another way to increase the capacity is to improve the SNR by using optical amplifiers that have lower noise properties and/or by making use of the nonlinearity mitigation that enables higher optical signal launch powers to be used. The two main fundamental limitations in fiber-optic transmission systems are the amplifier noise that defines the linear Shannon limitation and the fiber nonlinearity that defines the nonlinear (NL) Shannon limitation for the achievable SE [14]. The origin of fundamental capacity limitations can be explained by Fig. 1.3 that originates from reference [21]. In Fig. 1.3, the optical transmission system performances are shown for four different system configurations. The black curve stands for the linear Shannon limitation determined by the amplified

18

spontaneous emission (ASE) noise. The linear Shannon limit will increase to a higher SE with the signal input power P_{in} increase, as the SNR increases. It must be noted, that the SNR and the OSNR (optical SNR) on the x-axis is attributed to the linear Shannon limitation and do not account for the SNR decrease caused by the fiber nonlinearity.
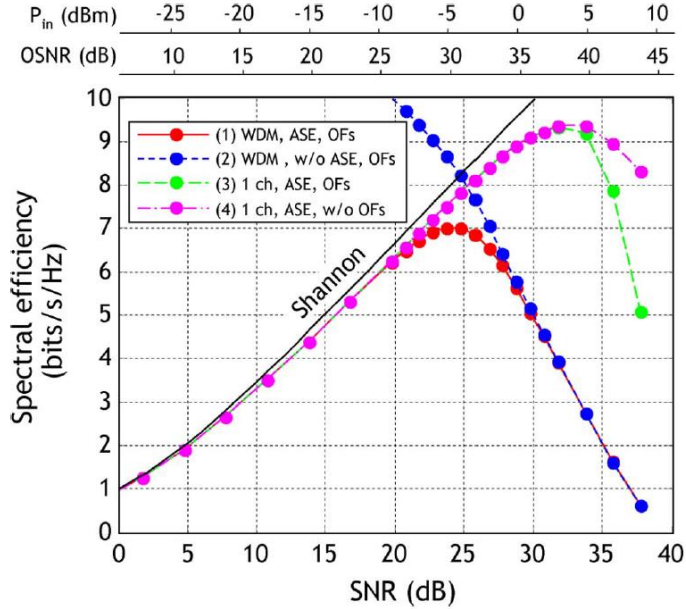
Figure 1.3 An illustration from reference [21] showing the spectral efficiency for four fiber-optic transmission system cases. The black curve and the blue curve of case (2) are showing the linear and nonlinear Shannon limitation boundaries respectively.

The case (1) in Fig. 1.3, a WDM system with an ASE noise and optical filters (OFs), shows that in an actual system, the SE has a maximum possible value at an optimal input power P_{in}, and the further increase in a signal input power will lead to a SE degradation. This is caused by the fiber nonlinearity, that limits the maximum usable input power of a fiber-optical transmission system. The case (2) shows an unrealistic noiseless scenario, where no ASE noise is present in a WDM system and the only limiting factor is the fiber nonlinearity. As the black curve stands for the linear Shannon limitation, then the case (2) shows the NL Shannon limitation caused by the fiber nonlinearity that degrades the achievable SE with an increasing input power. The cases (3) and (4) show that single-channel transmission systems can tolerate a much higher input power than WDM systems, therefore a higher spectral efficiency can be achieved.

The two operating regimes (linear or nonlinear) of a transmission system can be also distinguished. A system operates in a linear regime, if a signal launch power is lower than the optimal input power and the system performance is ASE noise limited. An operation in a nonlinear regime is achieved, if the optimal input power

is exceeded by a signal launch power and the system performance is limited by the transmission fiber nonlinearity.

The phase-sensitive amplifiers (PSAs) have gained a lot of interest in recent years due to their simultaneous low noise amplification and nonlinearity mitigation capability [22]. It must be noted that PSAs due to their complexity are not yet feasible for a commercial use. Also much smaller and shorter nonlinear waveguides than a highly-nonlinear fiber must be developed first. One of such a candidate could be based on a silicon nitride [23]. However, all research and knowledge related to PSAs is interesting and important to the optical society, while PSAs have shown a great potential for free-space optical links. The current record of the one-photon-per-bit receiver sensitivity has been achieved by using a PSA [24]. This allows us to predict that the future free-space optical links between planets will probably deploy PSAs.

1.2.   State of the art

The four main methods of mitigating nonlinear distortions induced by the Kerr effect in an optical fiber are the optical phase conjugation (OPC) that is also known as the mid-link spectral inversion (MLSI), the digital back-propagation (DBP), the phase-conjugated twin-waves (PCTW) approach and the use of phase-sensitive amplifiers (PSAs) [25]. There are also other methods proposed that increase a receiver robustness towards nonlinearly distorted signals, e.g. some methods based on nonlinear Volterra filtering techniques are the nonlinear equalization [26] or the digital pre-distortion [27, 28] or a combination of nonlinear equalization and a nonlinearity mitigation method to further improve an overall nonlinearity mitigation such as the Volterra-assisted optical phase conjugation [29]. Also machine learning techniques have been proposed for fiber-optics [30] and an interesting addition to the four main nonlinearity mitigation methods is the nonlinear Fourier transform (NFT) based optical nonlinearity mitigation method [31, 32]. The NFT method uses an inverse NFT in a transmitter to allow the eigenvalue composition of transmitted signals in such a way, that the spectrum is kept invariant during a nonlinear propagation.

- **Optical phase conjugation**

The optical phase conjugation (OPC) method was already proposed in 1983 for the nonlinearity mitigation [33]. It is continuously a hot research topic even for today [34, 35, 36], while the method is very robust to implement, requires a minimal redesign of a fiber link, is implemented all-optically and has the same spectral efficiency as a conventional transmission link. The alternative name, mid-link spectral inversion (MLSI) [37], comes from an idea about the OPC method, where an OPC device performs the optical phase-conjugation in the middle of a transmission link, where also a spectrum of a signal is inverted during the OPC

process. In the case of a symmetric link, the accumulated nonlinear distortions in the first half of the link are mitigated by the nonlinear distortions accumulated in the second half of the link. This is possible due to the phase conjugation process that will reverse the accumulated dispersion sign, while also the generated phase distortions of the first half of the link are reversed. The main problems with the method are related to the fact that a symmetric link assumption is not achievable in real-life. Also this method can deploy multiple OPC devices throughout a fiber-optic transmission link [34, 35, 36].

- **Digital back-propagation**

The digital back-propagation (DBP) method was first proposed in 2005 to mitigate nonlinear distortions [38]. The DBP is a hot topic for research ever since, due to a very good Kerr nonlinearity mitigation capability [39]. The basic idea is to digitally back-propagate (reverse a nonlinear propagation) the nonlinear Schrödinger equation (NLSE) that is used to model the nonlinear propagation effects in an optical fiber transmission. It can be implemented before the transmission, in a transmitter DSP, resulting in a signal digital pre-distortion or after the fiber transmission in a receiver DSP. The DBP idea shows that in the absence of stochastic noise, all the nonlinear distortions are deterministic and therefore reversible. However, the DBP is far from being practical in real-life applications as it requires a tremendous computational effort for numerical back-propagation calculations [40]. Some methods have been proposed to reduce this computational effort [40, 41, 42, 43]. It has been shown with the help of the DBP, that it is crucial to use frequency referenced carriers for WDM systems in order to effectively mitigate nonlinear distortions [44, 45].

- **Phase conjugated twin-waves**

The phase-conjugated twin-waves (PCTW) approach is a digital signal processing approach where a signal and its phase-conjugated copy are digitally coherently superpositioned in a receiver DSP. The twin waves can be separated in different polarizations (polarization multiplexed) [46], time-slots (time-division multiplexed) [47], wavelengths (wavelength-division multiplexed) [48, 49, 50] or spatial dimensions (spatial-division multiplexed) [51]. A more detailed description of the PCTW nonlinearity mitigation mechanism is presented in section 3.4 on page 56, while the basic idea behind the PCTW nonlinearity mitigation is the same as for the PSA approach. The PCTW approach offers a 3 dB SNR advantage in the linear regime and in the nonlinear regime, even larger performance improvements could be achieved due to the nonlinearity mitigation [46, 48, 49]. However, it is important to note that due to the use of a phase conjugated copy in fiber transmission, the spectral efficiency is halved by a factor of two [52].

- **Phase-sensitive amplifier**

An alternative way to perform the coherent superposition of a signal and its phase-conjugated copy is by using fiber-optic parametric amplifiers (FOPAs) in a two-mode phase-sensitive amplifier (PSA) mode [22, 53]. The coherent addition during the phase-sensitive process is performed all-optically and at the end of each transmission span that is amplified by a PSA, that also requires a span-wise in-line dispersion management before each PSA. ("Span" in this thesis context means an optical transmission link section that consists of an optical fiber that is followed by an optical amplifier.) In a two-mode single-polarization PSA link, a signal and its conjugated copy are located at different wavelengths. Similarly to the PCTW, the PSA approach also reduces the spectral efficiency by a factor of two. PSAs offer an improved performance for both linear and nonlinear transmission regimes and additionally benefit from a very low-noise (0 dB quantum limited noise figure, 1.1 dB noise figure experimentally achieved [54]) amplification. The experimental comparison of the PCTW and PSA methods in a single-span link have been investigated in [50].

The idea about optical amplifiers such as PSAs that could provide amplification without adding noise, dates back to 1962 [55, 56]. However, it took 20 years more after the PSA noise properties were formulated and an understanding to achieve noiseless amplification was established [57, 58]. It must be noted that in this thesis context, the one-mode PSAs are not relevant, since they are not multi-channel compatible and cannot provide a modulation format independent operation in contrast to two-mode PSAs.

The first pioneering experiment with a two-mode PSA was already conducted in 1986 [59], but the generation of phase-locked waves was a problem and the first demonstration of a data transmission amplified by a two-mode PSA was presented almost 20 years later [60]. In this experiment [60], an optical double-sideband modulation scheme was used for the frequency- and phase-locked waves generation, where the bandwidth was limited by the used modulators bandwidth. Additionally, in this latter scheme, the two sidebands contain the same information (no conjugate copy of a signal) that leads to a squeezing of one signal quadrature component, while a modulation format independent operation cannot be achieved. A modulation independent and a WDM compatible PSA can be realized by using a copier-PSA scheme, where the frequency- and phase-locked waves are first generated in a phase-insensitive FOPA [61, 62]. The bandwidth of a FOPA can be very large [63] that does not yield a limitation.

During the years 2010-2012, the research with PSA amplified transmission systems based on a copier-PSA scheme were mainly conducted, where the focus was to investigate the properties of PSA links and verify the noise figure improvement compared to the phase-insensitively amplified links [54, 64, 62, 65, 66]. The PSA WDM capability was shown in [65] and the record-low noise figure of 1.1 dB was experimentally measured in [54].

The further work in fiber-optic transmission systems using two-mode PSAs was made possible by the introduction and demonstration of a pump recovery system that enabled a transmission in spans with more than 40 dB loss in 2012 [67, 68]. In [69], the first experimental demonstration of a PSA link nonlinearity mitigation capability is presented. It was shown a year later, that the PSA nonlinearity mitigation performance is dependent on the used span dispersion map [53]. A further numerical investigation of a single-span PSA dispersion map optimization was presented in [22], although a full experimental dispersion map optimization study was not made, since the tunable dispersion compensators were not used. In 2014, the first long-haul two-mode PSA amplified transmission system in a circulating loop setup was presented, where a threefold transmission reach improvement was observed, if in-line PSAs, that enabled low-noise amplification and nonlinearity mitigation, were used instead of conventional EDFAs in a 10 GBaud QPSK signal transmission [70].

The dispersion map dependence was also noted for twin-waves in a PCTW approach study [46]. According to the first-order perturbation theory, it has been suggested in [46] that a symmetric power map and an anti-symmetric dispersion map should be used for superior nonlinearity mitigation performance that is not achievable in a lumped amplified link. The perturbation theory assumption has inspired a numerical study [71] that investigates nonlinearity mitigation aspects in a hybrid Raman/phase-sensitive amplifier links for more power symmetrical and ideal Raman amplified scenarios. However, such an experimental study was not carried out in previous work for the PSA links.

1.3.   This thesis

This thesis focuses on the nonlinearity mitigation aspects that are dependent on the deployed dispersion maps in a two-mode PSA amplified optical transmission link. A comprehensive study both numerically and experimentally has been presented in Papers A - E, that include an experimental demonstration of the highest transmission reach improvement achieved by using in-line PSAs, the first demonstration (both numerically and experimentally) of a multi-span dispersion map optimization for PSA links and the first experimental demonstration of a power symmetrized Raman assisted PSA link, in order to gain more insight about the dispersion compensation role in the PSA links.

1.3.1.   Problem statement and research questions

It is evident from the state of the art, that a dispersion map plays a significant role in the PSA link performance by influencing the nonlinearity mitigation effectiveness. However, so far, only few studies have been carried out to single-span optimize a dispersion map of a two-mode PSA amplified transmission link [53, 22], where the optimum dispersion maps were determined only by a numerical study. In the

fiber-optical society, numerical studies usually correspond well to experimental observations, but all the concepts have to be proven by an experimental study for a quality assurance. In Papers A, B and E an experimental investigation is presented. The Papers C and D present only numerical studies, while the experimental study seems not feasible to carry out for more than a two-span PSA link dispersion map optimization by considering current laboratory setup possibilities. The validity of the Papers C and D numerical studies is assumed to rely on the fact, that the numerical and experimental study in the Paper B coincide well with each other.

As the use of tunable dispersion compensators makes it easy to optimize a dispersion map experimentally and also switch between different dispersion map configurations for PSA and PIA case, an experiment was conducted in Paper A to measure the reach extension achieved, if PSAs are used instead of PIAs in an in-line amplified and dispersion in-line compensated circulating loop transmission system. The main idea is to demonstrate for the first time the reach extension in the case, where PSA and PIA links have both optimized dispersion maps. The previous work presented in [70] did not use tunable dispersion compensators, so the PSA and PIA link comparison presented was not actually dispersion map optimized.

In Paper B, it has been demonstrated for the first time, both numerically and experimentally, that different dispersion maps in a two-span PSA link will enhance nonlinearity mitigation performance. It is inherent only to PSA amplified links (and not to conventional phase-insensitive amplified (PIA) links) in the case of a high symbol rate transmission, when the span dispersive length is smaller than the span length, e.g. 28 GBaud QPSK case that was studied in the Paper B. However, the experimental part was made possible due to the tunable dispersion compensators, so the span dispersion maps could be easily altered without a need to change an experimental setup and without introducing any significant penalties.

The concept of multi-span dispersion map optimization has been investigated further and extended up to four-span optimized PSA links in Papers C and D. In Paper C a four-span optimization with a coarse step size shows a significant improvement in the highly nonlinear transmission regime. In paper D, a more thorough numerical investigation of nonlinearity mitigation aspects with a more precise optimization step size has been carried out. Additionally a complete benchmarking that shows possible long-haul reach extension improvements by the use of dispersion map optimized PSA links instead of PIA dispersion in-line compensated and dispersion in-line unmanaged links, is presented.

The first-order perturbation theory suggest a symmetric span power map and an anti-symmetric dispersion map for efficient nonlinearity mitigation for a PCTW approach [46], that would also apply for a two-mode PSA link. The numerical simulation study in [71] predicted significant improvement, if power-symmetric PSA spans are deployed. One way to symmetrize a span power map is to use multiple backward Raman pumped amplified span setup together with a single lumped PSA at the end of a span, that performs coherent superposition. In Paper

E, such an experimental investigation and demonstration has been presented for the first time.

- **Research questions**

The most relevant research questions raised and answered in this thesis are:

1. What is the experimentally achieved transmission reach improvement for a long-haul dispersion map optimized QPSK link operating in the 10 GBaud regime, if PSAs are used instead of PIAs in an in-line dispersion managed long-haul circulating loop setup?

2. Does the PSA link simulation study for the 28 GBaud regime show that the use of multi-span optimized dispersion maps outperform widely used single-span optimized dispersion map solution for multi-span PSA links?

3. Is it possible to design experimentally a two-span PSA link that utilizes different dispersion map configuration in each span by using only one available PSA amplifier?

4. Are we able to observe experimentally any performance improvement by using a two-span dispersion map optimized PSA link configuration instead of a single-span optimized two-span PSA link?

5. Does the further number of spans dispersion map optimization increase the nonlinearity mitigation performance of a 28 GBaud PSA link?

6. How sensitive is the nonlinearity mitigation performance to a multi-span dispersion map optimization accuracy of a 28 GBaud PSA link?

7. What are the possible transmission reach improvements, if multi-span dispersion map optimized PSA links are used instead of PIA links in long-haul fiber-optic 28 GBaud transmission systems?

8. Why the multi-span dispersion map optimization that allows the use of different span dispersion maps in each span can improve the nonlinearity mitigation capability of a PSA?

9. Are we able to observe experimentally an enhanced nonlinearity mitigation performance for a Raman assisted span power map symmetrized PSA link working in a 28 GBaud regime?

1.3.2. Contributions of the thesis

The main contributions are given in the form of the main claims of this thesis as follows:

1. The first experimental demonstration of a significant transmission reach improvement by a factor of 5.6 at optimal launch powers has been demonstrated, if PSAs are used instead of PIAs in a long-haul single-span dispersion map optimized 10 GBaud QPSK fiber-optic transmission link. Such a significant transmission reach improvement is enabled by the low-noise amplification and nonlinearity mitigation capability of PSAs. [Paper A]

2. A method to allow and optimize the use of different span dispersion maps in a two-mode 28 GBaud QPSK PSA amplified fiber-optic transmission link has been proposed. The method is not so self-evident, while conventional recirculating loop experiments conducted in laboratories use only single-span setup to loop through the same span in order to emulate a long-haul fiber-optic transmission link. [Paper B]

3. The first experimental demonstration of a two-span dispersion map optimized 28 GBaud QPSK PSA fiber-optic transmission link is presented, that will outperform a single-span optimized two-span PSA link. This is possible due to the improved nonlinearity mitigation capability of a PSA link enabled by an allowance to use different span dispersion maps in each span. [Paper B]

4. The first and extensive numerical study up to four-span dispersion map optimization in a 28 GBaud QPSK PSA amplified fiber-optic transmission link has been carried out and the investigation of nonlinearity mitigation properties are presented. [Paper C and D]

5. The first benchmarking of up to four-span dispersion map optimized PSA links and in-line span-wise dispersion compensated and dispersion in-line unmanaged EDC compensated PIA links in a long-haul 28 GBaud QPSK fiber-optic transmission link numerical study has been carried out and presented. [Paper D]

6. The first generic explanation about the nonlinearity mitigation mechanism for multi-span dispersion map optimization, that is based on a power map symmetry and dispersion map anti-symmetry condition of a phase-conjugated twin-waves, is presented. [Subsection 4.2.2 on page 70]

7. The first experimental demonstration of distributed Raman amplification assisted 28 GBaud QPSK PSA fiber-optic transmission link is presented and the nonlinearity mitigation properties of such a span power map symmetrized PSA link have been investigated. [Paper E]

1.3.3. Thesis outline

This thesis is organized as follows. In Chapter 2 an overall introduction to an optical signal propagation through a fiber, the optical fiber propagation effects and the main building parts of a fiber-optic transmission system are presented. In Chapter 3, a general theory of the two-mode phase-sensitive amplification, that is realized by using FOPAs, has been described. A bit more detailed description than usually necessary is briefly presented in Chapters 2 and 3, while this is (to the best of author's knowledge at least) the first PhD thesis defended in Estonia concerning nonlinear fiber-optic communication systems.

The aspects of dispersion map optimization, especially in PSA links and the PSA nonlinearity mitigation mechanism dependence on dispersion maps is discussed in Chapter 4. In Chapter 5 an overview of the publications is presented and finally, Chapter 6 concludes the work presented in this thesis with a discussion and in addition, some interesting future prospects are deduced from the discussion.

2. SIGNAL PROPAGATION IN FIBER-OPTIC TRANSMISSION SYSTEMS

A fiber-optic transmission link as a communication channel for transmitting digital data from point A to point B follows the basic principle of any generic digital communication channel [5, 72] that is illustrated in Fig. 2.1. The digital data in the form of a bit sequence b from the point A is sent to a transmitter where the data is modulated to a carrier suitable for the physical layer signal delivery through a transmission channel. After the transmission channel, the transmitted signal is detected by a receiver and converted into a digital bit sequence $\hat{b}$. It is important to note that the quality of transmitted signals degrades during signal transmission, therefore different measures have to be taken into account to assure that the transmitted data for the recipient B should contain the same information as it was sent from the point A.
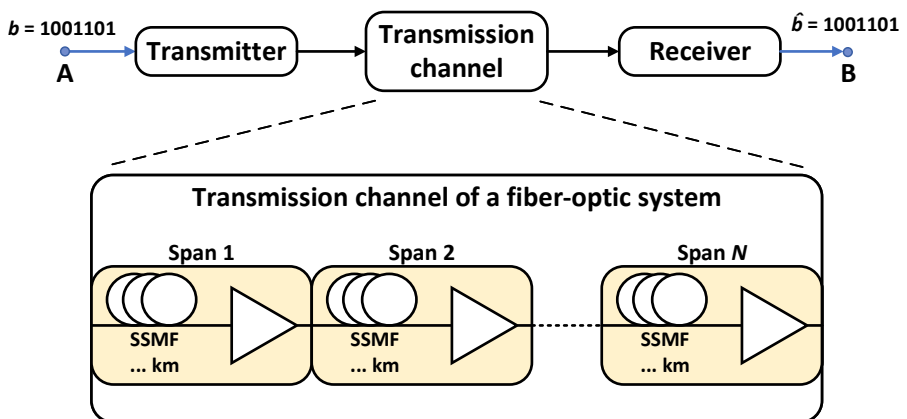
Figure 2.1 Illustration of a basic digital communication channel and the main building blocks of a fiber-optic transmission channel.

Fiber-optic transmission systems use lightwaves as information carriers, that propagate through a fiber-optical transmission channel. A transmission channel for such systems usually consists of many fiber-spans and optical amplifiers, that compensate for a fiber-span attenuation. A span of optical fiber, usually a SSMF, and an optical amplifier in the end of each fiber-span are usually called

the span, as shown in Fig. 2.1. In multi-span long-haul systems, the span length is usually chosen from 50 to 100 km. The longest transmission reaches of long-haul fiber-optic links without electronic regenerators have been demonstrated extending up to 12000 km [73], while the longest fiber-optic link around the globe (FLAG) extends to 28000 km [74].

The development of fiber-optic coherent transmission systems has enabled a better sensitivity over traditional direct-detection transmission systems and to improve the spectral efficiency [75]. The direct-detection method uses a photodiode in a receiver that can detect only the envelope of an optical field, while the phase information of a signal is ignored [76]. However, the adaption of coherent transmitter and receiver has made possible the use of higher modulation formats that require simultaneous detection of amplitude and phase information and enabled the mitigation of linear impairments in the digital signal processing (DSP) domain.

In this chapter an overview of a long-haul coherent fiber-optical communication link through the main building blocks of a communication channel is presented. However, the dispersion management building blocks - dispersion compensators, are not included in this chapter, while the dispersion management of fiber-optic transmission systems is discussed in more detail in section 4.1 on page 62.

2.1. Optical transmitters

The two main parts of a coherent optical transmitter are a coherent light source for generating carrier waves and an I/Q-modulator that consists of Mach-Zender modulators (MZMs) for modulating in-phase (I) and quadrature (Q) components of an electrical input signal shown in Fig. 2.2 [77]. After the coherent light source, such as a laser, the optical carrier is splitted by a polarization beam splitter into two paths. The upper path is used to modulate the carrier for the X polarization and the lower path for the Y polarization of an optical field. In these two almost identical paths, the signal is splitted again into two paths for modulating the I and Q components of an electrical input signal separately in each MZM modulator. The input bit streams for every I and Q channel (I_x, Q_x, I_y, Q_y) are converted in the digital to analog converters (DACs) and amplified with radio frequency (RF) amplifiers before the MZM electrical inputs. In the I/Q-modulator Q path, the optical signal is phase shifted by $\pi/2$ and then recombined with the I path signal. Such a setup consisting of two MZMs and a $\pi/2$ phase-shifter forms the I/Q-modulator. A polarization rotator has to be used at one of the paths to assure the orthogonality of the combined signal polarizations. The polarization beam combiner is used to combine X and Y polarization components into single polarization-multiplexed optical signal.

In Fig. 2.2 the structure of a dual-polarization transmitter is shown. However, a single-polarization transmitter can also be built. A single-polarization transmitter
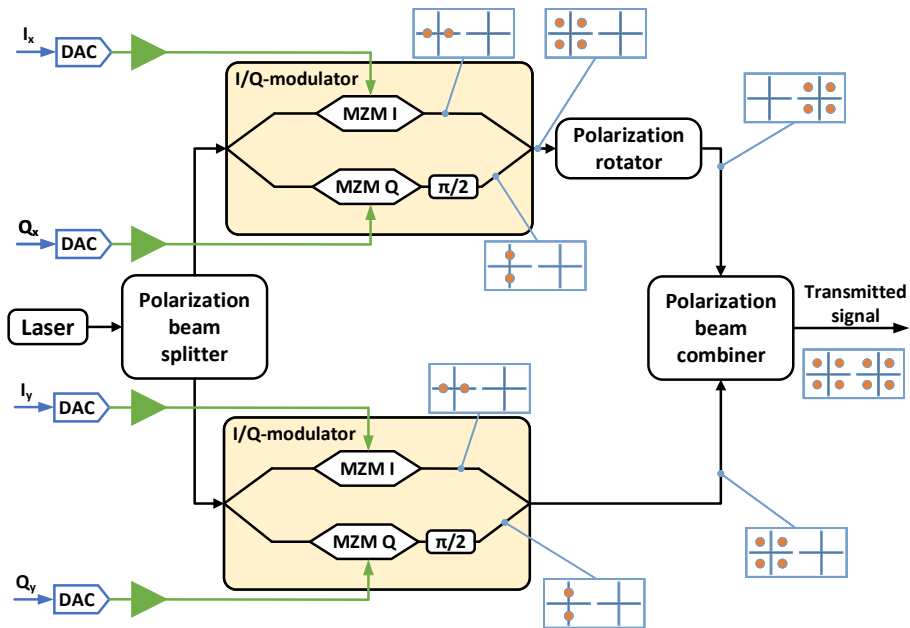
Figure 2.2 Schematic of an optical coherent transmitter [77]. Colored paths show signal type: blue - digital, green - analog, black - optical signal. The constellations illustrate a generation of a QPSK signal, where the left side constellation stands for the X polarization and the right side constellation for the Y polarization.

is simpler consisting of a laser and the lower path shown in Fig. 2.2 without polarization beam splitter and combiner elements. In this thesis only a single-polarization transmitter and transmission are used.

In any coherent transmitter, the coherence of a light source is the most important parameter, since the carrier phase is modulated. An ideal laser spectral shape would be the delta function at the carrier frequency. In real-life, the presence of phase noise broadens the spectral shape, that can be modeled using the Lorentzian shape [78, 79]. The amount of phase noise is typically characterized by the linewidth that conveys the stability of a phase over time. The phase noise can be modeled as Wiener process

$$\Phi_i = \Phi_{i-1} + \Delta n_i, \tag{2.1}$$

where Φ_i is the phase of the ith sample and Δn_i is an independent and identically distributed Gaussian random variable with zero mean and variance

$$\sigma_\Phi^2 = 2\pi\Delta\nu T_\mathrm{s}, \tag{2.2}$$

where $\Delta\nu$ is the linewidth of a laser and T_s is a sampling interval [80].

2.2. Optical fiber

An optical-fiber is lossy, dispersive and nonlinear transmission medium. The linear fiber effects are attenuation and fiber dispersion. The fiber dispersion in this thesis context means mainly group-velocity dispersion (GVD), if not stated otherwise. The polarization-mode dispersion (PMD) is caused by fiber birefringence i.e. due to a fiber asymmetry the refractive index slightly varies between orthogonal polarizations causing traveling speed difference that is dependent on the state of polarization. In this thesis a single polarization transmission is assumed resulting in negligible PMD effects, therefore a more detailed discussion about PMD is not included. It should be noted that also intermodal dispersion that is present in multi-mode fibers is not discussed here, since SSMFs (standard single-mode fibers) are used in long-haul fiber-optic transmission links. In the following section an overview of a fiber attenuation, dispersion and nonlinear fiber effects are presented. Also the principle of the Split-step Fourier method as the main tool to numerically simulate a fiber-optic propagation environment is presented.

2.2.1. Attenuation

The optical fiber attenuation is caused mainly by the material absorption and the Rayleigh scattering. The attenuation introduces power loss to a signal propagating through a fiber-optic link that can be governed under quite general conditions by Beer's law [5] that can be written in the form:

$$P(z) = P_{\text{in}}\exp(-\alpha z), \tag{2.3}$$

where P_{in} is the power launched into a fiber, α is the attenuation coefficient (unit m^{-1}) and $P(z)$ is the optical field power at the propagated distance z. Typically, if an output power at the end of a fiber is under interest, then the Eq. 2.3 is given by

$$P_{\text{out}} = P_{\text{in}}\exp(-\alpha L), \tag{2.4}$$

where P_{out} is the optical field power at the end of a fiber of length L. After the introduction of silica fibers in 1970s, optical fibers with practical attenuation coefficients became available [81]. A typical attenuation coefficient value for a SSMF is round 0.2 dB/km at 1550 nm wavelength region [82] where most of the modern long-haul fiber-optic systems are operated. It should be noted that usually the attenuation coefficient is given in unit dB/km, but it should be converted into unit m^{-1} in order to use it in Eq. 2.3 and 2.4.

2.2.2. Fiber dispersion

A phenomenon, that is present in fiber-optics and referred to as the group-velocity dispersion (GVD), intramodal dispersion or fiber dispersion [5], is responsible for an optical pulse broadening during a propagation in a transmission fiber. During the propagation in a dispersive medium such as an optical fiber, different spectral components of an optical pulse travel at different group velocities. As a result, a delay between different frequency components is introduced. This is caused by the frequency dependent change of the refractive index that is described by equation:

$$\bar{n}_g = \bar{n} + \omega(d\bar{n}/d\omega), \tag{2.5}$$

where $\bar{n}$ is the refractive index, ω is frequency and $\bar{n}_g$ is the group index. This refractive index difference results in different propagation path lengths for different frequency components that causes different delays to each frequency component, while the propagation path lengths are different.

A delay between traveling times of different frequency components results in the time domain broadening of a pulse shown in Fig. 2.3, where an optical pulse propagation in a fiber over 200 km in the presence of dispersion effects is illustrated. The pulse peak amplitude lowers and the pulse spreads over neighboring symbol slots during the propagation. The pulse broadening itself was a problem for older systems using direct-detection receivers. However, in modern systems with coherent detection receivers, the fiber dispersion can be compensated electronically in a receiver. Also modern systems without the span-wise dispersion compensation scheme are more tolerant to nonlinear impairments [83, 84].

The GVD parameter β_2 (unit $\mathrm{ps}^2/\mathrm{km}$) is the second derivative of the linear propagation constant $\beta_\mathrm{L}(\omega) = \bar{n}(\omega) \cdot \omega/c$ and conveys a propagation speed difference over frequency components

$$\beta_2 = \frac{d^2\beta_\mathrm{L}}{d\omega^2}. \tag{2.6}$$

The dispersion parameter D (unit $\mathrm{ps}/\mathrm{nm}/\mathrm{km}$) is related to the GVD parameter β_2 as

$$D = -\frac{2\pi c}{\lambda^2}\beta_2, \tag{2.7}$$

where c is a constant of the speed of light and λ is the operating wavelength. A length scale for the dispersion is named the dispersion length and defined

$$L_\mathrm{D} = T_0^2/|\beta_2|, \tag{2.8}$$

where T_0 is the half-width at 1/e intensity point and relates to the pulse full-width at half-maximum as

$$T_\mathrm{FWHM} = 2(\ln 2)^{1/2}T_0 \approx 1.665T_0. \tag{2.9}$$
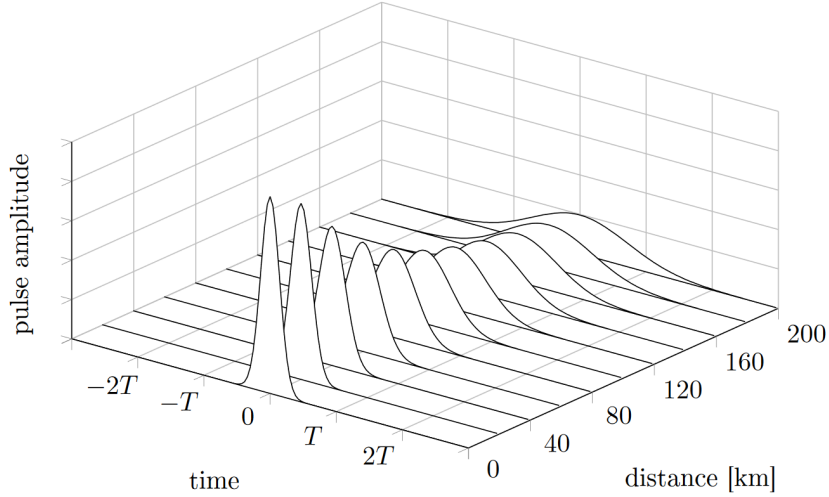
33

Figure 2.3 Illustration showing the broadening of an optical pulse in the time domain over adjacent symbol slots during a dispersive propagation in a fiber-optic link over 200 km from reference [85].

Also the third-order dispersion parameter known as the differential-dispersion parameter or the dispersion slope parameter S (unit $\mathrm{ps/nm^2/km}$) represents the frequency (or wavelength) dependence of the dispersion

$$S = \frac{dD}{d\lambda} = (2\pi c/\lambda^2)^2 \beta_3 + (4\pi c/\lambda^3)\beta_2, \qquad (2.10)$$

where β_3 is the third-order derivative of $\beta_\mathrm{L}(\omega)$. The differential-dispersion parameter is important to consider in WDM systems, where different channels have slightly different GVD values. Additionally in PSA systems, the differential-dispersion parameter affects the phase-matching as a signal and its phase conjugate are located at different wavelengths and therefore have slightly different GVD values, which results in slightly different relative phase-shifts after the propagation in a fiber.

The dispersion can be an anomalous dispersion or a normal dispersion dependent on the used wavelength region. A typical SSMF [82] at the wavelengths higher than 1.3 μm results in the anomalous dispersion regime where the group velocity of higher frequencies is higher than for lower frequencies and the dispersion parameter D value is positive. The opposite is true for the normal dispersion regime at the wavelengths smaller than 1.3 μm. Modern fiber-optic communication systems operate typically at anomalous dispersion wavelengths around 1.55 μm. For the both dispersion regimes, nonlinear effects affect a signal during the propagation in a fiber differently [75].

The total dispersion of a fiber consists of the material dispersion and the waveguide dispersion that are the main parameters in the fiber design process.

The material dispersion is related to a dependence of the cladding material's group index on the frequency, while the waveguide dispersion is attributed to a mode dependence on the frequency [5]. Therefore different fibers can be designed by using the properties of material and waveguide dispersion e.g. a dispersion-shifted fiber (DSF), a dispersion-flattened fiber (DFF) or a dispersion compensating fiber (DCF).

2.2.3. Nonlinear fiber effects

Often fiber nonlinear effects are called the Kerr effect after a Scottish physicist John Kerr, who discovered in 1875 [86, 87] that the refractive index of any material can be changed with an applied electromagnetic field. In addition to the refractive index wavelength dependence, the refractive index dependence on the instantaneous intensity of the light has to be included in the refractive index equation [88]

$$n(\omega, I) = n_0(\omega) + n_2 I,$$ (2.11)

where $n(\omega, I)$ is the frequency and light intensity dependent refractive index, $n_0(\omega)$ is the linear and n_2 is the nonlinear refractive index and I is the instantaneous intensity of a propagating light. The nonlinearity coefficient that specifies a nonlinearity strength in a fiber is given [89]

$$\gamma = \frac{2\pi n_2}{\lambda A_{eff}},$$ (2.12)

where A_{eff} is the effective area of a fiber mode. The value of γ is round $1.3\ W^{-1}km^{-1}$ for a typical SSMF.

- **Self-phase modulation**

The fundamental Kerr effect phenomenon is the self-phase modulation (SPM). In the SPM process, a wave that propagates through a nonlinear medium, such as a fiber, modulates its own phase by inducing a refractive index change, which results in a signal spectral broadening. The nonlinear phase shift can be described by

$$\phi_{\mathrm{NL}} = \gamma P L_{\mathrm{eff}},$$ (2.13)

where P is the power of a propagating wave, and L_{eff} is the effective length of a fiber described by

$$L_{\mathrm{eff}} = \frac{1 - \exp(-\alpha L)}{\alpha}.$$ (2.14)

The effective length is defined to express the strength of the nonlinear effect. It shows a length, where the accumulated nonlinear phase shift $\phi_{\mathrm{NL}}(L)$ of a fiber link with a realistic attenuating power profile at the end of the link would be the same as for an unrealistic attenuation-less link, where the power of a propagating

wave would be constant, thus giving the same accumulated nonlinear phase shift over a shorter distance L_{eff} than the physical length L. It can be written as

$$\phi_{\text{NL}}(L) = \gamma P(0)L_{\text{eff}}, \qquad (2.15)$$

where $P(0)$ is the input power to a fiber. Another way to express the impact of nonlinearity is the nonlinear length described by

$$L_{\text{NL}} = \frac{1}{\gamma P(0)}, \qquad (2.16)$$

that can be substituted into Eq. 2.15. The maximum nonlinear phase shift can be calculated as a ratio between effective and nonlinear lengths as

$$\phi_{\text{NL,max}} = \gamma P(0)L_{\text{eff}} = L_{\text{eff}}/L_{\text{NL}}. \qquad (2.17)$$

However, it should be noted that Eq. 2.17 is a quantitative measure and valid only for cases where the dispersion can be neglected, e.g. a slowly-varying input signal or an operation near or at the zero-dispersion wavelength. In most cases, a numerical solution should be used as the interplay between dispersion and SPM effects should be considered. For example it is known from the generation of optical solitons that the dispersion and nonlinear effects can cancel each other out [90, 91].

- **Cross-phase modulation**

In this thesis only single-channel PSA links are under investigation and therefore multi-channel propagation effects like the cross-phase modulation (XPM) are not studied in papers A - E. However, a brief introduction of the XPM is presented.

As it is already said, the XPM occurs in a multi-channel (WDM) scenario when two or more optical channels are transmitted simultaneously. For the SPM case, the nonlinear phase shift depends only on the power of that channel. For the XPM case, also the power of adjacent channels will add up to the nonlinear phase shift of that channel and the phase shift for the jth channel for the co-polarized waves is described as

$$\phi_{\text{NL},j} = \gamma L_{\text{eff}}(P_j + 2\sum_{m \neq j} P_m), \qquad (2.18)$$

where the sum extends over multiple channels [5]. The factor 2 shows that the effect of XPM i.e. the nonlinear phase-shift dependence from adjacent channels, is twice as effective as the effect of SPM in the case of equal channel powers. In reality the effect of XPM is difficult to estimate as optical pulses in different channels travel with different speeds due to the dispersion and the XPM effect occurs only if two pulses in different channels overlap in time. Therefore a numerical approach should be used (analogically to the SPM) to evaluate the impact of XPM.

- **Four-wave mixing**

The four-wave mixing (FWM) or alternatively the four-photon mixing process happens similarly to the XPM in the presence of multiple waves at different frequencies. The concept of four-photon mixing can be described in several ways including the quantum-mechanical or the vector FWM interpretation [92, 93]. In this thesis, the most commonly used classical interpretation is preferred.

The four-photon mixing concept according to the classical interpretation is as follows. Two waves at different frequencies ω_1 and ω_2 are co-propagating through an optical fiber, where they generate a varying intensity field with a beat tone at a frequency $\omega_2 - \omega_1$. The generated beat tone will modulate the index of refraction through the Kerr nonlinearity. If an additional third wave is also co-propagating through the fiber at a frequency ω_3 , it will experience a phase modulation with the frequency $\omega_2 - \omega_1$, thus generating sidebands at frequencies $\omega_3 \pm (\omega_2 - \omega_1)$. The phase modulations are also caused by the beatings between the waves at ω_3 and at ω_1, thus introducing sidebands $\omega_2 \pm (\omega_3 - \omega_1)$ and between the waves at ω_3 and at ω_2 resulting in sidebands $\omega_1 \pm (\omega_3 - \omega_2)$. All the possible combinations of generating new frequency components with three frequencies at the input can be described by

$$\omega_{jkl} = \omega_j + \omega_k - \omega_l, \tag{2.19}$$

where the three new components are a product of the non-degenerate FWM $j, k, l \in 1, 2, 3, j \neq k, j \neq l, k \neq l$ and the six new components are produced in the degenerate FWM $j, k, l \in 1, 2, 3, j = k, j \neq l, k \neq l$. The total number of new frequency components created from three input waves in the FWM process is nine. An illustration of the three input waves and the FWM process produced frequency components are shown in Fig. 2.4.
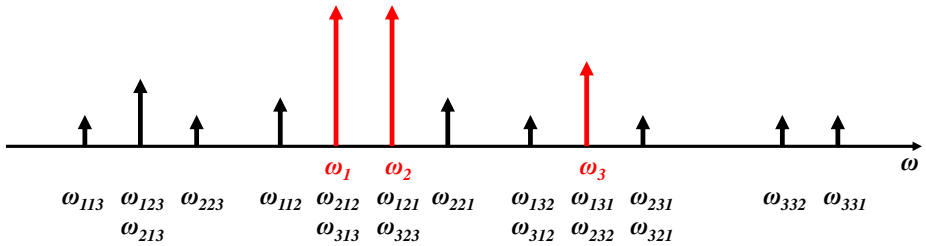

Figure 2.4 Illustration of the FWM generated nine new frequency components from the three input frequency components $\omega_1, \omega_2, \omega_3$.

The FWM can cause major limitations in WDM systems [94], where the number of frequency components is large and the possibility to create many new components can cause severe crosstalk effects. However, the FWM process is utilized to realize fiber-optic parametric amplification and also phase-sensitive fiber-optic parametric amplification.

- **Nonlinear scattering effects**

All the previously described nonlinear effects are elastic nonlinear processes, where no energy exchange happens between the propagating lightwaves and the propagation medium, therefore the total energy of propagating waves is conserved. The Raman and Brillouin scattering on the other hand are inelastic nonlinear processes, where the lightwaves exchange energy through the vibrational excitation modes with the propagation medium. According to the quantum-mechanical perspective, a photon is annihilated, but a new one at a lower frequency together with a phonon (vibration) is created during the inelastic nonlinear process. The latter two scatterings are distinguished by the created phonons, where the Raman scattering involves optical phonons and the Brillouin scattering involves acoustic phonons [75].

The spontaneous Raman scattering process was discovered in 1928 by Raman [95], while the stimulated Raman scattering (SRS) effect was first discovered in 1962 [96]. During the SRS process, a power from one lightwave (which is usually the pump wave) is transferred to another lightwave at a lower frequency (Stokes wave). If the frequency shift conditions are met, then these two waves at the input of a fiber cause a chain reaction, where pump photons are annihilated and optical phonons as well as photons at the lower frequency are created. The creation of phonons increases the vibrational energy, therefore stimulating the process further. During the process, the Stokes wave experiences amplification, therefore the SRS effect can be utilized for a distributed amplification [89, 97, 98]. As the downshifted photons can travel in forward or backward directions, the both, forward and backward pumped Raman amplification schemes are possible to implement.

During the Brillouin scattering process, the energy transfer to a medium results as acoustic vibrations. In contrast to the SRS, the generated Stokes wave from the Brillouin scattering process propagates usually in the backward direction. However, a weak forward propagation phenomenon can also happen if the conditions are met for the guided acoustic wave Brillouin scattering (GAWBS) [99].

The stimulated Brillouin scattering (SBS) was discovered in 1964 [100]. The SBS effects start to dominate after the pump wave power reaches a certain threshold, therefore limiting the input power. The SBS causes problems in nonlinear fiber devices with the high input power of a pump e.g. phase-sensitive parametric amplifiers. Various methods and a detailed discussion about the SBS suppression for parametric amplifiers can be found in [101].

2.2.4. Split-step Fourier method

The fundamental equation to model the propagation of lightwaves in fiber-optic links is the nonlinear Schrödinger equation (NLSE). The NLSE can be given in

the form of generalized (or extended) NLSE [75] given by

$$\frac{\partial A}{\partial z} + \frac{\alpha}{2}A + \frac{i\beta_2}{2}\frac{\partial^2 A}{\partial T^2} - \frac{\beta_3}{6}\frac{\partial^3 A}{\partial T^3} = i\gamma(|A|^2 A + \frac{i}{\omega_0}\frac{\partial}{\partial T}(|A|^2 A) - T_R A\frac{\partial|A|^2}{\partial T}),$$
(2.20)

where A is the amplitude of the propagating light field, z is the propagation distance, α is the attenuation coefficient, β_2 is the GVD parameter, β_3 is the third-order dispersion parameter, T is the pulse width, γ is the nonlinearity coefficient, ω_0 is the center frequency and T_R is related to the slope of the Raman gain spectrum [102]. However, Eq. 2.20 can be simplified by neglecting the parameters $(\omega_0 T_0)^{-1}$ and T_R/T_0 that are small in the case of an initial pulse width $T_0 > 5$ ps. The third-order dispersion term is also negligible if a carrier wavelength is not close to a zero-dispersion wavelength. The simplified NLSE formula that includes terms for the attenuation, GVD and nonlinear effects becomes

$$i\frac{\partial A}{\partial z} + \frac{i\alpha}{2}A - \frac{\beta_2}{2}\frac{\partial^2 A}{\partial T^2} + \gamma|A|^2 A = 0.$$
(2.21)

If the propagation of a light in the both polarizations are under interest, then the coupled equations [103, 104] of the Manakov model [105] can be used to describe an optical field propagation

$$\frac{\partial A_X}{\partial z} = -\frac{\alpha}{2}A_X - i\frac{\beta_2}{2}\frac{\partial^2 A_X}{\partial T^2} + i\frac{8}{9}\gamma(|A_X|^2 + |A_Y|^2)A_X,$$
(2.22)

$$\frac{\partial A_Y}{\partial z} = -\frac{\alpha}{2}A_Y - i\frac{\beta_2}{2}\frac{\partial^2 A_Y}{\partial T^2} + i\frac{8}{9}\gamma(|A_Y|^2 + |A_X|^2)A_Y,$$
(2.23)

where A_X and A_Y are the propagating field amplitudes for X and Y polarization correspondingly.

Unfortunately, the NLSE equation does not have an analytical solution and therefore numerical methods have to be used. The most extensively used method to model an optical field propagation in fiber-optical communication links numerically is the split-step Fourier method (SSFM) [75, 106]. The SSFM each step ∂z calculation is divided into two parts, therefore the Eq. 2.20 is more useful to write in the form of

$$\frac{\partial A}{\partial z} = (\hat{D} + \hat{N})A,$$
(2.24)

where $\hat{D}$ is a differential operator that accounts for the dispersion and attenuation within a linear medium and $\hat{N}$ is a nonlinear operator that governs the effect of fiber nonlinearity on pulse propagation [75]. The substituted parts from Eq. 2.20 defining these two operators are

$$\hat{D} = -\frac{i\beta_2}{2}\frac{\partial^2}{\partial T^2} + \frac{\beta_3}{6}\frac{\partial^3}{\partial T^3} - \frac{\alpha}{2},$$
(2.25)

39

$$\hat{N} = i\gamma(|A|^2 + \frac{i}{\omega_0}\frac{1}{A}\frac{\partial}{\partial T}(|A|^2 A) - T_R\frac{\partial|A|^2}{\partial T}). \qquad (2.26)$$

In reality, the effects of dispersion and nonlinearity will act together during the propagation of lightwaves along a fiber. The SSMF assumes that by choosing the step distance h small enough, the dispersive and nonlinear effects can be accounted independently, still providing a good approximate solution.

The basic idea behind the symmetrized SSFM that is used for numerical computer simulations, is illustrated in Fig. 2.5 and mathematically described as

$$A(z + h, T) \approx \exp(\frac{h}{2}\hat{D})\exp(\int_z^{z+h} \hat{N}(z')dz')\exp(\frac{h}{2}\hat{D})A(z, T), \qquad (2.27)$$

that provides approximate solution for Eq. 2.24. The fiber span length L_{span} is divided into small segments of a length h and a lightwave propagation is modeled segment by segment according to the Eq. 2.27. In a single segment, the optical field is first accounted only for the dispersion operator for a distance $h/2$. In the middle of the segment at $z+h/2$, the optical field is accounted only for the nonlinear term over the whole segment length h. The remaining distance $h/2$ is accounted again with the dispersion operator only and the result $A(z + h, T)$ is obtained that is also the input for the next segment calculation. It must be noted, that if the step distance h is small enough, the middle exponential in Eq. 2.27 that accounts for the nonlinear interaction can be approximated by $\exp(h\hat{N})$ [75]. Under normal conditions, the chosen step distance should be much smaller than the fiber span nonlinear length or the dispersion length.
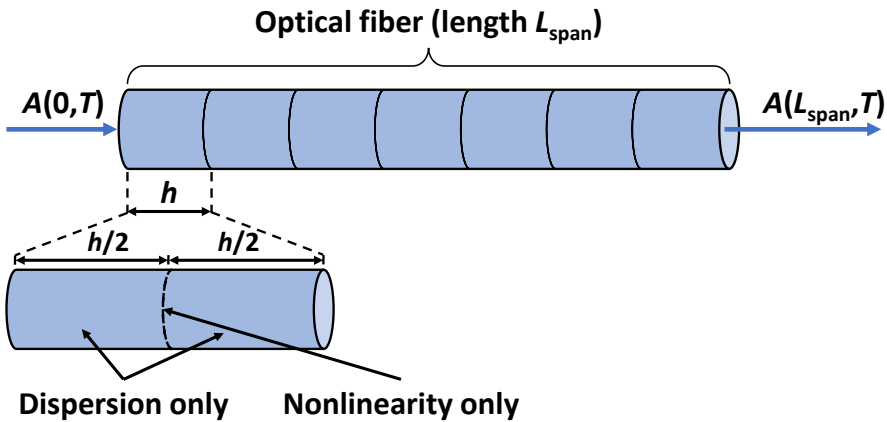

Figure 2.5 Illustration of the symmetrized split-step Fourier method (SSFM) that is used for numerical simulations of an optical field propagation in an optical fiber of length L_{span} with the SSFM step distance h.

2.3.   Optical Amplification

The optical fiber is a lossy medium where the optical field attenuation occurs during the propagation of lightwaves. In order to propagate lightwaves over long distances, an optical amplification should be used, while an optical receiver in the receiving end requires a minimum signal power for a signal detection. However, optical amplifiers add the amplified spontaneous emission (ASE) noise during an amplification process, therefore deteriorating the optical signal-to-noise ratio (OSNR) and thereby the signal-to-noise ratio (SNR) i.e. the quality of a transmitted signal.

During the evolution of fiber-optic communication systems, optical amplifiers were not used before the mid-90's. In fact, before the mid-90's, optoelectronic repeaters were used to manage a fiber attenuation by a periodic detection and regeneration of the transmitted signals. In fact, the repeaters were not practical for WDM systems at all, since every wavelength channel needs one receiver-transmitter pair. The optical amplifiers such as the erbium-doped fiber amplifiers (EDFAs) after their introduction in the second half of the 80's [107, 10, 11], led to a significant breakthrough in the adoption of WDM transmission systems. There are also other types of optical amplifiers commercially available, that are capable to operate in the C-band (1530–1565 nm), e.g. Raman amplifiers [98], semiconductor optical amplifiers (SOAs) [108] and fiber-optical parametric amplifiers (FOPAs) [109]. In this section a brief overview of a conventional EDFA and a distributed Raman amplification is presented. More detailed description of FOPAs and especially PSAs are presented in chapter 3 on page 49.

2.3.1.   Lumped amplification

The most conventional and commercially widespread optical amplifier for a lumped amplification is the EDFA (erbium-doped fiber amplifier). It is a phase-insensitive amplifier with the gain bandwidth about 40 nm (5.3 THz) and is mainly used in the C-band (1530–1565 nm) [107, 10, 11]. Also the L-band (1570-1610 nm) [110] and S-band (1490-1520 nm) [111] operation has been demonstrated. An addition of the ASE noise and thereby the amplifier noise figure (NF) of an EDFA is dependent on the pumping wavelength and the used pumping scheme. The pumping can be applied at 980 nm and 1480 nm, while the 980 nm pumping results in a better noise performance [112]. The pumping schemes are a unidirectional (forward or backward) or a bidirectional pumping scheme. A NF as low as 3.1 dB has been demonstrated [113], while the quantum-limited (theoretical) NF of EDFA is 3 dB [57], but an actual NF in commercial EDFAs can be as high as 4-8 dB.

The power evolution inside a multi-span lumped amplified fiber-optic link and the ASE noise accumulation by in-line optical amplifiers are shown in Fig. 2.6. After a signal has attenuated in a fiber (usually a SSMF), the signal power is

amplified up by a lumped amplifier with a gain G at the end of each span. The ASE noise is added to the transmitted signal in every amplification stage with a noise figure NF, but also the accumulated noise that was added to the signal from previous amplification stages, is also amplified. The ASE noise power spectral density in an amplification stage is defined as [5]

$$S_{ASE}(\nu) = \eta_{\text{sp}} h \nu_0 (G - 1), \tag{2.28}$$

where η_{sp} is the spontaneous emission factor, h is the Planck constant, ν_0 is the light frequency and G is the amplifier gain. A lumped amplifier NF is defined as [5]

$$\text{NF} = \frac{\text{SNR}_{\text{in}}}{\text{SNR}_{\text{out}}} \approx 2\eta_{\text{sp}}, \tag{2.29}$$

where SNR_{in} and SNR_{out} are the electrical SNRs at an amplifier input and output port respectively. The electrical SNR is the ratio of the electrical signal power to the electrical noise power, that are measured by using an ideal photodetector, assuming that an input signal is only degraded by the shot noise (the shot noise limited operation) [114, 115]. It is also important to note that the link NF definition is sometimes used. The link NF is defined similarly to Eq. 2.29, by using $\text{SNR}_{\text{link,in}}$ and $\text{SNR}_{\text{link,out}}$ as the electrical SNRs at the link input and output respectively.
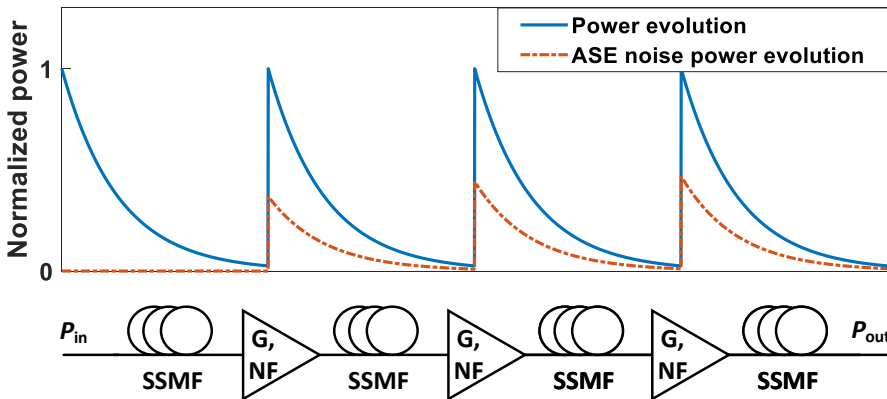

Figure 2.6 Illustration of the ASE noise addition by lumped in-line optical amplifiers with gain G and noise figure NF during a signal propagation in a multi-span fiber-optic link. P_{in} and P_{out} denote the link input and output power respectively.

The ASE noise is originating from spontaneously emitted photons due to the population inversion. Photons are emitted with a random phase, wavelength (inside an EDFA bandwidth) and state-of-polarization. Therefore the ASE noise addition is typically modeled as the uncorrelated additive white Gaussian noise (AWGN) with zero mean [5] for a fiber-optic transmission link simulation model.

2.3.2. Distributed Raman amplification

The distributed Raman amplification is briefly introduced in this thesis context, while it is used in Paper E to flatten the span power map profile in a PSA amplified transmission link in order to observe and compare the nonlinearity mitigation performance of lumped and distributed amplified PSA links. The distributed Raman amplification is especially interesting, while it provides in contrast to the lumped amplification, an amplification in a transmission fiber itself. Dependent on the pumping scheme of a unidirectional (forward, backward) or a bidirectional, different span power map configurations can be implemented. In Fig. 2.7 are shown different span power map profiles for a bidirectionally pumped Raman amplifier with the forward and backward pumping ratio being altered.
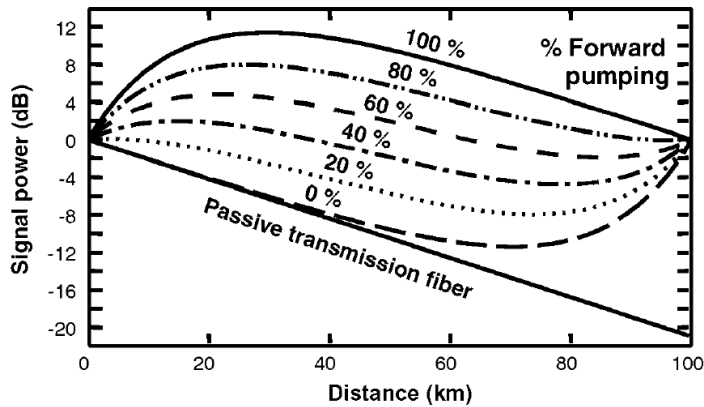

Figure 2.7 Evolution of a signal power in a bidirectionally pumped 100-km-long Raman amplified span as the contribution of forward pumping is varied from 0 to 100%, from reference [116].

The Raman amplification utilizes the stimulated Raman scattering (SRS) phenomenon (introduced in subsection 2.2.3 on page 35) for a signal amplification. The Raman amplification is fiber based, where a power from a pump wave is transferred to a signal wave at a lower frequency through the SRS process. The achievable amplifier gain is dependent on the pump power, the frequency separation of the pump and the signal waves and the polarization of the waves. The gain bandwidth is about 40 THz (320 nm) and the highest peak gain occurs at wavelengths 13 THz below the pump frequency in silica-based fibers [116]. The Raman amplifiers are suitable for WDM systems due to their large bandwidth gain profile.

The ASE noise in the Raman amplification comes from the spontaneous Raman scattering. Compared to the EDFA amplified transmission, the Raman amplification can improve a system NF. Therefore a measure of the equivalent noise figure NF_{eq} [117] is often used for such a comparison. The NF_{eq} represents

a concept of the noise figure that a lumped amplifier that is placed at the end of a transmission span instead of the Raman amplified span, would need to achieve for the same SNR as the Raman amplified span would provide. These two equivalent systems are shown in Fig. 2.8. The NF of the system consisting of a span and a lumped amplifier in Fig. 2.8(b) becomes

$$\mathrm{NF}_{\mathrm{sys}} = \mathrm{NF}_{\mathrm{eq}} \alpha_s L, \tag{2.30}$$

where α_s is the span attenuation coefficient and L is the length of the span. As the noise figures of the equivalent system and the Raman amplified system are assumed to be equal $\mathrm{NF}_{\mathrm{sys}} = \mathrm{NF}_{\mathrm{R}}$, the $\mathrm{NF}_{\mathrm{eq}}$ becomes

$$\mathrm{NF}_{\mathrm{eq}} = \frac{\mathrm{NF}_{\mathrm{R}}}{\alpha_s L}. \tag{2.31}$$

Eq. 2.31 shows that the $\mathrm{NF}_{\mathrm{eq}}$ can be less than one or in a dB-scale, less than a zero. Such an amplifier is not physically realizable, but the $\mathrm{NF}_{\mathrm{eq}}$ shows that the Raman amplification provided performance is superior, that is not achievable by a lumped amplification at the end of a span.
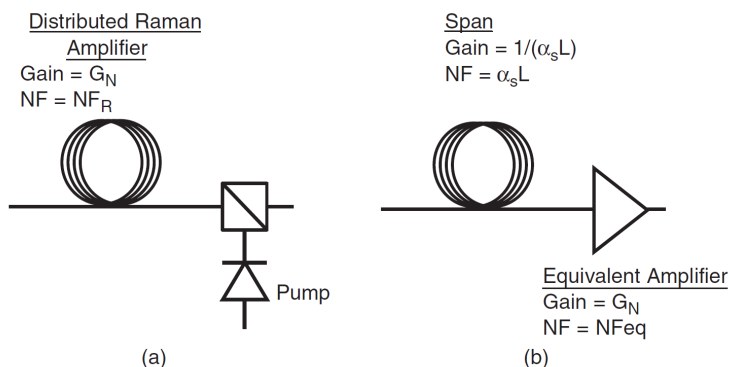

Figure 2.8 Schematic of (a) a distributed Raman amplified system and (b) the equivalent system that consists of a transmission span and a lumped amplifier from reference [116].

2.4. Optical receivers

The final part in a coherent optical information transmission path is the coherent optical receiver. Although the name stands for "optical", this receiver consists of two major parts. The first part is the optical front end, that detects the optical photons and converts them into electrical currents. The second part is completely in the electrical (digital) domain,where the digital signal processing (DSP) is applied to the processed signals for information estimation and decoding.

An extensive overview and description of a conventional digital optical receiver is presented in [118]. In this thesis we present a simplified optical receiver shown in Fig. 2.9. Some of the building blocks such as analog-to-digital conversion, de-skew, orthonormalization are not presented here, since they are not relevant in the context of this thesis. It must be noted, that in Papers A - E, a conventional digital optical receiver is used, although there is a small exception in Paper B, where a straightforward modification in the receiver DSP is included, that performs the coherent superposition of a second span. It should be stated in addition that here only the receiver DSP processing is presented, although the DSP processing can be implemented also at the transmitter side [119], for example the dispersion pre-compensation, digital pre-distortion or pulse shaping.
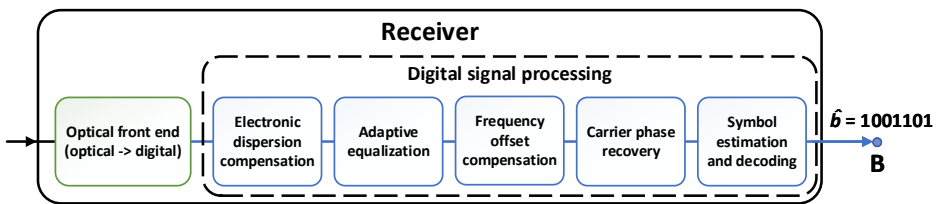

Figure 2.9 Schematic of a simplified coherent optical receiver.

- **Optical front end**

The optical front end shown in Fig. 2.10 performs an optical signal field conversion into a digital signal for the DSP processing. An input optical signal two polarizations are separated by a polarization beam splitter (PBS). The optical signal is mixed with the local oscillator signal using two 90° hybrids for the detection of both polarizations separately. The output of the hybrids corresponds to signal quadratures in the two polarizations. To detect these quadratures, four balanced photodetectors are located at the outputs of the hybrids, that map an optical field to an electric. Thereafter the signal components are amplified before sampled by the analog-to-digital converters (ADCs) and the digital signals of the four quadratures for the DSP processing are obtained. In this stage the receiver local oscillator phase noise adds up to the signal as well as the frequency offset due to the phase and frequency difference between the transmitter laser and the local oscillator.

- **Electronic dispersion compensation**

The electronic dispersion compensation (EDC) stage is present in a conventional fiber-optic link receiver if the dispersion is not completely inline compensated inside an optical link. In PSA links, the dispersion is inline compensated and therefore this part is optional in the PSA receiver setup. Nevertheless this building block performs a static equalization that compensates for the delay between
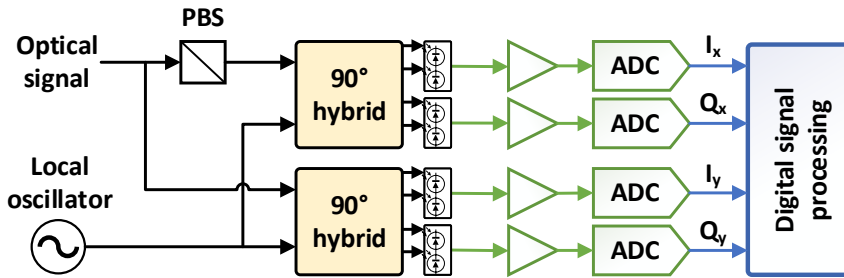
Figure 2.10 Schematic of a conventional optical front end setup for a coherent optical receiver. Different colors of the signal paths stand for: black - optical signal, green - analog electrical signal, blue - digital signal.

different signal frequency components that has been introduced by the dispersion during the propagation of lightwaves in a fiber. The finite-impulse response (FIR) filters [118] or alternatively the infinite-impulse response (IIR) filters [120] can be implemented for the compensation. This building block can be replaced in systems that use the DSP nonlinearity mitigation technique by the digital back-propagation building block [39, 121].

• **Adaptive equalization**

The adaptive equalization building block is also related with the polarization tracking and the compensation of polarization caused effects e.g. the polarization mode dispersion (PMD). In this thesis only one polarization is used for a signal transmission in Papers A - E, but the butterfly filter configuration used in the equalizer shown in Fig. 2.11 is included, since it belongs to a conventional optical receiver standard setup. The butterfly configuration usually consists of four adaptive FIR-filters that filter taps are complex valued [118, 122, 123]. The adaptive filter itself can mitigate intersymbol interference (ISI) and residual dispersion (at least up to some extent) as it approximates towards matched filtering.

An adaptive algorithm should be chosen according to the used modulation format. A very common algorithm for the quadrature phase shift keying (QPSK) modulation format that has constant constellation point values on a unit power circle, is the constant modulus algorithm (CMA). The CMA was first introduced in 1980 [124], but modified later for the four-dimensional signal space i.e. the polarization multiplexed QPSK (PM-QPSK) for optical communications [118, 125]. However, the CMA does not work directly for polarization switched QPSK (PS-QPSK) modulation format, unless the cost function is modified for proper demultiplexing of the polarization states [126].

The higher order quadrature amplitude modulation (QAM) formats do not have one constant symbol amplitude, however the CMA still works with 16-QAM, though the convergence and a steady-state performance is suboptimal [127, 128].
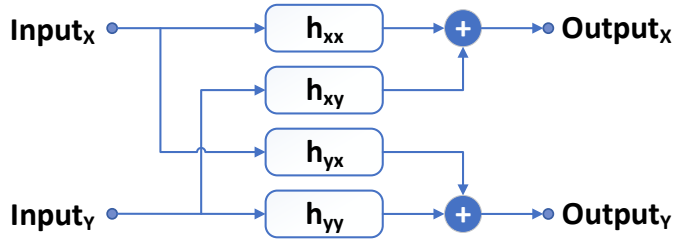
Figure 2.11 Adaptive equalizer filters in butterfly structure, subscripts X and Y denote polarization.

For the higher order QAM, the most common algorithm is the decision-directed least mean square (DD-LMS). The main idea is to minimize adaptive coefficients to the distance closest to a constellation point. Before the equalizer can be switched to a DD-LMS operation, a pre-convergence has to be performed. Usually, the CMA is used for pre-convergence [127]. In contrast to the CMA, the frequency and phase estimation and polarization multiplexing have to be implemented before or within the DD-LMS loop. Other adaptive algorithms for a higher order QAM are the radius-directed equalizer [118, 129, 130] and the independent component analysis [131].

- **Frequency offset compensation**

The frequency offset compensation can be implemented in the time domain or in the frequency domain. In the time domain the fourth-order methods can be utilized that use the four-fold rotational symmetry property of the PM-QAM constellations [132]. The frequency domain methods are matching a center peak of the spectrum around the zero frequency [133].

- **Carrier phase recovery**

The carrier phase estimation can be similarly estimated as a frequency offset by using the fourth-order method i.e. the Viterby-Viterby method [134], that is also used in this thesis. Also methods that will perform an error function calculation over a set of possible test phases are proposed [135]. The problem of cycle slips can also happen in this building block. It is possible to use a differential coding to minimize the effect of cycle slips or use data-aided algorithms by inserting pilots [136].

- **Symbol estimation and decoding**

During this stage, symbols that are corresponding to one sample per symbol are mapped into information bits. Also if coding is used, the decoding is performed. The forward error correction (FEC) can be applied with the soft-decision or hard-decision decoding [137]. Although the latter is more common due to a lower complexity, the soft-decision has also attracted a lot of interest recently [138]. In this thesis Papers A - E, a FEC is not used in the simulations and experiments.

3. PHASE-SENSITIVE AMPLIFIED TRANSMISSION

In this chapter an overview of phase sensitive fiber-optic parametric amplifiers is presented. The phase sensitive amplifiers (PSAs) are a type of fiber-optic parametric amplifiers, that operate in the phase-sensitive mode. PSAs have caught a lot of attention due to their combined ultra-low-noise and nonlinearity mitigation properties [54, 64, 22, 139]. It means that PSA amplified optical links are capable of lowering an amplifier noise limitation dictated by the ASE noise and also tolerate higher launch powers due to the increased nonlinearity tolerance of a transmission system. A conventional EDFA amplifier has the quantum-limited NF of 3 dB, and that holds also true for all the optical phase-insensitive amplifiers (PIAs) [57]. On the other hand, the quantum-limited (theoretical) NF of a PSA is 0 dB [57, 140], however a NF as low as 1.1 dB has been demonstrated in practice [54, 141].

It is practical to talk about an achievable distance improvement when PSAs are used instead of PIAs. In laboratory experiments so far, PSAs are usually compared with PIA amplified links, that also deploy an in-line span-wise dispersion compensation [22, 70, 142, 69]. This also holds true for this thesis Papers A - E. However, the PIA links without the in-line span-wise dispersion compensation (PIA links with the EDC) are more tolerant to nonlinear impairments [83, 84], but the comparison between an in-line dispersion compensated PSA and an EDC PIA link is not feasible, since it requires a complete modification of an experimental setup. Therefore in Paper D, a simulation based comparison of the PSA and PIA 28 GBaud QPSK links with and without the in-line span-wise dispersion compensation schemes are presented to express the first such benchmarking.

The achievable transmission reach improvements are dependent on the used signal symbol rates and amplification scheme. In this thesis, Paper A reports a significant 5.6 times transmission reach improvement achieved experimentally in a 10 GBaud fiber-optic link with a lumped amplification scheme. However, the results from the Raman (distributed amplified) assisted PSA link work in Paper E clearly show that the nonlinearity mitigation capability degrades with higher symbol rates such as in a 28 GBaud QPSK link. Only a transmission reach improvement by a factor of 2.9 between the phase-sensitive and phase-insensitive mode operations for a 28 GBaud QPSK link for the Raman assisted case and an improvement by a factor of 3.8 for the lumped amplified case was measured in Paper E. It can be also confirmed by a later experiment by Vijayan [142],

where similar maximum transmission reach improvement factors for 10 GBaud and 28 GBaud QPSK links were observed. In Papers B, C and D the idea of multi-span dispersion map optimization has been proposed, to further increase the achievable transmission reach extension for higher signal symbol rates, such as a 28 GBaud QPSK case. It should be noted beforehand, that PSA links operating at lower signal symbol rates such as 10 GBaud, do not benefit from multi-span dispersion map optimization. Further details and discussion about dispersion map optimization is presented in chapter 4 on page 61.

3.1. Fiber-optic parametric amplifiers

The fiber-optic parametric amplifiers (FOPAs) realize their amplification through the four-wave mixing process (FWM - nonlinear process, presented in 2.2.3 on page 35) in optical fibers. The gain is achieved from an energy transfer between the interacting waves, thus no energy is stored in a medium. The gain mechanism is therefore called the parametric gain or the parametric amplification. Both $\chi^{(2)}$-nonlinear materials [143, 144] and $\chi^{(3)}$-nonlinear materials [145, 146] are suitable to obtain a parametric amplification. Since a parametric amplifier is a "fiber-optic" (implemented by using an optical fiber), then in an optical fiber (silica glass - SiO_2) only the 3rd-order susceptibility dominates, that causes the FWM process and therefore the parametric gain. In most communication related applications, a continuous wave (CW) for a pump is necessary to use, but the first FOPA demonstrations used pulsed pumps [145, 147, 148].

The FOPAs with CW pumps were not possible to demonstrate until the mid-1990's [149], since the requirements for a FOPA implementation such as fibers with high nonlinear coefficients and low zero-dispersion wavelength variations or high-power pump sources were not available in hardware. The FOPA bandwidth and operating range is determined by the used nonlinear fiber. FOPAs have been demonstrated with a large bandwidth range 155 nm (≈ 20 THz) in a dual-pump configuration [150] and 270 nm (≈ 34 THz) in a single-pump configuration [63]. A gain value as high as 70 dB has been demonstrated [151]. A NF of 3.7 dB for a phase-insensitive FOPA [152] and 1.1 dB for a phase-sensitive FOPA [54, 141] have been demonstrated. Due to the ultra-fast gain mechanism with a femtosecond response time, FOPAs are suitable also for nonlinear signal processing applications [153, 154, 155, 156].

3.1.1. Phase-matching

The phase-matching is directly related to the efficiency of a FWM process. It means that a relative phase between the interacting waves that propagate through a nonlinear medium, should be held constant in the parametric amplification process during the interaction length to maximize the energy transfer.

A set of equations from reference [109] can be derived that define the pump P_p, signal P_s, idler P_i power and the relative phase θ evolutions as:

$$\frac{dP_\mathrm{p}}{dz} = -4\gamma(P_\mathrm{p}^2 P_\mathrm{s} P_\mathrm{i})^{1/2}\sin(\theta), \qquad (3.1)$$

$$\frac{dP_\mathrm{s}}{dz} = \frac{dP_\mathrm{i}}{dz} = -2\gamma(P_\mathrm{p}^2 P_\mathrm{s} P_\mathrm{i})^{1/2}\sin(\theta), \qquad (3.2)$$

$$\frac{d\theta}{dz} = \Delta\beta + \gamma(2P_\mathrm{p} - P_\mathrm{s} - P_\mathrm{i}) + \gamma\left(\sqrt{\frac{P_\mathrm{p}^2 P_\mathrm{s}}{P_\mathrm{i}}} + \sqrt{\frac{P_\mathrm{p}^2 P_\mathrm{i}}{P_\mathrm{s}}} - 4\sqrt{P_\mathrm{s} P_\mathrm{i}}\right)\cos(\theta), \quad (3.3)$$

where γ is the nonlinear coefficient and $\Delta\beta$ is the propagation constant mismatch defined as

$$\Delta\beta = 2\beta_\mathrm{p} - \beta_\mathrm{s} - \beta_\mathrm{i}, \qquad (3.4)$$

where β_p, β_s and β_i are the propagation constants of pump, signal and idler waves respectively and the relative phase

$$\theta = 2\phi_\mathrm{p} - \phi_\mathrm{s} - \phi_\mathrm{i}, \qquad (3.5)$$

where $\phi_\mathrm{p}, \phi_\mathrm{s}$ and ϕ_i are the phases of pump, signal and idler waves. In order to maximize the FWM efficiency, the relative phase should satisfy $\theta = \pi/2$ as it is seen from equations 3.1 and 3.2. In that case the process is phase-matched (maximal energy transfer when $\sin(\pi/2)$). It is also important to note that the relative phase in equations 3.1 and 3.2 determines the direction of energy transfer i.e. from pump waves to signal and idler waves or vice versa.

If the phase-matching condition is satisfied ($\theta = \pi/2$), the last term in equation 3.3 becomes zero, signal and idler powers are negligible as the pump power is assumed to be much larger and the condition to keep the phase-matched condition satisfied during the interaction length becomes

$$\kappa \equiv \Delta\beta + 2\gamma P_\mathrm{p} = 0, \qquad (3.6)$$

where κ describes the phase-matching. It is clear form the derivation of Eq. 3.6, that for an efficient parametric gain process, the relative phase should be kept constant during the interaction length in a nonlinear fiber. Problems arise as the first term $\Delta\beta$ in equation 3.6 represents the linear phase-shift and the second term $2\gamma P_\mathrm{p}$ represents the nonlinear phase shift that both should cancel each other out in order to keep relative phase constant. The linear phase-shift is induced by the different propagation constant values of the interacting waves. The nonlinear phase-shift is induced by the SPM and XPM nonlinear effects. In order to satisfy equation 3.6, the first term (linear) should be negative. For the single (degenerate)

pump case, assuming that the pump frequency ω_p is close to the fiber zero dispersion frequency ω_0, then Eq. 3.6 can be given as [109]

$$\kappa = \beta_3(\omega_p - \omega_0)(\omega_s - \omega_p)^2 + 2\gamma P_p = 0, \tag{3.7}$$

where β_3 is the third derivative of the propagation constant at ω_0 and ω_s is the signal frequency. There are two implications from Eq. 3.7. First it can be seen that the pump should be in the anomalous dispersion regime to satisfy the phase-matching condition. Secondly it shows that there are only two signal frequencies located symmetrically around the pump frequency, that will satisfy $\kappa = 0$.

3.1.2. Parametric amplification

The parametric signal gain according to [109] by assuming no pump depletion (pump waves are much stronger during the parametric process than signal and idler waves) can be described by

$$G = \{1 + [\frac{\gamma P_p}{g}\sinh(gL_{\text{eff}})]\}^2, \tag{3.8}$$

where the parametric gain coefficient g is defined as

$$g^2 = [(\gamma P_p)^2 - (\frac{\kappa}{2})^2] \tag{3.9}$$

and the effective length L_{eff} is defined in Eq. 2.14. Under the perfect nonlinear phase-matching assumption ($\kappa = 0$ and $\gamma P_p L_{\text{eff}} \gg 1$), Eq. 3.8 simplifies and the exponential gain regime (the signal gain grows exponentially with respect to the pump power) [109] can be described by

$$G \approx \frac{1}{4}\exp(2\gamma P_p L_{\text{eff}}). \tag{3.10}$$

When the signal and pump waves are located at the same wavelength (there is no relative phase-shift due to the dispersion) and $\kappa = -2\gamma P_p$, the signal gain becomes quadratic (signal gain grows quadratically with respect to pump power) and in the case of quadratic gain regime [109]

$$G \approx (\gamma P_p L_{\text{eff}})^2. \tag{3.11}$$

An origin of the fundamental noise source in FOPAs, the parametric ASE, is caused by the amplified quantum noise (AQN), that is generated by the FWM process between the strong pumps and the zero-point fluctuations, that are present at all wavelengths.

52

3.2. Phase-sensitive operation

The basic definition of the phase-sensitive or phase-insensitive FOPA is straightforward, whether the gain is dependent on the phases of the input waves. In the phase-insensitive case, an idler is not present at the input of a FOPA, but is generated at the FOPA output with a phase that satisfies the relative phase ($\theta = \pi/2$). The phase-insensitive FOPA gain is independent of the input signal phase. In contrast, if there is an idler at the correct frequency also present at the input of a FOPA, then the gain of such a FOPA will depend on the input signal phase and the FOPA operates in the phase-sensitive mode, that is called the phase-sensitive amplifier (PSA).

A PSA can be realized in multiple amplification configurations, dependent on the allocated frequency/wavelength setup at the input of a FOPA [157]. Examples of different PSA configurations implemented by using FOPAs is presented in Fig. 3.1. In this thesis, only the two-mode single-pump configuration PSA is used in Fig. 3.1(a). However, other possible configurations can also be implemented for example the two-mode dual-pump PSA configuration in Fig. 3.1(b), the one-mode single-pump (fully degenerate) PSA configuration in Fig. 3.1(c), the one-mode dual-pump PSA configuration in Fig. 3.1(d).
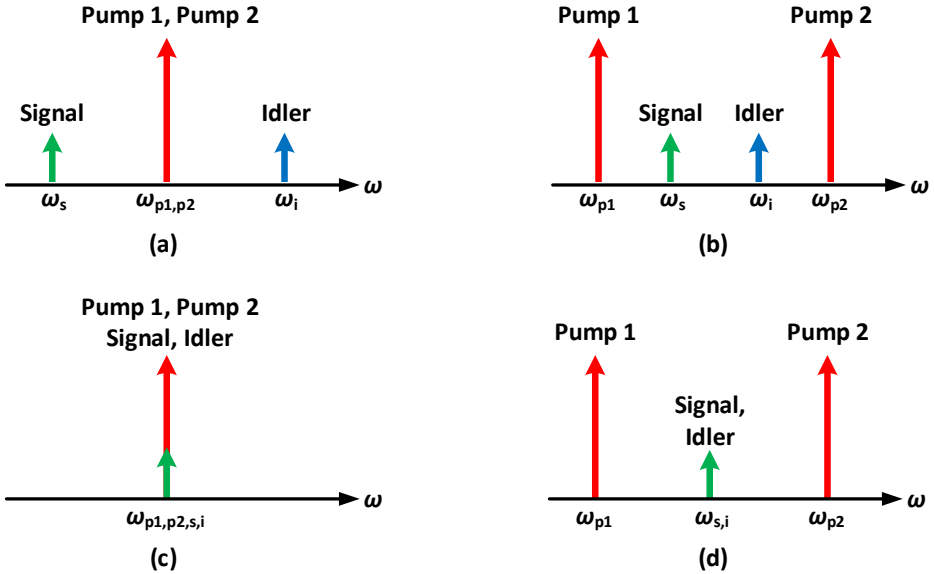

Figure 3.1 Schematic of possible PSA configurations, (a) two-mode single-pump PSA, (b) two-mode dual-pump PSA, (c) one-mode single-pump (fully degenerate) PSA, (d) one-mode dual-pump PSA.

Based on the signal and idler waves, a configuration with the degenerate signal and idler are called the one-mode and a configuration with the non-degenerate signal and idler are called the two-mode PSA. The same applies with the pump

waves. A configuration with the degenerate pump waves is called the single-pump and the non-degenerate configuration is the dual-pump. The one-mode PSAs are only capable of amplifying single-channel signals, while two-mode PSAs are multi-channel compatible [157, 158, 65, 159].

3.3. Two-mode phase sensitive amplifier

Parametric processes can be described by using a transfer matrix. The transfer matrix for a general two-mode parametric process, that describes signal and idler amplification, where the pump waves are assumed to be constant without any pump depletion, can be described by [160, 140]

$$
\begin{bmatrix} B_\mathrm{s} \\ B_\mathrm{i}^* \end{bmatrix} = \begin{bmatrix} \mu & \nu \\ \nu^* & \mu^* \end{bmatrix} \begin{bmatrix} A_\mathrm{s} \\ A_\mathrm{i}^* \end{bmatrix},
\tag{3.12}
$$

where s and i stand for the signal and idler waves of the input A and output B respectively, μ and ν are the complex transfer coefficients and * is the complex conjugate. The transfer matrix in Eq. 3.12 can be written in the form of a transfer function

$$
\begin{cases} B_\mathrm{s} = \mu A_\mathrm{s} + \nu A_\mathrm{i}^* \\ B_\mathrm{i} = \nu A_\mathrm{s}^* + \mu A_\mathrm{i}. \end{cases}
\tag{3.13}
$$

The complex transfer coefficients μ and ν depend on the pump power, phase-matching, nonlinear interaction strength and the state-of-polarization. More details and full expressions of μ and ν are presented in [140], but in this thesis context, it is important to know that μ and ν satisfy the relation [160]

$$
|\mu|^2 - |\nu|^2 = 1.
\tag{3.14}
$$

It has been shown in [161], that by substituting quadrature component variables in Eq. 3.13 and composing two independent modes, then one quadrature component of each mode will be amplified by $G = (|\mu| + |\nu|)^2$ and the other quadrature component is attenuated by $1/G = (|\mu| - |\nu|)^2$. This means that in the case of two independent quadrature components, a two-mode phase-sensitive FOPA can simultaneously amplify both quadratures.

In the following, the three possible operation schemes are presented based on a FOPA transfer matrix in Eq. 3.12. Relevant to this thesis context are the first and the third operation schemes.

- **Phase-insensitive operation with $A_\mathrm{i} = 0$**

In the first configuration, no idler is present at the FOPA input, i.e. $A_\mathrm{i} = 0$ and Eq. 3.12 can be written

$$
\begin{bmatrix} B_\mathrm{s} \\ B_\mathrm{i}^* \end{bmatrix} = \begin{bmatrix} \mu & \nu \\ \nu^* & \mu^* \end{bmatrix} \begin{bmatrix} A_\mathrm{s} \\ 0 \end{bmatrix}
\tag{3.15}
$$

and the corresponding transfer function becomes

$$
\begin{cases}
B_\mathrm{s} = \mu A_\mathrm{s} \\
B_\mathrm{i} = \nu A_\mathrm{s}^*.
\end{cases}
\tag{3.16}
$$

As a result, an idler is generated at the FOPA output, that is a phase-conjugated copy of the signal and the process is phase-insensitive. The signal is amplified by $G_\mathrm{PIA} = |\mu|^2$ and the phase-conjugated copy of the signal by $|\nu|^2 = G_\mathrm{PIA} - 1$. The noise figure of a phase-insensitive amplifier is given by [140]

$$
NF_\mathrm{PIA} = \frac{2G_\mathrm{PIA} - 1}{G_\mathrm{PIA}} = 2 - \frac{1}{G_\mathrm{PIA}},
\tag{3.17}
$$

which in the case of high gain ($G_\mathrm{PIA} \gg 1$) is a factor of 2 (3 dB).

The phase-insensitive FOPA capability to generate a phase-conjugated copy of the signal at its output has made possible to use them as a copier in the copier-PSA scheme, that has been used in Papers A, B and E for the idler generation.

- **Phase-sensitive operation with $A_\mathrm{i} = A_\mathrm{s}$**

In the second configuration, an idler, that is a direct copy of the signal, i.e. $A_\mathrm{i} = A_\mathrm{s}$, is present at the input of a FOPA, therefore Eq. 3.12 can be written

$$
\begin{bmatrix} B_\mathrm{s} \\ B_\mathrm{i}^* \end{bmatrix} = \begin{bmatrix} \mu & \nu \\ \nu^* & \mu^* \end{bmatrix} \begin{bmatrix} A_\mathrm{s} \\ A_\mathrm{s}^* \end{bmatrix},
\tag{3.18}
$$

and the corresponding transfer function becomes

$$
\begin{cases}
B_\mathrm{s} = \mu A_\mathrm{s} + \nu A_\mathrm{s}^* \\
B_\mathrm{i} = \mu A_\mathrm{s} + \nu A_\mathrm{s}^*.
\end{cases}
\tag{3.19}
$$

Eq. 3.21 states clearly, that in such case the output signal and idler are identical. From the substitution of quadrature components in Eq. 3.13 (see derivation in [161], one can see that only one signal quadrature component (either quadrature or in-phase) is amplified by $G_\mathrm{PSA} = (|\mu| + |\nu|)^2 = (\sqrt{G_\mathrm{PIA}} + \sqrt{G_\mathrm{PIA} - 1})^2$, while the other quadrature component is attenuated by $1/G_\mathrm{PSA}$. In the limit of a high gain ($|\mu| \approx |\nu|$), the PSA gain becomes $G_\mathrm{PSA} = 4G_\mathrm{PIA}$.

This kind of PSA operation is known as the signal and idler phase-squeezing and has found use in all-optical phase and amplitude regenerators [162, 163, 164, 165]. This PSA operation regime is irrelevant to the context of this thesis and is only described here to include all possible signal-idler input options for a complete transfer matrix description.

- **Phase-sensitive operation with $A_\mathrm{i} = A_\mathrm{s}^*$**

In the third configuration, an idler, that is a phase-conjugated copy of the signal, i.e. $A_\mathrm{i} = A_\mathrm{s}^*$, is present at the input of a FOPA, therefore Eq. 3.12 can be written

$$\begin{bmatrix} B_\mathrm{s} \\ B_\mathrm{i}^* \end{bmatrix} = \begin{bmatrix} \mu & \nu \\ \nu^* & \mu^* \end{bmatrix} \begin{bmatrix} A_\mathrm{s} \\ A_\mathrm{s} \end{bmatrix}, \tag{3.20}$$

and the corresponding transfer function becomes

$$\begin{cases} B_\mathrm{s} = \mu A_\mathrm{s} + \nu A_\mathrm{s} \\ B_\mathrm{i} = \mu A_\mathrm{s}^* + \nu A_\mathrm{s}^*. \end{cases} \tag{3.21}$$

It turns out that both signal quadrature components are amplified with a gain $G_\mathrm{PSA} = (|\mu| + |\nu|)^2$ (see the derivation in [161]). The NF is given by [140]

$$NF_\mathrm{PSA} = \frac{2G_\mathrm{PIA} - 1}{G_\mathrm{PSA}} = \frac{2G_\mathrm{PIA} - 1}{(\sqrt{G_\mathrm{PIA}} + \sqrt{G_\mathrm{PIA} - 1})^2}. \tag{3.22}$$

In the case of high gain operation ($G_\mathrm{PIA} \gg 1$) the NF of a PSA becomes -3 dB (1/2), if only an input signal is accounted for. The 6 dB (a factor of 4) PSA link NF advantage over PIA amplified links can be observed in the case of the copier-PSA scheme implementation, where the signal power at the link input and output is only considered. The idler is considered as an internal mode of the system, while it is generated after the copier. The idler power is considered in the case of the pure-PSA link, where the PSA link NF becomes 0 dB, that is 3 dB better than the quantum limited PIA NF.

3.4. Nonlinearity mitigation in PSA links

In this section a description of the nonlinearity mitigation mechanism for a two-mode single pump PSA amplified link is presented. In fact, the nonlinearity mitigation of a two-mode PSA and phase-conjugated twin-waves (PCTW) approaches are similar as they both use signal and idler waves that are the phase-conjugated twin-waves [53, 46]. The difference arises due to the fact that a two-mode PSA implementation requires signal and idler waves to be located at different wavelengths. In contrast to the PCTW approach, the signal and idler waves can use all available and possible dimensions, e.g. the signal and idler waves are separated in different polarizations (polarization multiplexed) [46], time-slots (time-division multiplexed) [47], wavelengths (wavelength-division multiplexed) [48, 49, 50] or spatial dimensions (spatial-division multiplexed) [51].

The basic idea of the phase-conjugated twin waves that co-propagate through a nonlinear fiber is illustrated in Fig. 3.2. The signal $E_\mathrm{s} = $ sig. and its phase-conjugate, the idler $E_\mathrm{i} = E_\mathrm{s}^* = $ sig.*, are launched into a transmission span.

In the transmission span, as the waves are co-propagating, they experience similar SPM (nonlinearity) induced nonlinear distortions (phase shifts $\delta\varphi$) resulting in $E_s + \delta E_s$ and $E_i + \delta E_i$. In a coherent superposition stage, the idler is phase-conjugated again and the coherent summation results in $CS_s = (E_s + \delta E_s) + (E_i + \delta E_i)^*$. If the phase distortions on the signal and idler waves are perfectly correlated ($\delta E_i = -\delta E_s^*$), a perfect cancellation is achieved, i.e. $CS_s = E_s + \delta E_s + E_i^* + \delta E_i^* = E_s + \delta E_s + E_s - \delta E_s = 2E_s$. If the phase distortions on the signal and idler waves are less correlated, the phase distortions are squeezed into amplitude distortions (δA) [53].
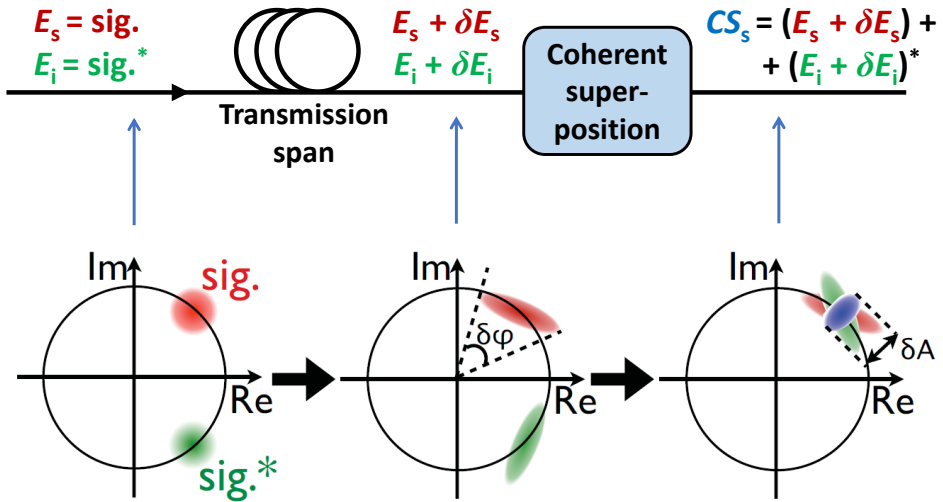
Figure 3.2 Illustration of the basic idea of the nonlinearity mitigation with phase-conjugated twin-waves after a propagation in a nonlinear medium and the result of a coherent superposition of the waves. The constellations are from reference [53], showing an example of the signal and idler constellation points evolution before and after a nonlinear transmission span and after the coherent superposition process.

The twin-wave structure is inherent to the two-mode PSA transmission systems. The PCTW approach coherent superposition is performed after a transmission link digitally in a DSP, but a PSA, if operated at the small-signal regime, performs a coherent summation of the signal and the phase-conjugated idler all-optically [54] at every PSA amplifier. The signal and idler coherent summation is silently integrated into the PSA nature as it is described by the transfer function in Eq. 3.13, where $B_s = \mu A_s + \nu A_i^*$ and $B_i = \nu A_s^* + \mu A_i$. The SPM induced nonlinearity mitigation performance is discussed in more detail in the next chapter 4 on page 61 as it is dependent on the dispersion management.

Another benefit by using PSA twin-wave approach is that the all-optical nonlinearity mitigation is performed span-wise (in every PSA amplification stage),

which also results in the mitigation of nonlinear phase noise (NLPN) (originating from nonlinear signal to amplifier-noise interaction) [139].

3.5. Design and implementation

In this section a brief overview of the main implementation considerations of PSA amplified transmission systems are given for both, numerical simulations and an experimental setup.

3.5.1. Simplified PSA simulation model

A PSA can be numerically modeled as a propagation of signal, idler and pump waves in a highly nonlinear fiber (HNLF), that is similar to a physical PSA implemented by using a FOPA. However, in this thesis context, the used PSA simulation model in numerical simulations is called the "simplified PSA simulation model". A PSA in a high-gain regime with low signal powers and assuming no pump depletion can be modeled according to the previously given matrix description in Eq. 3.20 with added noise terms [22] as

$$
\begin{bmatrix} B_\mathrm{s} \\ B_\mathrm{i}^* \end{bmatrix} = \begin{bmatrix} \mu & \nu \\ \nu^* & \mu^* \end{bmatrix} \begin{bmatrix} A_\mathrm{s} + n_\mathrm{s} \\ A_\mathrm{i}^* + n_\mathrm{i}^* \end{bmatrix},
\tag{3.23}
$$

and the corresponding transfer function becomes

$$
\begin{cases} B_\mathrm{s} = \mu(A_\mathrm{s} + n_\mathrm{s}) + \nu(A_\mathrm{i}^* + n_\mathrm{i}^*) \\ B_\mathrm{i} = \mu(A_\mathrm{i} + n_\mathrm{i}) + \nu(A_\mathrm{s}^* + n_\mathrm{s}^*), \end{cases}
\tag{3.24}
$$

where the noise terms n_s and n_i correspond to uncorrelated additive white Gaussian noises that were added to signal and idler waves at the PSA model input by following the so-called semi-classical model under high-photon-number assumption [166]. It must be noted that the noise terms were accounted only for the long-haul numerical simulations in Papers B, C and D with a noise figure of 1.1 dB.

A simplified PSA simulation model is shown in Fig. 3.3 in the absence of amplifier noise terms i.e. $n_\mathrm{s} = n_\mathrm{i} = 0$. First, the signal and idler waves are amplified and after that the both waves are divided between the main path and the middle path, were the signal and idler waves are phase-conjugated. In order to coherently superposition both waves as given by Eq. 3.24, the phase-conjugated waves constellations are rotated by introducing a necessary phase rotation that maximizes the PSA gain. The constellation alignment block is similar to the phase-locked loop (PLL) in the experimental setup as they both stand for the phase-matching of waves to achieve the maximum PSA gain. In the final PSA simulation model stage a coherent superposition is performed to signal and idler waves.
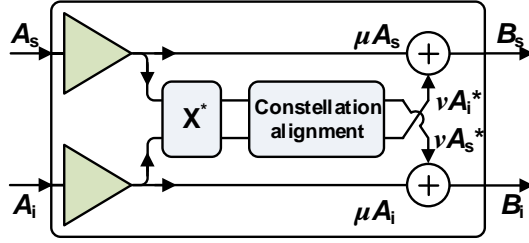
Figure 3.3 Simplified PSA model that is used in numerical simulations of this thesis.

3.5.2. The copier-PSA scheme

It is straightforward to generate a phase-conjugated twin-wave in numerical simulations just by conjugating the original signal for the idler generation. In an experimental setup of a PSA link, a phase-conjugated copy of the signal, the idler, is generated by using the copier, that is a FOPA operating in a phase-insensitive mode. The idler is generated at the phase-insensitive FOPA output as a standard product of the phase-insensitive FOPA amplification process. The copier-PSA scheme in a single-span PSA link is illustrated in Fig. 3.4.
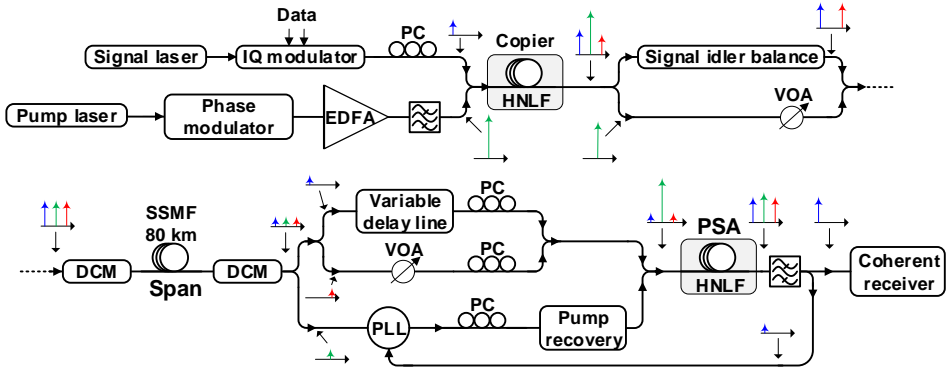
Figure 3.4 Illustration of the copier-PSA scheme implemented in a single-span PSA link. The blue, green and red spectrum components illustrate the evolution of signal, pump and idler power respectively throughout the PSA link.

Figure 3.4 is used in the following to discuss the main implementation considerations and problems of the copier-PSA transmission system. A phase modulator after the pump laser is used to broaden the pump spectrum in order to reduce the SBS [167]. The SBS limits the amount of pump power that can be launched into the HNLF, therefore limiting the achievable gain. The pump is boosted with an EDFA and filtered to remove excess ASE noise. The polarization controller (PC) is used to tune the polarization for maximal gain, since the FWM process is polarization dependent. After that, the signal and pump waves are launched into the copier for the idler generation. After the copier the signal and

idler waves have to be balanced in power. The pump wave has to be attenuated by using a variable optical attenuator (VOA) before launched into an optical fiber transmission span to avoid the SBS effects.

The dispersion compensating modules (DCMs) are necessary to set the dispersion map of a transmission span and compensate fully for the dispersion before the PSA. After the transmission span, waves are separated, while the different delay introduced by dispersion between signal and idler has to be compensated for by using a variable delay line and also the power has to be balanced again before PSA by using a VOA in the idler path. Also the polarization has to be tuned again for all the waves before the PSA.

Before the PSA, the weak pump wave has to be recovered to a high power and high OSNR in a pump recovery stage. The pump OSNR should be at least higher than 65 dB to avoid noise transfer from pump to signal and idler waves [168]. The most crucial component for the pump recovery stage is the optical injection locking that detailed description can be found in [68]. The phase-locked loop (PLL) is used to stabilize the relative phase between the waves in order to maximize and stabilize the PSA gain.

4.   DISPERSION MAP OPTIMIZATION

The group velocity dispersion (GVD) (later on the dispersion) of an optical fiber causes different frequency components of an optical pulse to travel with different speeds, causing pulses to broaden during the propagation in an optical fiber. The dispersion itself is not a concern in modern fiber-optic transmission systems since the advent of coherent fiber-optic systems, that can recover highly dispersed signals. The problem with dispersion arises from a complex interplay between dispersive and nonlinear effects in conjunction with the transmission medium attenuation that results in different communication system performances that are dependent on the applied dispersion compensation, i.e. nonlinear distortions can be more or less severe dependent on the used dispersion map of an optical link.

The dispersion map optimization has been investigated for coherent in-line span-wise dispersion compensated PIA links [169, 170, 171]. However an interest has been lost over a decade ago, since the advent of the electronic dispersion compensation (EDC) has rendered in-line dispersion compensated PIA links obsolete, while EDC links are more tolerant to nonlinear impairments [83, 84]. The EDC links show very little dependence on the used dispersion map, but are mostly considered with 50% pre- (at the transmitter side EDC) and 50% post-compensation (at the receiver side EDC) [172, 173]. A full EDC cannot be implemented for PSA amplified links, since the accumulated dispersion needs to be compensated before every PSA, in order to compensate for a time delay introduced by the dispersion to the signal, idler and pump waves arrival times and to fulfill the phase-matching conditions [22].

This thesis focuses mainly on the aspects of the nonlinearity mitigation performance dependent on the used dispersion map configuration in PSA links. By the time this thesis work started with PSAs in 2015, only a single-span PSA dispersion map optimization was briefly investigated. However, it was shown and known by then, that the single-span dispersion map optimization plays a major role in the PSA link performance [53, 22]. It was evident from [53], that an optimum dispersion map found by a simulation study, outperformed dispersion maps that were fully pre- or post-compensated in an experimental study. A numerically optimized single-span dispersion map was also used for the long-haul transmission experiment in [70]. In Paper A, it is shown that an experimental optimization allowed by tunable dispersion compensators, is extremely important, while the maximum reach extension improvement by using PSAs instead of PIAs in a

10 GBaud link, is achieved by a factor of 5.6 compared to a factor of 3 that was presented previously [70].

The single-span PSA dispersion map optimization was only considered before, since it is not feasible to alter a dispersion compensation setup in every span of a circulating loop experiment. Therefore a dispersion map study, where different dispersion compensation values for each span are allowed (resulting in two-, three-, four-span optimized dispersion maps presented in Papers B, C and D), were not considered beforehand at all. However, it was predicted for phase-conjugated twin-waves (PCTW) approach by the first-order perturbation theory in [46] and investigated numerically for hybrid Raman/phase-sensitive amplified links in [71], that a symmetric power map and an anti-symmetric dispersion map result in the best possible nonlinearity mitigation performance. Therefore an additional experimental study of a 28 GBaud PSA link nonlinearity mitigation in a more power symmetrical (Raman assisted) transmission span in Paper E was carried out.

It should be noted that in this thesis, two different fiber-optic transmission link regimes dependent on a symbol rate, are considered. Firstly, the 10 GBaud regime, where the dispersion length is much larger than the span length ($L_\mathrm{D} \gg L_\mathrm{span}$) and secondly, the 28 GBaud regime, where the dispersion length is smaller than the span length ($L_\mathrm{D} < L_\mathrm{span}$). It can be seen, that the 10 GBaud regime provides better reach improvement and therefore nonlinearity mitigation capability than the 28 GBaud regime (Papers A, D and E), where the nonlinearity mitigation capability has degraded. The two proposed methods, the multi-span dispersion map optimization (Papers B, C and D) and the Raman assisted phase-sensitive amplified link (Paper E) are studied in this thesis mainly for a 28 GBaud regime, where $L_\mathrm{D} < L_\mathrm{span}$.

4.1. Dispersion management

A generic illustration of a dispersion compensation concept after an optical pulse has propagated through a dispersive fiber-optic span is presented in Fig. 4.1(a). During the propagation in a standard single-mode fiber (SSMF), an optical pulse broadens in time domain due to the different travel speeds of a signal frequency components. In the dispersion compensation stage, a linear time delay induced by the dispersion is compensated and the pulse is narrowed to its original pulse-width in the time domain. In the case of a dispersion pre-compensation, the dispersion compensation pre-broadens the pulse, so that the frequency components that travel faster, are delayed more to compensate for the travel speed and the pulse is narrowed to its original pulse-width during propagation in an optical fiber. The dispersion pre-compensation in Fig. 4.1(b) and post-compensation in Fig. 4.1(a) that are performed in dispersion compensation modules (DCMs) or EDC modules are named after the principle, whether the dispersion compensation is applied before or after the transmission in an optical fiber. In Fig. 4.1(a) and (b) full

dispersion compensation is described for pre- and post-compensation, but also the combination of pre- and post-compensation stages can be used as it can be seen in Fig. 4.1(c) and (d).
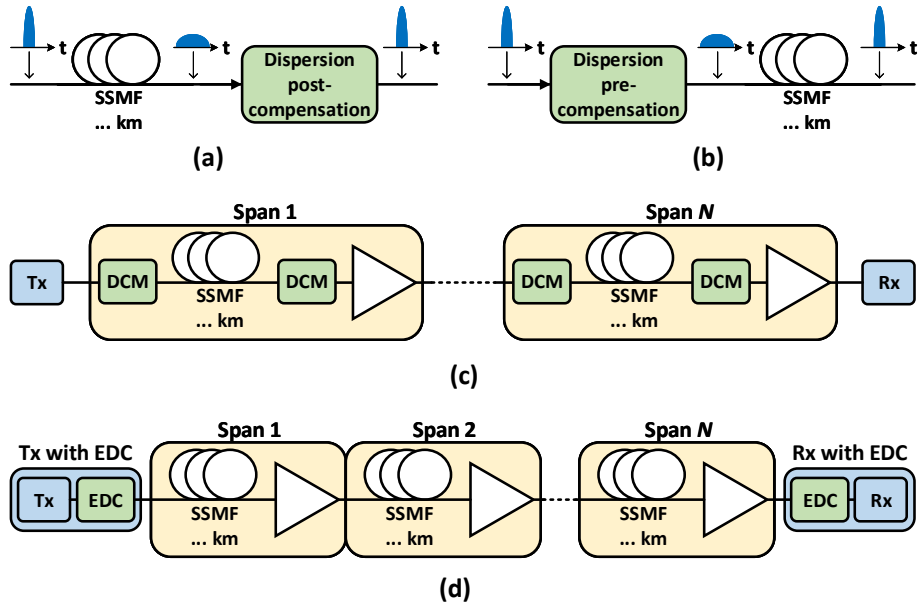

Figure 4.1 Schematic of possible dispersion management schemes, where (a) and (b) illustrate an optical pulse broadening during the propagation in a standard single-mode fiber (SSMF) for the dispersion post- and pre-compensated cases respectively, (c) shows dispersion in-line span-wise compensated link that dispersion compensating modules (DCMs) are positioned correspondingly to a PSA link setup, (d) shows a dispersion unmanaged link with the transmitter (Tx) and receiver (Rx) side electronic dispersion compensation (EDC).

4.1.1. Dispersion management schemes

The dispersion management schemes can be divided into two main categories based on the classification that is better preferred. One option is to divide schemes by the dispersion management location, where a dispersion compensation is applied i.e. in-line span-wise dispersion compensation with DCMs in Fig. 4.1(c) or dispersion unmanaged transmission link with EDC modules that has been applied in the transmitter and/or in the receiver in Fig. 4.1(d). The other option is to divide schemes by the dispersion management domain, i.e. in-line span-wise dispersion compensation in Fig. 4.1(c) is performed in the all-optical domain and the EDC in Fig. 4.1(d) is carried out in the digital domain in the transmitter/receiver side digital signal processing. Hence the categories classification can be named on different basis, the actual schemes remain the same in Fig. 4.1(c) and Fig. 4.1(d). It should be noted that the in-line span-wise dispersion compensation in Fig. 4.1(c)

is in a configuration that is inherent to PSA links. In a PIA link, the second DCM that performs dispersion post-compensation can be removed and the remaining post-compensation can be related with the pre-compensation DCM in the next span.

It is important to note that every DCM that has been inserted into the in-line span-wise dispersion compensation transmission link, introduces an extra loss in reality. In Paper D, where a benchmarking and a comparison has been carried out between dispersion map optimized PSA links and in-line span-wise compensated and EDC compensated PIA links based on numerical simulation results, an in-line DCM extra loss has not been accounted for, since the actual comparison between nonlinearity tolerance of these transmission links was intended. However, in reality, one must always consider that there is a possibility for PSA links, that are in-line span-wise compensated in their nature, that the PSA link with optimized dispersion map in the sense of nonlinear tolerance, could not provide it's best performance. It is attributed to the fact that the equivalent NF of a span is lower for the scenario, where only the dispersion pre-compensation module is present, since the module is at the beginning of a span, where the power is relatively high causing negligible NF degradation compared to the PSA link having both compensators. However, this is beyond the scope of this thesis, but should always be considered in the design of PSA links. It can be also an interesting study subject, since to the best of this thesis author's knowledge, no such study has been presented yet.

4.1.2. Dispersion compensation methods

- **Dispersion compensating fiber**

A dispersion compensating fiber (DCF) [174] is an optical fiber that has been designed to reverse the dispersion effects (the dispersion parameter is designed with the opposite sign), so that a broadened optical pulse propagating in a DCF is narrowed back. A DCF must have a certain length that is determined by the length of the SSMF transmission span fiber and the dispersion parameter that is usually larger, resulting in the shorter length of a DCF than a transmission fiber. The modern DCFs are accurate and also designed with a good dispersion slope matching for certain SSMFs [174].

However, there are also major drawbacks that has to be considered. DCFs will add loss and have a relatively high nonlinear coefficient that will become a problem in the case of high optical launch powers or in a case, when an optical power is high also at the output of a transmission span. For example a DCF according to [175] has an attenuation coefficient 0.231 dB/km and a dispersion parameter -38.0 ps/nm/km. The largest drawback related to the experimental work presented in this thesis is the fact that a DCF cannot be designed to be a tunable dispersion compensator.

- **Fiber Bragg grating**

An in-line dispersion compensation can also be performed by using the fiber-Bragg grating (FBG) based DCMs. A FBG consists of a short piece of fiber that refractive index grating is inscribed by using a laser light [176]. The dispersion compensation can be achieved by the design of a chirped grating [177]. It is also possible to design tunable DCMs based on the channelized FBG technology [178]. Tunable FBG based DCMs have been used for all of the experimental work presented in this thesis Papers A, B and E, because the dispersion pre- and post-compensation ratio tuning was essential for the conducted experiments.

The two major advantages by using FBGs instead of DCFs, is the lower loss and negligible fiber nonlinearity, since the fiber in a FBG is very short. The insertion loss of DCMs used in experiments according to [179] was 3.0 dB. However, the FBG technology suffers from the group delay ripple (GDR) that is induced by non-ideal fabrication process of the grating [180, 181, 182]. The GDR is random fluctuations in the phase response of a FBG, that cause additional unwanted penalties to the bandpass characteristics.

- **Electronic dispersion compensation**

The electronic dispersion compensation (EDC) is a dispersion compensating method performed digitally in a receiver or in a transmitter DSP. The necessary assumption to perform the receiver side EDC is a coherent receiver. That means, if the phase of a signal is detected, then it is a straightforward implementation [118] to reverse the linear distortion caused by the dispersion. The EDC does not suffer any signal degrading effects that are inherent to DCFs or FBGs, as the EDC is performed digitally. However, one must consider the increased energy consumption of a DSP and an extra processing time, while the optical channels are detected separately, the EDC has to be performed to every channel separately. There is an additional major drawback for PSA links, since the EDC can be implemented only at the transmitter and receiver side, so the dispersion cannot be compensated span-wise manner before each PSA in a multi-span PSA link.

4.2. Dispersion map optimization for PSA links

A simplified schematic of a PSA amplified transmission span used for the dispersion map optimization simulations in this thesis is presented in Fig. 4.2. The easiest and so-called "brute forced" way to find an optimal dispersion map, is to simulate numerically or measure (experimentally) through all the possible interesting dispersion map configurations by changing the applied dispersion pre- and post-compensation $D_{\text{pre,n}}$ and $D_{\text{post,n}} = 100\% - D_{\text{pre,n}}$ values by a pre-determined step value i.e. sweeping through dispersion compensation values. A dispersion map configuration that results in the best system performance is

defined as an optimal dispersion map. In this thesis, the brute forced optimization has been mainly used, although the higher number of optimized spans such as three and four-span optimization in Papers C and D cannot be implemented by brute forcing, while it leads to an enormous computational effort. Therefore a more coarse optima were found and more precise dispersion map sweeps were performed only in small regions. More details are provided in Papers C and D.
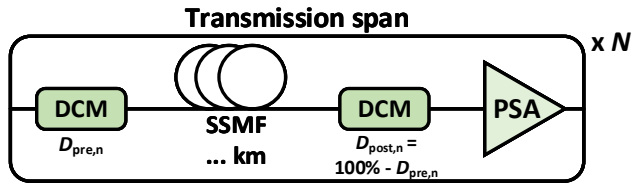

Figure 4.2 Generic schematic of a PSA transmission span model used for numerical simulations in this thesis, where $D_{\mathrm{pre,n}}$ and $D_{\mathrm{post,n}}$ stand for the percentage of applied dispersion pre- and post-compensation respectively from the total accumulated dispersion per span and $n = 1, ..., N$ is the transmission span number.

An example of a single-span 10 GBaud at 12 dBm signal launch power and 28 GBaud at 6 dBm signal launch power PSA link numerical dispersion map optimization from Paper D is shown in Fig. 4.3. The error vector magnitude (EVM) as a function of applied dispersion pre-compensation is used as a metric, to show the PSA link performance dependent on the used dispersion map configuration. The EVM metric expresses an error vector (difference) in the constellation IQ-plane between the received symbols and the ideal symbols [183]. The optimum configurations are 23 % dispersion pre-compensation and 77 % post-compensation for a 10 GBaud PSA link and 19 % dispersion pre-compensation and 81 % post-compensation for a 28 GBaud PSA link.

One can see from Fig. 4.3 that the 10 GBaud case optimum is much sharper than the 28 GBaud case. If 1 dB worse EVM than the optimum would be tolerated for both cases, then an offset of 2% for the 10 GBaud case compared to an offset of 8% for the 28 GBaud case from the optimum point would be allowed. It can be deduced, that the 10 GBaud case, that provides better nonlinearity mitigation capability, is more intolerant to a dispersion map optimum offset. As the single-span optimized case results in a good nonlinearity mitigation performance, the 10 GBaud regime does not benefit further from the multi-span dispersion map optimization as it is shown in Paper D. It can be attributed to the fact that the dispersion length is much larger than the span length ($L_{\mathrm{D}} \gg L_{\mathrm{span}}$), therefore a better combination by using different span dispersion maps does not exist. The opposite is true for the 28 GBaud regime, where the dispersion length is smaller than the span length ($L_{\mathrm{D}} < L_{\mathrm{span}}$) and the nonlinearity mitigation capability can be improved by combining different span dispersion maps by performing the multi-span dispersion map optimization as shown in Papers B, C and D.
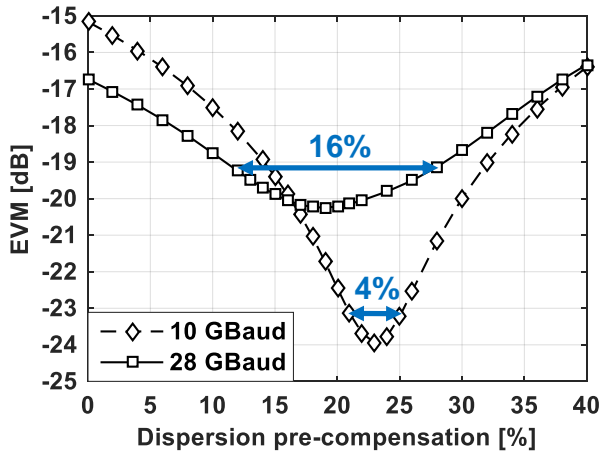
Figure 4.3 Example of a single-span PSA link numerical dispersion map optimization from Paper D.

4.2.1. Nonlinearity mitigation capability

The basic idea behind the nonlinearity mitigation mechanism in a PSA link was already presented in section 3.4 on page 56. However a bit more complicated explanation should be introduced to describe the degradation mechanism of the nonlinearity mitigation capability for higher symbol rate PSA links such as a 28 GBaud regime ($L_D < L_{span}$), where the dispersion in conjunction with the fiber attenuation play the key role for the dispersion map optimization.

A good starting point for this explanation would be to explore further the idea of a span power map symmetry and the dispersion map anti-symmetry condition, that would result in the best possible nonlinearity mitigation performance of the phase-conjugated twin waves according to the first order perturbation theory [46]. Such a symmetric power map condition can be met by designing a theoretical single-span fiber-optic link without accounting any fiber attenuation and performing numerical simulations. The propagating light-field power is constant in such a link, that satisfies power map symmetry condition. The first order perturbation theory for the phase-conjugated twin waves [46] suggest that the dispersion map should be anti-symmetric, which means that the 50% dispersion pre- and post-compensation should be applied. In Fig. 4.4 the results of a numerical dispersion map optimization of such a theoretical link are shown. The simulation study confirms the prediction from theory, that the best performance of such a link is achieved by using 50% dispersion pre- and post-compensation scheme.

The power evolution in Fig. 4.5(a) and the accumulated dispersion in Fig. 4.5(b) as a function of a propagated distance are illustrated for such a theoretical single-span 80 km long PSA link. In Fig. 4.5(b), a blue line shows anti-symmetric
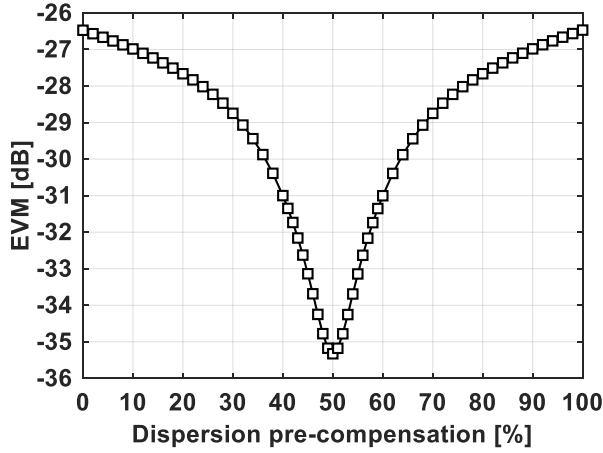
Figure 4.4 Example of the numerical dispersion map optimization of a single-span power symmetric 28 GBaud PSA link, where the optical fiber attenuation is neglected in order to simulate constant (lossless) power evolution of an optical signal.

dispersion map for the signal and idler waves during the propagation in a fiber. During the phase-sensitive amplification process, the idler wave is conjugated and coherently added to the signal wave. Now, if the idler wave is conjugated, it means that the accumulated dispersion will take the opposite sign. It also means that the conjugated idler (Idler*) accumulated dispersion during the propagation in a span can be abstractly represented by a mirrored dashed green line that is the opposite of the signal and idler accumulated dispersion.

By this latter abstract addition, it is possible to see all the signal and conjugate idler dispersion states throughout the propagation in a 80 km span in Fig. 4.5(b). While the symmetric power map and anti-symmetric dispersion map result in the best PSA link performance, it is evident, that the effective nonlinearity mitigation from the coherent superposition of the signal and idler conjugate distortions (δx_{Sig} and $\delta x_{\text{Idl*}}$) can only happen if the signal and idler conjugate distortions were generated by the same accumulated dispersion states with equal optical power. The latter conclusion can be expressed for that particular case shown in Fig. 4.5 as

$$\begin{aligned}
\delta x_{\text{Sig}}(z_1) + \delta x_{\text{Idl*}}(z_2) = \delta x_{\text{Sig}}(DS(z_1), P(z_1)) + \\
\delta x_{\text{Idl*}}(DS(L_{\text{span}} - z_1), P(L_{\text{span}} - z_1)) = 0,
\end{aligned} \tag{4.1}$$

if $DS(z_1) = DS(z_2)$ and $P(z_1) = P(z_2)$, while $z_2 = L_{\text{span}} - z_1$, where $DS(z)$ is the dispersion state at distance z , $P(z)$ is the optical power at distance z and L_{span} is the span length.

The dispersion state in this thesis context means an optical pulse shape broadening state during propagation in an optical fiber, where the signal and idler conjugate signals are having the same shape and chirp caused by the dispersion
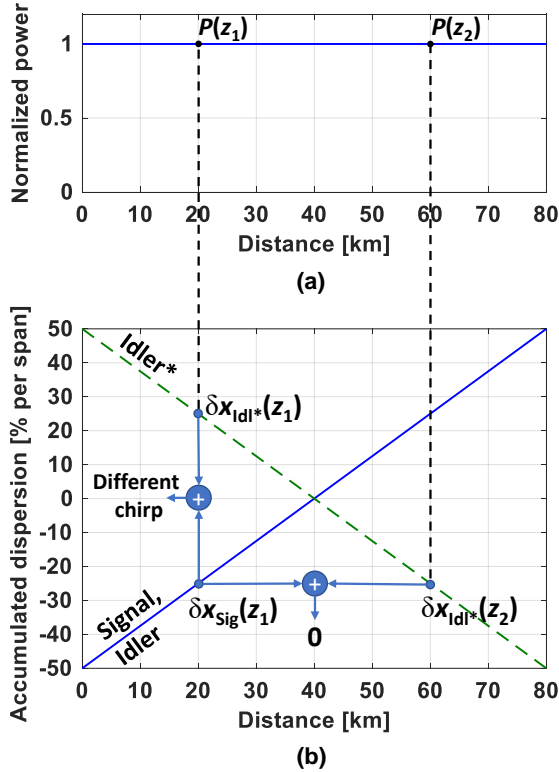
Figure 4.5 Illustration of (a) a constant (lossless) power map, that is symmetric of a theoretical 80 km PSA single-span link and (b) the anti-symmetric dispersion map of such a link, showing the accumulated dispersion evolution of signal, idler and idler conjugated waves during propagation as a function of a distance.

effect. It is also evident that the nonlinear distortions of dispersion states of the signal $\delta x_{\mathrm{Sig}}(DS(z_1), P(z_1))$ and the idler conjugate $\delta x_{\mathrm{Idl*}}(DS(z_1), P(z_1))$ at the same distance (and same optical power), that are differently chirped, do not provide complete nonlinearity mitigation, otherwise the symmetric power map and anti-symmetric dispersion map condition would not be necessary to fulfill.

In order to validate once more this provided explanation, Fig. 4.5 can be represented for some other dispersion map case, where the PSA link performance in Fig. 4.4 has degraded compared to an optimal anti-symmetric dispersion map case. In Fig. 4.6 such an illustration is presented, where the 35% dispersion pre- and 65% post-compensation has been applied. One can see, that when the dispersion map anti-symmetry condition does not hold, then all the nonlinear distortions generated in the last part of the PSA span, remain uncompensated, while there are no such opposite compensating distortions generated in the first part of the PSA link.
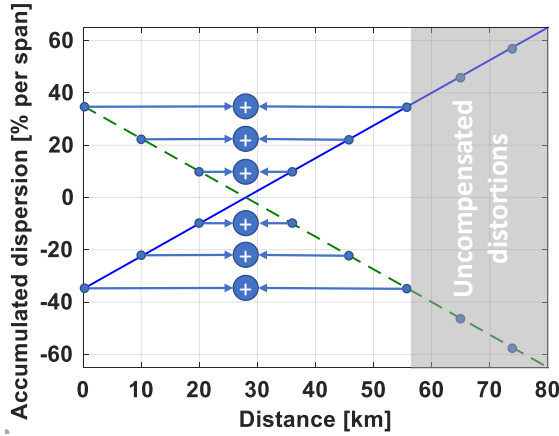
69

Figure 4.6 Illustration showing the not anti-symmetric dispersion map of a power symmetric single-span PSA link and accumulated dispersion evolution therein during optical signal propagation. The gray area shows the region where the generated nonlinear distortions remain uncompensated, therefore degrading the PSA link performance.

One possibility to design a more power symmetric PSA link for an experimental study, is by making use of the distributed Raman amplification. In Paper E a single-span PSA link that consists of three backward Raman amplified spans was built in order to power symmetrize a PSA span. Although the experimental results were not as good as expected, a nearly anti-symmetric optimum dispersion map was found to provide the best performance, that is consistent with the theory. Now, more insight has been gained and the mediocre nonlinearity mitigation performance observed in this experiment could be explained by the power symmetry condition. By building a PSA span out of three 27 km backward Raman pumped spans, actually more power symmetry was introduced in a PSA span, but as a matter of fact all the high powered parts of that span were out of power balance to each other (see measured power map in Paper E Fig. 1 and 2(b)), that cause much unmitigated nonlinear distortions to be generated. Also a slight shift in the dispersion pre-compensation value from 40.5 km (in theory) to 39 km (experimentally measured) can be explained by looking at the measured power map of the experiment.

4.2.2. Multi-span dispersion map optimization

The simulation study in Paper D showed that the multi-span dispersion map optimization is beneficial only to the 28 GBaud regime, where $L_{\mathrm{D}} < L_{\mathrm{span}}$. To better understand the difference between 10 GBaud and 28 GBaud regimes, a formula that expresses an evolvement of a Gaussian pulse envelope during a dispersive propagation can be useful for a visualization. According to [75], a

Gaussian pulse envelope during the optical fiber propagation can be described by

$$U(z,T) = \frac{T_0}{[T_0^2 - i\beta_2 z(1+iC)]^{1/2}} \exp(-\frac{(1+iC)T^2}{2[T_0^2 - i\beta_2 z(1+iC)]}), \quad (4.2)$$

where T_0 is the initial pulse width, β_2 is the GVD parameter and C is the chirp parameter. In Fig. 4.7 an evolvement of a Gaussian pulse peak power during propagation in (a) 10 GBaud and (b) 28 GBaud 80 km long single-span link is presented, where 23% and 19% dispersion pre-compensation has been applied respectively. The measure of a peak power to convey the pulse broadening is used, while the peak power of an optical pulse will generate the strongest nonlinear distortions. The dashed blue curves present the pulse peak power evolvement $|U(z,0)|^2$ by using Eq. 4.2, that does not take into account a fiber loss. The dashed black curves show the power evolution in a fiber optic link according to Eq. 2.3 by taking into account attenuation coefficient $\alpha = 0.2$ dB/km and an input power that is in the case of normalized power equal to one. In order to find the real Gaussian pulse peak power evolution (red curve) that also takes into account the fiber attenuation, Eq. 4.2 can be substituted into Eq. 2.3, resulting in
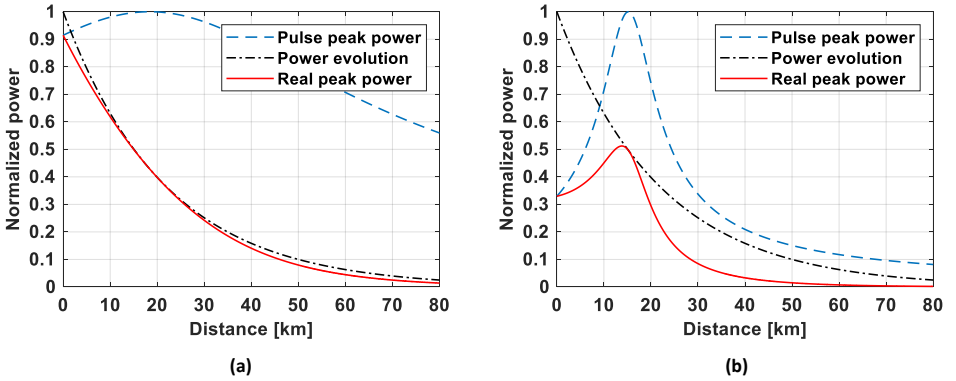
$$P(z) = |U(z,0)|^2 \exp(-\alpha z). \quad (4.3)$$

Figure 4.7 A Gaussian pulse evolution as a function of a distance for (a) 10 GBaud and (b) 28 GBaud 80 km long fiber-optic link, where 23% and 19% dispersion pre-compensation has been applied respectively. The dashed blue curves represent the pulse peak power evolvement without attenuation, the dashed black curves show the power evolution in a fiber optic link and the red curves show the real Gaussian pulse peak power evolution by taking into account the fiber attenuation.

It is evident by comparing the results of Fig. 4.7(a) and (b) that the dispersion plays a significant role for the pulse real peak power evolvement during the propagation for the 28 GBaud case compared to the 10 GBaud case. However, while the dispersion states for the 28 GBaud regime are significantly different

during the propagation throughout the link, it is possible that the PSA nonlinearity mitigation can be enhanced by combining different span dispersion maps in different spans of a PSA link that has been shown in Papers B, C and D.

In Fig. 4.8(a) to (d) are shown Gaussian pulse peak power evolvements in a four-span dispersion map optimized 28 GBaud PSA link with dispersion pre-compensation values 4%, 12%, 22% and 52% according to Paper D. The multi-span dispersion map optimization (to the best of our understanding so far) can enhance PSA nonlinearity mitigation in power unsymmetrical links for higher symbol rate regimes, while it allows to combine the same dispersion states over multiple spans for the best possible power-balancing between signal and idler waves.
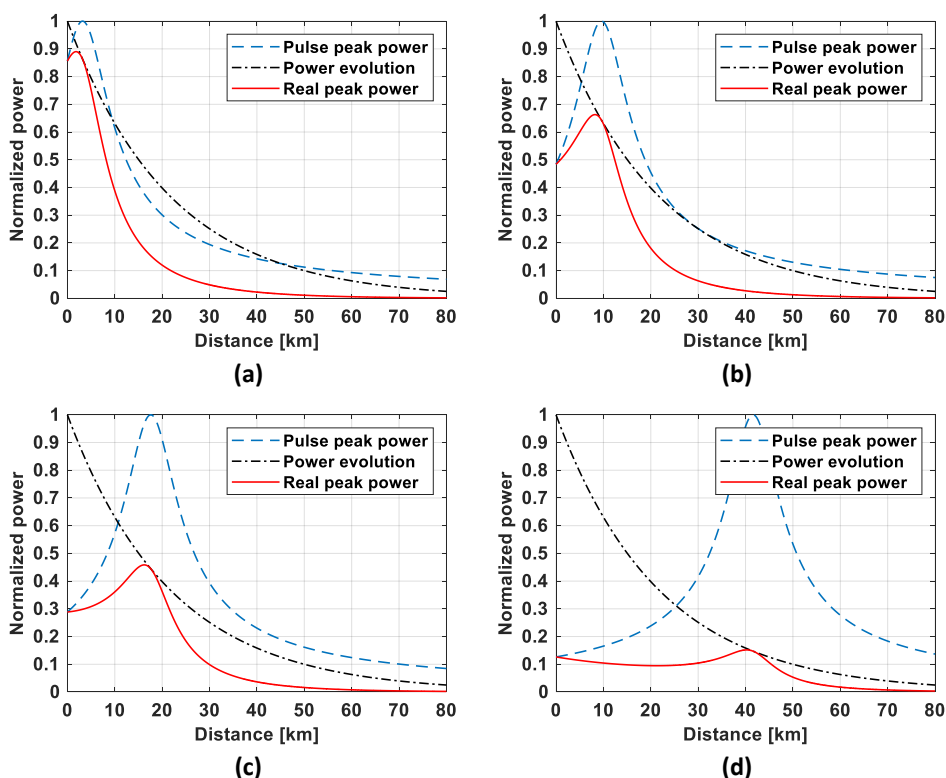

Figure 4.8 A Gaussian pulse evolution as a function of a distance for a 28 GBaud four-span dispersion map optimized fiber-optic PSA link, where (a) 4%, (b) 12%, (c) 22% and (d) 52% dispersion pre-compensation has been applied in the first, second, third and fourth span respectively.

More insight can be derived from Fig. 4.9, where an example has been given that shows 28 GBaud four-span optimized PSA link case, where the distortions generated by the same state of dispersion at certain distance with certain power are summed up in the four span PSA link. The multi-span dispersion map

optimization allows the possibility to combine different configurations from different spans. The summation shown with orange happens between two signal and four idler conjugate generated distortions. The summation with blue shows the combination between single signal and four idler conjugate generated distortions. The multi-span optimization allows to re-design the generation of nonlinear distortions over the whole multi-span PSA link as the best possible power-equalized combination of all the distortions generated by all the possible dispersion states in all available spans. The whole PSA link becomes more similar to a single power symmetric span, where the generated nonlinear distortions of the first part of the span are equal in power to the distortions generated in the second part of the span of all the possible dispersion states (see Fig. 4.5). The allowed number of optimized spans determine the degrees of freedom for optimization where the increasing degrees of freedom allow better optimization and improved nonlinearity mitigation of a multi-span PSA link.
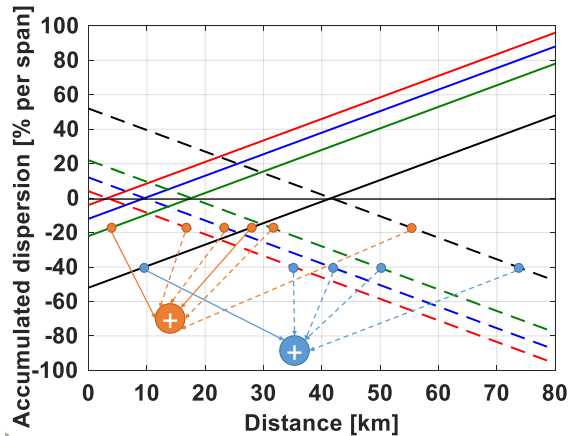

Figure 4.9 Example of the two summations of the same dispersion states generated nonlinear distortions in the four-span optimized PSA link dispersion maps plane. The solid lines represent the signal and the dashed lines for the idler conjugate dispersion states.

It is almost impossible to fulfill the power symmetry condition of an optical fiber span in the real world, but the multi-span dispersion map optimization for a higher symbol rate transmission in a dispersive medium can provide an artificial symmetrization of the generated nonlinear distortions with the help of many different span dispersion maps. However, the multi-span optimization turns out to be computationally devastating to be carried out and also such optimized PSA links are rather not flexible.

Additionally, it would be better in terms of a link noise figure, if the post-dispersion compensation could be completely removed. An alternative solution for PSA links to avoid dispersion induced effects and the degraded nonlinearity mitigation capability, would be to use dispersion-shifted fibers or

to create conditions for very low dispersion fiber-optic transmission. If the dispersion caused broadening would be negligible, then the span power map symmetry condition does not need to hold anymore, while the signal and the idler conjugate will have exactly the same dispersion states at the same distance, meaning that all the signal and idler nonlinear distortions are generated with an equal power. Therefore an ultimate nonlinearity mitigation would be expected, while the mechanism for PSA nonlinearity mitigation presented in Fig. 4.5, where $\delta x_{\mathrm{Sig}}(z_1) + \delta x_{\mathrm{Idl*}}(L_{\mathrm{span}} - z_1) = 0$, would change in the very low GVD condition as

$$\delta x_{\mathrm{Sig}}(z_1) + \delta x_{\mathrm{Idl*}}(z_1) = 0, \tag{4.4}$$

if $D \to 0$.

A numerical study of a PSA link performance for comparing an optical fiber transmission in a SSMF (dispersion parameter $D = 17$ ps/nm/km) with nearly a zero dispersion case ($D = 0.2$ ps/nm/km) is presented in Fig. 4.10. Figure 4.10 shows that the PSA link performance has improved significantly as expected in a low dispersion regime, up to 14.9 dB improvement in terms of the EVM. However, an unexpected result is yet a strong dependence on the chosen dispersion map of a low dispersion regime transmission. The strong dependence can also be attributed to a better nonlinearity mitigation performance, that was also observed at the 10 GBaud transmission regime. It is also interesting to note that the low dispersion regime offers 6.1 dB better EVM performance for a purely pre-compensated dispersion map case over the $D = 17$ ps/nm/km dispersion map optimized case.
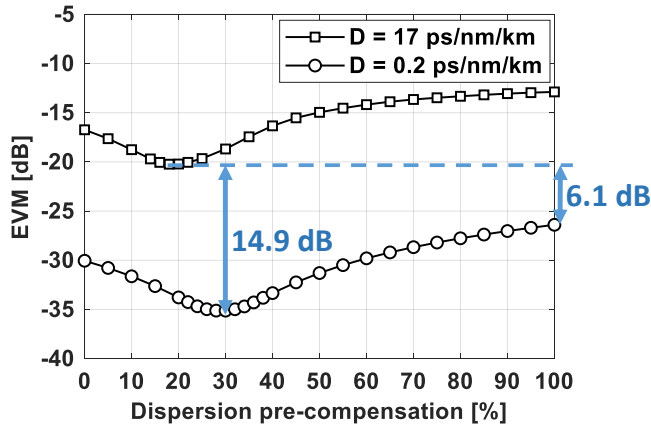

Figure 4.10 Numerical dispersion map optimization of a single-span PSA link at 6 dBm signal launch power, where the two optical transmission fiber dispersion parameters are $D = 17$ ps/nm/km and $D = 0.2$ ps/nm/km.

5. OVERVIEW OF THE PUBLICATIONS

- **Paper A**

S. L. I. Olsson, H. Eliasson, **E. Astra**, M. Karlsson and P. A. Andrekson, "Long-haul optical transmission link using low-noise phase-sensitive amplifiers," *Nature Communications*, no. 9 (2018): 2513.

In this paper a multi-channel compatible and a modulation format independent long-haul 10 GBaud QPSK fiber-optic transmission link that is deploying in-line two-mode PSAs is experimentally demonstrated. The experimental optimization of the single-span dispersion map has been enabled by the use of tunable dispersion compensators. For the first time, a significant reach extension improvement by a factor of 5.6 of a PSA link, compared to the link amplified by conventional EDFAs, is demonstrated. It is possible due to the low amplifier noise and the nonlinearity mitigation capability provided by the in-line PSAs. Such a demonstrated PSA link is able to tolerate the total accumulated nonlinear phase shift of 6.2 rad at optimal launch power.

My contribution: I contributed as a co-author by planning and designing the experiment, assembling the equipment for the experimental setup and conducting measurements.

- **Paper B**

E. Astra, S. L. I. Olsson, H. Eliasson and P. A. Andrekson, "Dispersion management for nonlinearity mitigation in two-span 28 GBaud QPSK phase-sensitive amplifier links," *Optics Express*, 25, no. 12 (2017): 13163–13173.

In this paper an initial simulation study was carried out to investigate whether by allowing different span dispersion maps in different spans of a two-span 28 GBaud QPSK PSA link would improve the PSA nonlinearity mitigation capability. Based on the positive simulation results an experiment was conducted, where an improved mitigation of nonlinearity was also observed in the highly nonlinear transmission regime for the two-span optimized dispersion map case, resulting in the EVM improvement of 1.4 dB and 2 dB higher launch power tolerance compared to a single-span optimized case. However, the dispersion

maps were not optimized experimentally, therefore it is possible that even a larger improvement could be observed. In the design of a two-span PSA link, only one PSA was available to use, therefore the second coherent superposition was performed digitally in DSP, that also enabled to observe constellation diagrams before and after the second coherent superpositioning (nonlinearity mitigation process) of twin-waves. Such a strong two-span dispersion map dependence on the link performance is only inherent to PSA links. Additionally, a long-haul simulation study is presented that shows a 2.1 fold transmission reach improvement in the nonlinear transmission regime and a 1.5 fold transmission reach increase at optimal launch powers of a two-span dispersion map optimized case compared to the single-span optimized case.

My contribution: I am the main author, proposed the idea, wrote the simulation program and carried out all the simulations. E.A, S.O. and H.E. together planned, designed and built the experimental setup and conducted measurements. I carried out the analysis of the results, prepared the figures, and wrote the manuscript.

- **Paper C**

E. Astra, H. Eliasson and P. A. Andrekson, "Four-span dispersion map optimization for improved nonlinearity mitigation in phase-sensitive amplifier links," in Proc. *European Conference on Optical Communication (ECOC)*, Gothenburg, Sweden (2017): paper P2.SC6.14.

In this paper the dispersion map optimization has been numerically investigated further up to four-span optimized maps to explore the nonlinearity mitigation properties of 28 GBaud QPSK PSA links. The optimization has been carried out with a coarse step size of 5%. The highly nonlinear transmission regime after the propagation up to 12 spans shows a significant EVM reduction of 6 dB. Additionally this significant reduction of both phase and amplitude distortions can be also observed from the corresponding constellations. It is also noteworthy that the four-span optimized case after propagation up to four spans results almost the same EVM as single-span optimized case after propagation only one span. The long-haul simulations at optimal launch powers show the four-span optimized case transmission reach improvement of 2.1 times at BER = 10^{-3} compared to a single-span optimized PSA link. Also the four-span optimized case constellation shows more stochastic nature than one-span optimized case, where larger phase distortions can be observed at optimal launch powers at BER = 10^{-3} in long-haul simulations.

My contribution: I proposed the idea for the paper, wrote the simulation program and performed numerical simulations. I did an analysis of the results, prepared the figures, and wrote the manuscript. As a main author, I presented the paper at ECOC in Gothenburg, Sweden in 2017.

• **Paper D**

E. Astra, H. Eliasson, T. Ruuben and P. A. Andrekson, "Improved mitigation of self-phase modulation induced impairments in 28 GBaud phase-sensitive amplified links," *Optics Express*, 27, no. 4 (2019): 4304–4316.

In this paper the dispersion map optimization up to four-span in 28 GBaud QPSK PSA links has been numerically investigated more thoroughly by extensive numerical simulations. The optimization precision has been evaluated by comparing the results of 5% and 1% dispersion optimization sweep step size. We expect an improvement in the results by introducing more precise dispersion maps for the the improved nonlinearity mitigation scenarios with two-, three- and four-span optimized cases. The expectation should be evident from the comparison of 10 GBaud and 28 GBaud single-span PSA links, where a 10 GBaud link yields almost 10 dB better nonlinearity mitigation capability, but it requires a more precise optimization of a dispersion map. However, although two- and three-span cases show a little improvement in the long-haul simulations at optimal launch powers, then no such significant improvement is noted for the four-span optimization case in the long-haul simulations at optimal launch powers, where the same results can be observed for the both optimization precision cases. The comparison of the maximal transmission reaches up to four-span optimized PSA links with the dispersion in-line span-wise managed PIA (6.9 times improvement by using PSAs) and in-line unmanaged EDC PIA (4.3 times improvement by using PSAs) links in the long-haul simulations at BER = 10^{-3} are presented. Additionally, the SPM mitigation capability in the WDM scenario is also briefly investigated, where the signal and idler waves can be separated far away in the wavelength dimension and the effect of third-order dispersion can become relevant.

My contribution: As a main author, I proposed the idea, wrote the simulation program and performed all the numerical simulations. I analyzed the results, prepared the figures, and wrote the paper.

• **Paper E**

H. Eliasson, K. Vijayan, B.Foo, S.L.I. Olsson, **E. Astra**, M. Karlsson and P. A. Andrekson, "Phase-sensitive amplifier link with distributed Raman amplification," *Optics Express*, 26, no. 16 (2018): 19854–19863.

In this paper distributed Raman amplification assisted 28 GBaud QPSK PSA link with more symmetrical span power maps has been experimentally investigated. The PSA span power map design is symmetrized by three backward Raman pumped spans. In long-haul experiments, the Raman assisted PSA link shows a transmission reach improvement by a factor of 2.9, if the Raman assisted PSAs are used instead of PIAs. The lumped amplification configuration

(when Raman pumps turned off) long-haul experiments show a transmission reach improvement by a factor of 3.8, if PSAs are used instead of PIAs. As the experimental results turned out different than what was expected, the effects caused by the dispersion compensating module group delay ripple were evaluated additionally by a numerical simulation study.

My contribution: I contributed by planning, designing and assembling the equipment for the experimental setup and conducting measurements.

6. CONCLUSIONS

In this thesis the nonlinearity (SPM) mitigation aspects dependent on the deployed dispersion map in a single-channel single-polarization two-mode PSA amplified fiber-optic transmission link are investigated. The effect of dispersion on the PSA mitigation capability is different for lower symbol rate and higher symbol rate transmission regimes. The lower symbol rate regime (the dispersion length is larger than the transmission span length) is assumed for a 10 GBaud QPSK PSA link and the higher symbol rate regime (the dispersion length becomes shorter than the transmission span length) is assumed for a 28 GBaud QPSK PSA link.

A significant transmission reach improvement in Paper A by a factor of 5.6 at optimal launch powers, if PSAs are used instead of PIAs, has been demonstrated for a single-span dispersion map optimized 10 GBaud PSA link. The use of tunable dispersion compensators enabled the experimental optimization of the single-span dispersion maps. However, the nonlinearity mitigation capability of a PSA transmission link degrades if higher symbol rates, such as 28 GBaud, are considered. In this thesis, two methods are proposed and investigated that could improve the nonlinearity mitigation capability of a 28 GBaud PSA link. First, the method of multi-span dispersion map optimization, that allows different span dispersion maps to be used in different spans, is presented in Papers B, C and D. Secondly, a method to symmetrize PSA link span power map by the three backward pumped Raman amplifiers is proposed and experimentally investigated in Paper E.

It was demonstrated in Paper B both numerically and experimentally, that by allowing different span dispersion maps in a two-span PSA link instead of single-span optimized dispersion maps, can improve the nonlinearity mitigation performance significantly.   However, in Paper B the dispersion maps were not optimized experimentally, which means that the experimentally measured performance improvement could be even higher than 1.4 dB in terms of the EVM in a highly nonlinear transmission regime.

In Paper C a short-haul transmission numerical study in a highly nonlinear transmission regime shows significant nonlinearity mitigation improvements up to four-span optimized PSA links. The four-span optimized case after a signal propagation up to four-spans in a PSA link yields almost the same low EVM as a single-span optimized PSA link after propagating only one span. It shows the great potential of the proposed method for the SPM mitigation.

In Paper D a four-span dispersion map optimization precision was evaluated by comparing the 5% and 1% optimization precision cases. It turns out that the further optimization with 1% precision does not benefit for long-haul 28 GBaud PSA link simulations in contrast to expectations from a single-span optimized 10 GBaud PSA link, where a single-span dispersion map optimum is narrow and requires precise tuning.

The numerical simulation study in Paper D showed that the optimization precision has not to be very precise, even though the nonlinearity mitigation capability is improved significantly, resulting in the PSA link transmission reach extension of 2.1 times when the four-span optimized dispersion maps are used instead of the single-span optimized maps. It must be also noted that the multi-span optimized dispersion maps cannot be chosen by a chance. However, a complete mathematical understanding has to be yet developed to better understand the choice of optimal dispersion maps for a two-mode PSA link.

In Paper E an experimental evaluation of a method to improve a PSA link nonlinearity mitigation performance by designing more power symmetrical transmission spans is presented. The power symmetrized link is built by using three backward Raman pumps. However, opposite to the expectations, the designed symmetrized power map scenario did not lead to a better nonlinearity (SPM) mitigation performance as predicted by theory. However, the optimum dispersion map configuration with almost 50% pre- and post-compensation was consistent to the theory. In fact, the nonlinearity mitigation capability, that is evaluated by the transmission reach increase factor between PSA and PIA amplified scenarios, dropped from the factor of 3.8 to the factor of 2.9, if Raman assisted symmetrized power map configuration was implemented in a long-haul transmission experiments. It was proposed that the GVD ripple by the same DCMs in a circulating loop setup will probably degrade the performance. Secondly, the noise accumulation and not perfectly flat Raman gain spectrum can play their own role by introducing imperfections. Another explanation can be also provided that takes into account the power symmetry condition. It means that the design of a PSA span power map that consisted of three Raman backward pumped spans, actually became more imbalanced. Due to the imbalance in the high-powered parts of the power map, the nonlinear distortions became more severe.

It is clear from the work conducted in this thesis, that an increased nonlinearity (SPM) mitigation capability of a PSA cannot be realized by using hybrid Raman PSA approach to design more symmetrical span power maps and the only working solution proposed here is the multi-span dispersion map optimization, that is unfortunately not practical in long-haul laboratory experiments in the current situation, where PSAs are not yet compact and straightforward to implement. Secondly, the multi-span dispersion map optimization also requires a good mathematical explanation in order to design the link dispersion map without the need for brute-forced optimization that becomes immense by the increasing number of spans. However, single-span dispersion map optimized PSA links

are still beneficial at lower symbol rate regimes (such as 10 GBaud), where the dispersion length is much more larger than the span length and dispersion affects the nonlinearity (SPM) mitigation performance less.

6.1.   Future outlook

In this thesis a method of multi-span optimization for higher symbol rate PSA links has been proposed for the SPM induced nonlinearity mitigation.   The optimization is carried out up to four-span optimized links numerically by computer simulations.   Although a generic explanation of the optimization mechanism has been provided in this thesis, yet a mathematical understanding of the optimization procedure has not been developed.

Additionally, this thesis is mainly based only on the aspects of the dispersion map optimization. As the main mechanism for multi-span optimization is to find optimal span dispersion maps that can equalize the power of generated nonlinear distortions on signal and idler waves for the same dispersion states, it can be expected, that also by allowing different launch powers in different spans together with the dispersion map optimization, might improve the nonlinearity mitigation performance for the PSA links.

A natural extension of this work would be also to investigate WDM PSA links to study the effects of (multi-span) the dispersion map optimization on the XPM nonlinearity mitigation. It has been proposed in this thesis that a PSA link operating in a low dispersion transmission (for example $D = 0.2$ ps/nm/km) will improve significantly the SPM induced nonlinearity mitigation capability. It could be realized experimentally by using a dispersion shifted fiber in a PSA link. However, the XPM effects and a WDM scenario would be interesting to study in a low dispersion transmission.

An operation in the zero dispersion regime should allow to remove a dispersion post-compensation module that degrades mainly a PSA link OSNR due to an additional loss.   However, to the best of author's knowledge, it has not been studied yet whether the removal of a dispersion post-compensation module (reduced nonlinearity mitigation performance, but a better SNR performance) would degrade the PSA link overall performance.

REFERENCES

[1] G. J. Holzmann and B. Pehrson, *The early history of data networks*. Wiley, 2003.

[2] D. Koenig, "Telegraphs and telegrams in revolutionary France," *The Scientific Monthly*, vol. 59, no. 6, pp. 431–437, 1944.

[3] A. A. Huurdeman, *The worldwide history of telecommunications*. Wiley - IEEE Press, 2003.

[4] A. G. Bell, "U.S. Patent No. 174 465," Tech. Rep., 1876.

[5] G. P. Agrawal, *Fiber-optic communication systems*. Wiley, 2010.

[6] T. H. Maiman, "Stimulated optical radiation in ruby," *Nature*, vol. 187, no. 4736, pp. 493–494, 1960.

[7] K. Kao and G. A. Hockham, "Dielectric-fibre surface waveguides for optical frequencies," *in Proceedings of the Institution of Electrical Engineers*, vol. 113, no. 7, pp. 1151–1158, 1966.

[8] I. Hayashi, M. B. Panish, P. W. Foy, , and S. Sumski, "Junction lasers which operate continuously at room temperature," *Applied Physics Letters*, vol. 17, no. 3, pp. 109–111, 1970.

[9] F. P. Kapron, D. B. Keck, and R. D. Maurer, "Radiation losses in glass optical waveguides," *Applied Physics Letters*, vol. 17, no. 10, pp. 423–425, 1970.

[10] R. J. Mears, L. Reekie, I. M. Jauncey, and D. N. Payne, "Low-noise erbium-doped fibre amplifier operating at 1.54 μm," *Electronics Letters*, vol. 23, no. 19, pp. 1026–1028, 1987.

[11] E. Desurvire, J. R. Simpson, and P. C. Becker, "High-gain erbium-doped traveling-wave fiber amplifier," *Optics Letters*, vol. 12, no. 11, pp. 888–890, 1987.

[12] P. J. Winzer and R.-J. Essiambre, "Advanced modulation formats for high-capacity optical transport networks," *Journal of Lightwave Technology*, vol. 24, no. 12, pp. 4711–4728, 2006.

[13] P. J. Winzer, D. T. Neilson, and A. R. Chraplyvy, "Fiber-optic transmission and networking: the previous 20 and the next 20 years," *Optics Express*, vol. 26, no. 18, pp. 24 190–24 239, 2018.

[14] A. D. Ellis, J. Zhao, and D. Cotter, "Approaching the non-linear Shannon limit," *Journal of Lightwave Technology*, vol. 28, no. 4, pp. 423–433, 2010.

[15] D. J. Richardson, "New optical fibres for high-capacity optical communications," *Philosophical Transactions of the Royal Society A: Mathematical, Physical and Engineering Sciences*, vol. 374, p. 20140441, 2016.

[16] H. Kaushal and G. Kaddoum, "Optical communication in space: challenges and mitigation techniques," *IEEE Communications Surveys and Tutorials*, vol. 19, no. 1, pp. 57–96, 2016.

[17] J. Brodkin, "SpaceX seeks FCC OK for 1 million satellite broadband earth stations," *Ars Technica*, 2/11/2019.

[18] P. J. Winzer, "From first fibers to mode-division multiplexing," *Chinese Optics Letters*, vol. 14, no. 12, p. 120002, 2016.

[19] "The submarine cable map," [Online]. Available: https://www.submarinecablemap.com/, (Last accessed: June 13 2019).

[20] G. Li, N. Bai, N. Zhao, and C. Xia, "Space-division multiplexing: the next frontier in optical communication," *Advances in Optics and Photonics*, vol. 6, no. 4, pp. 413–487, 2014.

[21] R.-J. Essiambre, G. Kramer, P. J. Winzer, G. J. Foschini, and B. Goebel, "Capacity limits of optical fiber networks," *Journal of Lightwave Technology*, vol. 28, no. 4, pp. 662–701, 2010.

[22] S. L. I. Olsson, B. Corcoran, C. Lundström, T. A. Eriksson, M. Karlsson, and P. A. Andrekson, "Phase-sensitive amplified transmission links for improved sensitivity and nonlinearity tolerance," *Journal of Lightwave Technology*, vol. 33, no. 3, pp. 710—721, 2015.

[23] A. Fülöp, C. Krückel, D. Castelló-Lurbe, E. Silvestre, and V. Torres-Company, "Phase-sensitive resonant four-wave mixing in silicon nitride microresonators," *European Conference on Lasers and Electro-Optics - European Quantum Electronics Conference, 2015, paper CDP9*.

[24] R. Kakarla, J. Schröder, and P. A. Andrekson, "Dielectric-fibre surface waveguides for optical frequencies," *Conference on Lasers and Electro-Optics (CLEO), 2019, paper JTh5B.1*.

[25] I. Sackey, T. Richter, M. Nölle, M. Jazayerifar, K. Petermann, J. K. Fischer, and C. Schubert, "Qualitative comparison of Kerr nonlinearity mitigation schemes in a dispersion-managed link for 4×28-GBd 16-QAM signals," *Journal of Lightwave Technology*, vol. 33, no. 23, pp. 4815–4825, 2015.

[26] A. Bakhshali, W. Chan, J. C. Cartledge, M. O'Sullivan, C. Laperle, A. Borowiec, and K. Roberts, "Frequency-domain Volterra-based equalization structures for efficient mitigation of intrachannel Kerr nonlinearities," *Journal of Lightwave Technology*, vol. 34, no. 8, pp. 1770–1777, 2016.

[27] C. Eun and E. J. Powers, "A new Volterra predistorter based on the indirect learning architecture," *IEEE Transactions on Signal Processing*, vol. 45, no. 1, pp. 223–227, 1997.

[28] P. W. Berenguer, M. Nölle, L. Molle, T. Raman, A. Napoli, C. Schubert, and J. K. Fischer, "Nonlinear digital pre-distortion of transmitter components," *Journal of Lightwave Technology*, vol. 34, no. 8, pp. 1739–1745, 2016.

[29] G. Saavedra, G. Liga, and P. Bayvel, "Volterra-assisted optical phase conjugation: A hybrid optical-digital scheme for fiber nonlinearity compensation," *Journal of Lightwave Technology*, vol. 37, no. 10, pp. 2467–2479, 2019.

[30] D. Zibar, M. Piels, R. Jones, and C. G. Schäeffer, "Machine learning techniques in optical communication," *Journal of Lightwave Technology*, vol. 34, no. 6, pp. 1442–1452, 2016.

[31] H. Bülow, "Experimental demonstration of optical signal detection using nonlinear Fourier transform," *Journal of Lightwave Technology*, vol. 33, no. 7, pp. 1433–1439, 2015.

[32] A. Hasegawa and T. Nyu, "Eigenvalue communication," *Journal of Lightwave Technology*, vol. 11, no. 3, pp. 395–399, 1993.

[33] R. A. Fisher, B. R. Suydam, and D. Yevick, "Optical phase conjugation for time-domain undoing of dispersive self-phase-modulation effects," *Optics Letters*, vol. 8, no. 12, pp. 611–613, 1983.

[34] M. A. Z. Al-Khateeb, M. A. Iqbal, M. Tan, A. Ali, M. McCarthy, P. Harper, and A. D. Ellis, "Analysis of the nonlinear Kerr effects in optical transmission systems that deploy optical phase conjugation," *Optics Express*, vol. 26, no. 3, pp. 3145–3160, 2018.

[35] A. D. Ellis, M. E. McCarthy, M. A. Z. Al-Khateeb, and S. Sygletos, "Capacity limits of systems employing multiple optical phase conjugators," *Optics Express*, vol. 23, no. 16, pp. 20 381–20 393, 2015.

[36] M. E. McCarthy, M. A. Z. A. Kahteeb, F. M. Ferreira, and A. D. Ellis, "PMD tolerant nonlinear compensation using in-line phase conjugation," *Optics Express*, vol. 24, no. 4, pp. 3385–3392, 2016.

[37] I. Sackey, F. D. Ros, J. K. Fischer, T. Richter, M. Jazayerifar, C. Peucheret, K. Petermann, and C. Schubert, "Kerr nonlinearity mitigation: Mid-link spectral inversion versus digital backpropagation in 5×28-GBd PDM 16-QAM signal transmission," *Journal of Lightwave Technology*, vol. 33, no. 9, pp. 1821–1827, 2015.

[38] R.-J. Essiambre and P. J. Winzer, "Fibre nonlinearities in electronically pre-distorted transmission," *in European Conference on Optical Communications (ECOC), 2005, paper Tu3.2.2.*

[39] E. Ip and J. M. Kahn, "Compensation of dispersion and nonlinear impairments using digital backpropagation," *Journal of Lightwave Technology*, vol. 26, no. 20, pp. 3416–3425, 2008.

[40] D. Rafique, M. Mussolin, M. Forzati, J. Mårtensson, M. N. Chugtai, and A. D. Ellis, "Compensation of intra-channel nonlinear fibre impairments using simplified digital back-propagation algorithm," *Optics Express*, vol. 19, no. 10, pp. 9453–9460, 2011.

[41] Z. Tao, L. Dou, T. Hoshida, and J. C. Rasmusen, "Complexity reduction of perturbation pre-distortion by term combination," *Optoelectronics Communication/Int. Conf. Photon Switching, 2013, paper WR4-2.*

[42] F. P. Guiomar, S. B. Amado, N. J. Muga, J. D. Reis, A. L. Teixeira, and A. N. Pinto, "Dispersion compensating fibers," *39th European Conference and Exhibition on Optical Communication (ECOC), 2013, paper We.3.C.6.*

[43] S. B. Amado, F. P. Guiomar, N. J. Muga, J. D. Reis, S. M. Rossi, A. Chiuchiarelli, J. R. F. Oliveira, A. L. Teixeira, and A. N. Pinto, "Experimental demonstration of the parallel split-step method in ultra-long-haul 400G transmission," *European Conference on Optical Communication (ECOC), 2015, paper Th.2.6.2.*

[44] N. Alic, E. Myslivets, E. Temprana, B. P. . Kuo, and S. Radic, "Nonlinearity cancellation in fiber optic links based on frequency referenced carriers," *Journal of Lightwave Technology*, vol. 32, no. 15, pp. 2690–2698, 2014.

[45] E. Temprana, E. Myslivets, L. Liu, A. Pejkic, V. Ataie, B. P. . Kuo, D. Esman, A. Wiberg, N. Alic, and S. Radic, "Demonstration of digital phase-sensitive boosting to extend signal reach for long-haul WDM systems using optical phase-conjugated copy," *European Conference on Optical Communication (ECOC), 2015, paper Th.2.6.5.*

[46] X. Liu, A. R. Chraplyvy, P. J. Winzer, R. W. Tkach, and S. Chandrasekhar, "Phase-conjugated twin waves for communication beyond the Kerr nonlinearity limit," *Nature Photonics*, vol. 7, pp. 560–568, 2013.

[47] H. Eliasson, P. Johannisson, M. Karlsson, and P. A. Andrekson, "Mitigation of nonlinearities using conjugate data repetition," *Optics Express*, vol. 23, no. 3, pp. 2392–2402, 2015.

[48] Y. Tian, Y.-K. Huang, S. Zhang, P. R. Prucnal, and T. Wang, "Demonstration of digital phase-sensitive boosting to extend signal reach for long-haul WDM systems using optical phase-conjugated copy," *Optics Express*, vol. 21, no. 4, pp. 5099–5106, 2013.

[49] X. Liu, H. Hu, S. Chandrasekhar, R. M. Jopson, A. H. Gnauck, M. Dinu, C. Xie, and P. J. Winzer, "Generation of 1.024-Tb/s Nyquist-WDM phase-conjugated twin vector waves by a polarization-insensitive optical parametric amplifier for fiber-nonlinearity-tolerant transmission," *Optics Express*, vol. 22, no. 6, pp. 6478–6485, 2014.

[50] H. Eliasson, S. L. Olsson, M. Karlsson, and P. A. Andrekson, "Comparison between coherent superposition in DSP and PSA for mitigation of nonlinearities in a single-span link," *in European Conference and Exhibition on Optical Communication (ECOC), 2014, paper Mo.3.5.2*.

[51] M. Koga, A. Mizutori, T. Ohata, and H. Takara, "Optical diversity transmission with signal and its phase conjugate lights through multi-core fiber," *Optical Fiber Communications Conf., Los Angeles, 2015, paper Th1D.4*.

[52] Y. Yu, W. Wang, P. D. Townsend, and J. Zhao, "Modified phase-conjugate twin wave schemes for spectral efficiency enhancement," *European Conference on Optical Communication (ECOC), 2015, paper We.2.6.5*.

[53] B. Corcoran, S. L. I. Olsson, C. Lundström, M. Karlsson, and P. A. Andrekson, "Mitigation of nonlinear impairments on QPSK data in phase-sensitive amplified links," *in Proc. European Conference on Optical Communications (ECOC), 2013, paper We.3.A.1*.

[54] Z. Tong, C. Lundström, P. A. Andrekson, C. J. McKinstrie, M. Karlsson, D. J. Blessing, E. Tipsuwannakul, B. J. Puttnam, H. Toda, and L. Grüner-Nielsen, "Towards ultrasensitive optical links enabled by low-noise phase-sensitive amplifiers," *Nature Photonics*, vol. 5, no. 7, pp. 430–436, 2011.

[55] H. A. Haus and C. H. Townes, "Comments on "Noise in photoelectric mixing"," *Proceedings of the IRE,*, vol. 50, no. 6, pp. 1544–1545, 1962.

[56] B. M. Oliver, "Reply to H. A. Haus and C. H. Townes, 'Comments on "Noise in photoelectric mixing",'" *Proceedings of the IRE*, vol. 50, no. 6, pp. 1545–1546, 1962.

[57] C. M. Caves, "Quantum limits on noise in linear amplifiers," *Physical Review D*, vol. 26, no. 8, pp. 1817–1839, 1982.

[58] H. P. Yuen, "Amplification of quantum states and noiseless photon amplifiers," *Physical Letters A*, vol. 113A, no. 8, pp. 405–407, 1986.

[59] I. Bar-Joseph, A. A. Friesem, R. G. Waarts, and H. H. Yaffe, "Parametric interaction of a modulated wave in a single-mode fiber," *Optics Letters*, vol. 11, no. 8, pp. 534–536, 1986.

[60] R. Tang, P. S. Devgan, V. S. Grigoryan, and P. Kumar, "Inline frequency-nondegenerate phase-sensitive fibre parametric amplifier for fibre-optic communication," *Electronics Letters*, vol. 41, no. 19, pp. 1072–1074, 2005.

[61] R. Tang, J. Lasri, P. S. Devgan, V. Grigoryan, P. Kumar, and M. Vasilyev, "Gain characteristics of a frequency nondegenerate phase-sensitive fiber-optic parametric amplifier with phase self-stabilized input," *Optics Express*, vol. 13, no. 26, pp. 10 483–10 493, 2005.

[62] C. J. McKinstrie, M. Karlsson, and Z. Tong, "Field-quadrature and photon-number correlations produced by parametric processes," *Optics Express*, vol. 18, no. 19, pp. 19 792–19 823, 2010.

[63] A. V. M. Jamshidifar and M. E. Marhic, "Continuous-wave one-pump fiber optical parametric amplifier with 270 nm gain bandwidth," *In European Conference and Exhibition on Optical Communication (ECOC), 2009, paper 1.1.4.*

[64] Z. Tong, C. Lundström, P. A. Andrekson, M. Karlsson, and A. Bogris, "Ultralow noise, broadband phase-sensitive optical amplifiers, and their applications," *IEEE Journal of Selected Topics in Quantum Electronics*, vol. 18, pp. 1016–1032, 2012.

[65] Z. Tong, C. Lundström, E. Tipsuwannakul, M. Karlsson, and P. A. Andrekson, "Phase-sensitive amplified DWDM DQPSK signals using free-running lasers with 6-dB link SNR improvement over EDFA-based systems," *in Proc. European Conference and Exhibition on Optical Communication (ECOC), 2010, paper PDP1.3.*

[66] Z. Tong, C. J. McKinstrie, C. Lundström, M. Karlsson, and P. A. Andrekson, "Noise performance of optical fiber transmission links that use non-degenerate cascaded phase-sensitive amplifiers," *Optics Express*, vol. 18, no. 15, pp. 15 426–15 439, 2010.

[67] S. L. I. Olsson, B. Corcoran, C. Lundström, E. Tipsuwannakul, S. Sygletos, A. Ellis, Z. Tong, M. Karlsson, and P. A. Andrekson, "Optical injection-locking-based pump recovery for phase-sensitively amplified links," *in Optical Fiber Communication Conference (OFC), 2012, paper OW3C.3.*

[68] S. L. I. Olsson, B. Corcoran, C. Lundström, E. Tipsuwannakul, S. Sygletos, A. Ellis, Z. Tong, M. Karlsson, and P. A. Andrekson, "Injection locking-based pump recovery for phase-sensitive amplified links," *Optics Express*, vol. 21, no. 12, pp. 14 512–14 529, 2013.

[69] S. L. I. Olsson, B. Corcoran, C. Lundström, M. Sjödin, M. Karlsson, and P. A. Andrekson, "Phase-sensitive amplified optical link operating in the nonlinear transmission regime," *in Proc. European Conference on Optical Communications (ECOC), 2012, paper Th.2.F.1.*

[70] S. L. I. Olsson, C. Lundström, M. Karlsson, and P. A. Andrekson, "Long-haul (3465 km) transmission of a 10 GBd QPSK signal with low noise phase-sensitive in-line amplification," *in Proc. European Conference on Optical Communications (ECOC), 2014, paper PD.2.2.*

[71] H. Eliasson, S. L. I. Olsson, M. Karlsson, and P. A. Andrekson, "Mitigation of nonlinear distortion in hybrid Raman/phase-sensitive amplifier links," *Optics Express*, vol. 24, no. 2, pp. 888–900, 2016.

[72] J. G. Proakis, *Digital Communications*. McGraw-Hill Companies, 2000.

[73] "Engineers break power and distance barriers for fiber optic communication," (Published June 25, 2015 in PHYSORG by University of California - San Diego). [Online]. Available: https: //phys.org/news/2015-06-electrical-power-distance-barriers-fiber.html, (Last accessed: Apr. 13 2019).

[74] "Fiber-optic link around the globe," (Published version of the 11/15/2016). [Online]. Available: https://ipfs.io/ipfs/ QmXoypizjW3WknFiJnKLwHCnL72vedxjQkDDP1mXWo6uco/wiki/ Fiber-Optic_Link_Around_the_Globe.html, (Last accessed: Apr. 13 2019).

[75] G. P. Agrawal, *Nonlinear Fiber Optics, 4th ed.* Academic Press, 2007.

[76] C. Cox and R. Helkey, "Techniques and performance of intensity-modulation direct-detection analog optical links," *IEEE TRANSACTIONS ON MICROWAVE THEORY AND TECHNIQUES*, vol. 45, no. 8, pp. 1375–1383, 1997.

[77] A. M. Joshi, S. Datta, and A. Crawford, "NEXT-GEN COMMUNICATIONS FIBER: Multilevel modulation formats push capacities beyond 100 Gbit/s," *Laser Focus World*, vol. 48, no. 2, pp. 58–63, 2012.

[78] A. Demir, A. Mehrotra, and J. Roychowdhury, "Phase noise in oscillators: a unifying theory and numerical methods for characterization," *IEEE Transactions on Circuits and Systems I: Fundamental Theory and Applications*, vol. 47, no. 5, pp. 655–674, 2000.

[79] K. Petermann, *Laser Diode Modulation and Noise*. Springer Netherlands, 1988.

[80] F. Munier, E. Alpman, T. Eriksson, A. Svensson, and H. Zirath, "Estimation of phase noise for QPSK modulation over AWGN channels," in *in Proc. GigaHertz 2003 Symposium*, 2003.

[81] T. Miya, Y. Terunuma, T. Hosaka, and T. Miyashita, "Ultimate low-loss single-mode fibre at 1.55 μm," *Electronics Letters*, vol. 15, no. 4, pp. 106–108, 1979.

[82] "Corning SMF-28e optical fiber product information," [Online]. Available: http://www.tlc.unipr.it/cucinotta/cfa/datasheet_SMF28e.pdf, (Last accessed: Apr. 13 2019).

[83] S. J. Savory, G. Gavioli, R. I. Killey, and P. Bayvel, "Electronic compensation of chromatic dispersion using a digital coherent receiver," *Optics Express*, vol. 15, no. 5, pp. 2120–2126, 2007.

[84] V. Curri, P. Poggiolini, A. Carena, and F. Forghieri, "Dispersion compensation and mitigation of nonlinear effects in 111-Gb/s WDM coherent PM-QPSK systems," *IEEE Photonics Technology Letters*, vol. 20, no. 17, pp. 1473–1475, 2008.

[85] C. B. Czegledi, "Modeling and tracking of stochastic polarization drifts in fiber-optic systems," Ph.D. dissertation, Chalmers University of Technology, Gothenburg, Sweden, 2016.

[86] J. Kerr, "XL. A new relation between electricity and light: Dielectrified media birefringent," *The London, Edinburgh, and Dublin Philosophical Magazine and Journal of Science*, vol. 50, no. 332, pp. 337–348, 1875.

[87] J. Kerr, "LIV. A new relation between electricity and light: Dielectrified media birefringent (second paper)," *The London, Edinburgh, and Dublin Philosophical Magazine and Journal of Science*, vol. 50, no. 333, pp. 446–458, 1875.

[88] R. W. Boyd, *Nonlinear Optics*. Elsevier Science, 2008.

[89] G. P. Agrawal, *Nonlinear Fiber Optics, 5th ed.* Elsevier Science, 2013.

[90] A. Hasegawa and F. Tappert, "Transmission of stationary nonlinear optical pulses in dispersive dielectric fibers. I. anomalous dispersion," *Applied Physics Letters*, vol. 23, no. 3, pp. 142–144, 1973.

[91] L. F. Mollenauer, R. H. Stolen, and J. P. Gordon, "Experimental observation of picosecond pulse narrowing and solitons in optical fibers," *Physical Review Letters*, vol. 45, pp. 1095—1098, 1980.

[92] M. D. Reid and D. F. Walls, "Quantum theory of nondegenerate four-wave mixing," *Physical Review A*, vol. 34, no. 6, pp. 4929–4955, 1986.

[93] A. Lorences-Riesgo, "Phase-sensitive parametric signal processing in optical communications," Ph.D. dissertation, Chalmers University of Technology, Gothenburg, Sweden, 2016.

[94] A. R. Chraplyvy, "Limitations on lightwave communications imposed by optical-fiber nonlinearities," *Journal of Lightwave Technology*, vol. 8, no. 10, pp. 1548–1557, 1990.

[95] C. Raman and K. Krishnan, "A new type of secondary radiation," *Nature*, vol. 121, pp. 501–502, 1928.

[96] E. Woodbury and W. Ng, "Ruby laser operation in the near IR," *Proceedings of the IRE*, vol. 50, no. 11, p. 2367, 1962.

[97] R. H. Stolen and E. P. Ippen, "Raman gain in glass optical waveguides," *Applied Physics Letters*, vol. 22, no. 6, pp. 276–278, 1973.

[98] M. N. Islam, "Raman amplifiers for telecommunications," *IEEE Journal of Selected Topics in Quantum Electronics*, vol. 8, pp. 548–559, 2002.

[99] R. Shelby, M. Levenson, and P. Bayer, "Guided acoustic-wave Brillouin scattering," *Physical Review B*, vol. 31, no. 8, pp. 5244–5252, 1985.

[100] R. Chiao, C. Townes, and B. Stoicheff, "Stimulated Brillouin scattering and coherent generation of intense hypersonic waves," *Physical Review Letters*, vol. 12, pp. 592–595, 1964.

[101] C. Lundström, "Phase-sensitive fiber optic parametric amplifiers and their applications in optical communication," Ph.D. dissertation, Chalmers University of Technology, Gothenburg, Sweden, 2012.

[102] J. P. Gordon, "Theory of the soliton self-frequency shift," *Optics Letters*, vol. 11, no. 10, pp. 662–664, 1986.

[103] P. K. A. Wai and C. R. Menyuk, "Polarization mode dispersion, decorrelation and diffusion in optical fibers with randomly varying birefringence," *Journal of Lightwave Technology*, vol. 14, no. 2, pp. 148–157, 1996.

[104] D. Marcuse, C. R. Menyuk, and P. K. A. Wai, "Application of the Manakov-PMD equation to studies of signal propagation in optical fibers with randomly varying birefringence," *Journal of Lightwave Technology*, vol. 15, no. 9, pp. 1735–1746, 1997.

[105] S. V. Manakov, "On the theory of two-dimensional stationary self-focusing of electromagnetic waves," *Journal of Experimental and Theoretical Physics*, vol. 38, no. 2, pp. 248–253, 1974.

[106] T. R. Taha and M. I. Ablowitz, "Analytical and numerical aspects of certain nonlinear evolution equations. II. Numerical, nonlinear Schrödinger equation," *Journal of Computational Physics*, vol. 55, no. 2, pp. 203–230, 1984.

[107] S. B. Poole, D. N. Payne, R. J. Mears, M. E. Fermann, and R. I. Laming, "Fabrication and characterization of low-loss optical fibers containing rare-earth ions," *Journal of Lightwave Technology*, vol. LT-4, no. 7, pp. 870–876, 1986.

[108] M. J. Connelly, *Semiconductor optical amplifiers*.   Kluwer, 2004.

[109] J. Hansryd, P. A. Andrekson, M. Westlund, J. Li, and P.-O. Hedekvist, "Fiber-based optical parametric amplifiers and their applications," *IEEE Journal of Selected Topics in Quantum Electronics*, vol. 8, no. 3, pp. 506–520, 2002.

[110] F. A. Flood, "L-band erbium-doped fiber amplifiers," *in Optical Fiber Communication Conference (OFC), 2000, paper WG1*.

[111] J. B. Rosolem and A. A. Juriollo, "S band EDFA using standard erbium doped fiber, 1450 nm pumping and single stage ASE filtering," *in Optical Fiber Communication Conference (OFC), 2008, paper OTuN3*.

[112] E. Desurvire, *Erbium-doped fiber amplifiers*.   John Wiley & Sons, 1994.

[113] R. I. Laming, M. N. Zervas, and D. N. Payne, "Erbium-doped fiber amplifier with 54 dB gain and 3.1 dB noise figure," *IEEE Photonics Technology Letters*, vol. 4, no. 12, pp. 1345–1347, 1992.

[114] D. M. Baneya, P. Gallion, and R. S. Tucker, "Theory and measurement techniques for the noise figure of optical amplifiers," *Optical Fiber Technology*, vol. 6, no. 2, pp. 122–154, 2000.

[115] H. T. Friis, "Noise figures of radio receivers," *Proceedings of the IRE*, vol. 32, no. 7, pp. 419–422, 1944.

[116] C. Headley and G. P. Agrawal, *Raman Amplification in Fiber Optical Communication Systems*.   Elsevier Academic Press, 2005.

[117] J. Bromage, "Raman amplification for fiber communication systems," *Optical Fiber Communication Conference, Atlanta, GA, 2003, Paper TuC1*.

[118] S. J. Savory, "Digital coherent optical receivers: Algorithms and subsystems," *IEEE Journal of Selected Topics in Quantum Electronics*, vol. 16, no. 5, pp. 1164–1179, 2010.

[119] D. A. Morero, M. A. Castrillón, A. Aguirre, M. R. Hueda, and O. E. Agazzi, "Design trade-offs and challenges in practical coherent optical transceiver implementations," *Journal of Lightwave Technology*, vol. 34, no. 1, pp. 121–136, 2016.

[120] G. Goldfarb and G. Li, "Chromatic dispersion compensation using digital IIR filtering with coherent detection," *IEEE Photonics Technology Letters*, vol. 19, no. 13, pp. 969–971, 2007.

[121] N. V. Irukulapati, H. Wymeersch, P. Johannisson, and E. Agrell, "Stochastic digital backpropagation," *IEEE Transactions on Communications*, vol. 62, no. 11, pp. 3956–3968, 2014.

[122] S. J. Savory, "Digital filters for coherent optical receivers," *Optics Express*, vol. 16, no. 2, pp. 804–817, 2008.

[123] G. Li, "Recent advances in coherent optical communication," *Advances in Optics and Photonics*, vol. 1, no. 2, pp. 279–307, 2009.

[124] D. N. Godard, "Self-recovering equalization and carrier tracking in two-dimensional data communication systems," *IEEE Transactions on Communications*, vol. 28, no. 11, pp. 1867–1875, 1980.

[125] K. Kikuchi, "Polarization-demultiplexing algorithm in the digital coherent receiver," *in IEEE/LEOS Summer Topical Meetings*, p. paper MC2.2, 2008.

[126] P. Johannisson, M. Sjödin, M. Karlsson, H. Wymeersch, E. Agrell, and P. A. Andrekson, "Modified constant modulus algorithm for polarization-switched QPSK," *Optics Express*, vol. 19, no. 8, pp. 7734–7741, 2011.

[127] I. Fatadin, D. Ives, and S. J. Savory, "Blind equalization and carrier phase recovery in a 16-QAM optical coherent system," *Journal of Lightwave Technology*, vol. 27, no. 15, pp. 3042–3049, 2009.

[128] H. Louchet, K. Kuzmin, and A. Richter, "Improved DSP algorithms for coherent 16-QAM transmission," *in Proc. European Conference on Optical Communication (ECOC), 2008, paper Tu.1.E.6.*

[129] P. J. Winzer, A. H. Gnauck, C. R. Doerr, M. Magarini, and L. L. Buhl, "Spectrally efficient long-haul optical networking using 112-Gb/s polarizationmultiplexed 16-QAM," *Journal of Lightwave Technology*, vol. 28, no. 4, pp. 547–556, 2010.

[130] M. J. Ready and R. P. Gooch, "Blind equalization based on radius directed adaptation," *in Proc. International Conference on Acoustics, Speech, and Signal Processing, 1990, paper D11.16.*

[131] P. Johannisson, H. Wymeersch, M. Sjödin, A. S. Tan, E. Agrell, P. A. Andrekson, , and M. Karlsson, "Convergence comparison of the CMA and ICA for blind polarization demultiplexing," *Journal of Optical Communications and Networking*, vol. 3, no. 6, pp. 493–501, 2011.

[132] A. Leven, N. Kaneda, U.-V. Koc, and Y.-K. Chen, "Frequency estimation in intradyne reception," *IEEE Photonics Technology Letters*, vol. 19, no. 6, pp. 366–368, 2007.

[133] M. Selmi, Y. Jaouen, and P. Ciblat, "Accurate digital frequency offset estimator for coherent PolMux QAM transmission systems," *in Proc. European Conference on Optical Communication (ECOC), Vienna, Austria, 2009, p. P3.08.*

[134] A. Viterbi and A. Viterbi, "Nonlinear estimation of PSK-modulated carrier phase with application to burst digital transmission," *IEEE Transactions on Information Theory*, vol. 29, no. 4, pp. 543–551, 1983.

[135] T. Pfau, S. Hoffmann, and R. Noé, "Hardware-efficient coherent digital receiver concept with feedforward carrier recovery for M-QAM constellations," *Journal of Lightwave Technology,*, vol. 27, no. 8, pp. 989–999, 2009.

[136] M. Seimetz, *High-Order Modulation for Optical Fiber Transmission*. Springer, 2009.

[137] B. P. Smith and F. R. Kschischang, "Future prospects for FEC in fiber-optic communications," *IEEE Journal of Selected Topics in Quantum Electronics*, vol. 16, no. 5, pp. 1245–1257, 2010.

[138] L. Schmalen, A. J. de Lind van Wijngaarden, and S. ten Brink, "Forward error correction in optical core and optical access networks," *Bell Labs Technical Journal*, vol. 18, no. 3, pp. 39–66, 2013.

[139] S. L. I. Olsson, M. Karlsson, and P. A. Andrekson, "Nonlinear phase noise mitigation in phase-sensitive amplified transmission systems," *Optics Express*, vol. 23, no. 9, pp. 11 724—11 740, 2015.

[140] M. Vasilyev, "Distributed phase-sensitive amplification," *Optics Express*, vol. 13, no. 19, pp. 7563–7571, 2005.

[141] M. E. Marhic, P. A. Andrekson, P. Petropoulos, S. Radic, C. Peucheret, and M. Jazayerifar, "Fiber optical parametric amplifiers in optical communication systems," *Laser photonics reviews*, vol. 9, no. 1, pp. 50–74, 2015.

[142] K. Vijayan, H. Eliasson, B. Foo, S. L. I. Olsson, M. Karlsson, and P. A. Andrekson, "Optical bandwidth dependency of nonlinearity mitigation in phase-sensitive amplifier links," *in Proc. European Conference on Optical Communications (ECOC), 2018, paper We2.44*.

[143] J. A. Armstrong, N. Bloembergen, J. Ducuing, and P. S. Pershan, "Interactions between light waves in a nonlinear dielectric," *Physical Review*, vol. 127, no. 6, pp. 1918–1939, 1962.

[144] N. M. Kroll, "Parametric amplification in spatially extended media and application to the design of tuneable oscillators at optical frequencies," *Proceedings of the IEEE*, vol. 51, no. 1, pp. 110–114, 1963.

[145] R. H. Stolen, "Phase-matched-stimulated four-photon mixing in silica-fiber waveguides," *IEEE Journal of Quantum Electronics*, vol. 11, no. 3, pp. 100–103, 1975.

[146] R. H. Stolen and J. E. Bjorkholm, "Parametric amplification and frequency conversion in optical fibers," *IEEE Journal of Quantum Electronics*, vol. 18, no. 7, pp. 1062–1072, 1982.

[147] A. D. P. C. Lin, W. A. Reed and H. T. Shang, "Phase matching in the minimum-chromatic-dispersion region of single-mode fibers for stimulated four-photon mixing," *Optics Letters*, vol. 6, no. 10, pp. 493–495, 1981.

[148] K. I. K.Washio and S. Kishida, "Efficient large-frequency-shifted threewave mixing in low dispersion wavelength region in single-mode optical fibre," *Electronics Letters*, vol. 16, no. 17, pp. 658–660, 1980.

[149] M. M. F. Yang and L. Kazovsky, "CW fibre optical parametric amplifier with net gain and wavelength conversion efficiency > 1," *Electronics Letters*, vol. 32, no. 25, pp. 2336–2338, 1996.

[150] J. M. C. Boggio, S. Moro, E. Myslivets, J. R. Windmiller, N. Alic, and S. Radic, "155-nm continuous-wave two-pump parametric amplification," *IEEE Photonics Technology Letters*, vol. 21, no. 10, pp. 612–614, 2009.

[151] P. A. A. T. Torounidis and B.-E. Olsson, "Fiber-optical parametric amplifier with 70-dB gain," *IEEE Photonics Technology Letters*, vol. 18, no. 10, pp. 1194–1196, 2006.

[152] R. T. P. L. Voss and P. Kumar, "Measurement of the photon statistics and the noise figure of a fiber-optic parametric amplifier," *Optics Letters*, vol. 28, no. 7, pp. 549–551, 2003.

[153] P. A. Andrekson, "Picosecond optical sampling using four-wave mixing in fibre," *Electronics Letters*, vol. 27, no. 16, pp. 1440–1441, 1991.

[154] P. A. Andrekson, N. A. Olsson, J. R. Simpson, T. Tanbun-ek, R. A. Logan, and M. Haner, "16 Gbit/s all-optical demultiplexing using four-wave mixing," *Electronics Letters*, vol. 27, no. 11, pp. 992–924, 1991.

[155] K. Inoue, "Optical level equalisation based on gain saturation in fibre optical parametric amplifier," *Electronics Letters*, vol. 36, no. 12, pp. 1016–1017, 2000.

[156] G.-W. Lu and T. Miyazaki, "Optical phase erasure based on FWM in HNLF enabling format conversion from 320-Gb/s RZDQPSK to 160-Gb/s RZDPSK," *Optics Express*, vol. 17, no. 16, pp. 13 346–13 353, 2009.

[157] Z. Tong and S. Radic, "Low-noise optical amplification and signal processing in parametric devices," *Advances in Optics and Photonics*, vol. 5, no. 3, pp. 318–384, 2013.

[158] R. Tang, P. S. Devgan, V. S. Grigoryan, P. Kumar, and M. Vasilyev, "In-line phase-sensitive amplification of multi-channel CW signals based on frequency nondegenerate four-wave-mixing in fiber," *Optics Express*, vol. 16, no. 12, pp. 9046–9053, 2008.

[159] K. Vijayan, B. Foo, H. Eliasson, and P. A. Andrekson, "Cross-phase modulation mitigation in WDM transmission systems using phase-sensitive amplifiers," *in Proc. European Conference on Optical Communications (ECOC), 2018, paper We3H.4*.

[160] C. J. McKinstrie, S. Radic, and M. G. Raymer, "Quantum noise properties of parametric amplifiers driven by two pump waves," *Optics Express*, vol. 12, no. 21, pp. 5037–5066, 2004.

[161] S. L. I. Olsson, "Optical transmission systems based on phase-sensitive amplifiers," Ph.D. dissertation, Chalmers University of Technology, Gothenburg, Sweden, 2015.

[162] K. Croussore and G. Li, "Phase and amplitude regeneration of differential phase-shift keyed signals using phase-sensitive amplification," *IEEE Journal of Selected Topics in Quantum Electronics*, vol. 14, pp. 648–658, 2008.

[163] e. a. R. Slavik, "All-optical phase and amplitude regenerator for next-generation telecommunications systems," *Nature Photonics*, vol. 4, pp. 690–695, 2010.

[164] e. a. R. Slavik, "Field-trial of an all-optical PSK regenerator multicaster in a 40 Gbit/s, 38 channel DWDM transmission experiment," *Journal of Lightwave Technology*, vol. 30, pp. 512–520, 2012.

[165] T. Umeki, M. Asobe, H. Takara, Y. Miyamoto, and H. Takenouchi, "Multi-span transmission using phase and amplitude regeneration in PPLN-based PSA," *Optics Express*, vol. 21, no. 15, pp. 18 170–18 177, 2013.

[166] Z. Tong, A. Bogris, C. Lundström, C. J. McKinstrie, M. Vasilyev, M. Karlsson, and P. A. Andrekson, "Modeling and measurement of the noise figure of a cascaded non-degenerate phase-sensitive parametric amplifier," *Optics Express*, vol. 18, no. 14, pp. 14 820–14 835, 2010.

[167] S. K. Korotky, P. B. Hansen, L. Eskildsen, and J. J. Veselka, "Efficient phase modulation scheme for suppressing stimulated Brillouin scattering," *in International Conference Integrated Optics and Optical Fiber Communications (IOOC), 1995, paper WD2*.

[168] A. Durecu-Legrand, C. Simonneau, D. Bayart, A. Mussot, T. Sylvestre, E. Lantz, and H. Maillotte, "Impact of pump OSNR on noise figure for fiber-optical parametric amplifiers," *IEEE Photonics Technology Letters*, vol. 17, no. 6, pp. 1178–1180, 2005.

[169] J. K. Fischer, C.-A. Bunge, and K. Petermann, "Equivalent single-span model for dispersion-managed fiber-optic transmission systems," *Journal of Lightwave Technology*, vol. 27, no. 16, pp. 3425–3432, 2009.

[170] A. Cartaxo, N. Costa, and D. Fonseca, "Analysis of optimum dispersion maps for DQPSK systems," *in Proc. International Conference on Transparent Optical Networks (ICTON), 2010, paper Mo.D1.1*.

[171] Y. Frignac and P. Ramantanis, "Average optical phase shift as an indicator of the dispersion management optimization in PSK-modulated transmission systems," *IEEE Photonics Technology Letters*, vol. 22, no. 20, pp. 1488–1490, 2010.

[172] A. J. Lowery, "Fiber nonlinearity pre- and post-compensation for long-haul optical links using OFDM," *Optics Express*, vol. 15, no. 20, pp. 12 965–12 970, 2007.

[173] R. Sinha, A. K. Garg, and S. Tyagi, "Dispersion compensation techniques: a comprehensive review," *International Journal of Electronics, Electrical and Computational System*, vol. 6, no. 4, pp. 57–61, 2017.

[174] L. Grüner-Nielsen, M. Wandel, P. Kristensen, C. Jørgensen, L. V. Jørgensen, B. Edvold, B. Pálsdóttir, and D. Jakobsen, "Dispersion compensating fibers," *Journal of Lightwave Technology*, vol. 23, no. 11, pp. 3566–3579, 2005.

[175] "Corning vascade optical fiber product information," [Online]. Available: https://www.corning.com/media/worldwide/coc/documents/Fiber/PI1445_3.17.pdf, (Last accessed: July 25 2019).

[176] K. O. Hill and G. Meltz, "Fiber Bragg grating technology fundamentals and overview," *Journal of Lightwave Technology*, vol. 15, no. 8, pp. 1263–1276, 1997.

[177] K. O. Hill, F. Bilodeau, B. Malo, T. Kitagawa, S. Thériault, D. C. Johnson, J. Albert, and K. Takiguchi, "Chirped in-fiber Bragg gratings for compensation of optical-fiber dispersion," *Optics Letters*, vol. 19, no. 17, pp. 1314–1316, 1994.

[178] X. Liu, S. Chandrasekhar, P. J. Winzer, B. Maheux-L, G. Brochu, and F. Trepanier, "Efficient fiber nonlinearity mitigation in 50-GHz-DWDM transmission of 256-Gb/s PDM-16QAM signals by folded digital-backpropagation and channelized FBG-DCMs," *in Optical Fiber Communication Conference (OFC), 2014, paper Tu3A.8*.

[179] "TeraXion ClearSpectrum DCML dispersion compensation module," [Online]. Available: https://teraxion.blob.core.windows.net/media/1311/teraxion-clearspectrum-dcml-specsheet.pdf, (Last accessed: July 25 2019).

[180] M. Sumetsky, B. J. Eggleton, and C. M. de Sterke, "Theory of group delay ripple generated by chirped fiber gratings," *Optics Express*, vol. 10, no. 7, pp. 332–340, 2002.

[181] E. Tipsuwannakul, J. Li, T. A. Eriksson, L. Egnell, F. Sjöström, J. Pejnefors, P. A. Andrekson, and M. Karlsson, "Influence of fiber-Bragg grating-induced group-delay ripple in high-speed transmission systems," *Journal of Optical Communications and Networking*, vol. 4, no. 6, pp. 514–521, 2012.

[182] F. Ramos and J. Marti, "Influence of non-ideal chirped fibre grating characteristics on dispersion-compensated analogue optical links in presence of fibre-induced SPM," *Electronics Letters*, vol. 39, no. 4, pp. 353–355, 2003.

[183] R. A. Shafik, S. Rahman, and R. Islam, "On the extended relationships among EVM, BER and SNR as performance metrics," *in Proc. 4th International Conference on Electrical and Computer Engineering (ICECE), 2006*.

ACKNOWLEDGEMENTS

First of all I am very grateful to Prof. Peter Avo Andrekson for this once-in-a-lifetime opportunity and great experience to pursue a PhD degree and to collaborate with his fiber-optics team at the photonics laboratory at Chalmers University of Technology. It is a great privilege and an honor to be supervised by you.

During these approximately 250 days in total spent as a visiting PhD student at the photonics laboratory in Göteborg, I like to express my sincere gratitude to all of the members of the fiber-optics team for an inspiring work environment. I especially thank Dr. Samuel Olsson and Dr. Henrik Eliasson for the extensive guidance and mentoring during my PhD studies and all of the work and great ideas put into our common projects. I also want to acknowledge Dr. Benjamin Foo and Kovendhan Vijayan for many fruitful discussions and thank Prof. Magnus Karlsson and Dr. Pontus Johannison for insightful comments and Jeanette Träff for always organizing a convenient accommodation during these visits to the photonics laboratory in Göteborg.

Secondly, I like to thank both of my co-supervisors from Tallinn University of Technology. Prof. Toomas Ruuben (current co-supervisor) who is responsible for that this PhD position was introduced to me and Prof. Tõnu Trump (co-supervisor during first 2.5 years) who has mostly inspired me during my master's degree studies about the idea of having a PhD degree. I will always remember all the most challenging and fun adaptive filtering, communication and signal processing theory courses lectured by Prof. Tõnu Trump during my study years.

I thank my colleagues from Tallinn University of Technology: Dr. Maksim Butsenko, Dr. Sander Ulp, Julia Berdnikova, Hip Kõiv and Allan Tart, with whom we shared everyday PhD studies experience together. Maksim and Sander, without you guys, I have probably never considered the idea to commence PhD studies at all! I also thank Prof. Toomas Rang, the former head of the Thomas Johann Seebeck Department of Electronics, and Laur Lemendik, the head of the Thomas Johann Seebeck Department of Electronics for all the provided support and motivation. I thank Frederick Rang for providing me a computer with the CUDA core graphics processing that could boost the most time consuming SSFM numerical simulation calculations much much faster.

I acknowledge all the financial support from the European Research Council (ERC) (ERC-2011-AdG- 291618 PSOPA), the Estonian Research Council Project

And finally, my special gratitude goes to my family who has been very supportive and patient during these PhD study years: to my parents Aare and Carmen, especially to my dear wife Hanna-Liina for all your love and support during all these university study years, to my little daughter Helena-Eliis who has missed her dad all this time that was spent on writing the thesis and to my newborn son Hans-Evan, I hope that your father's PhD studies will inspire you both and lead you to make your own right choices.

Egon Astra
Tallinn, September 2019

ABSTRACT
Transmission Fiber Nonlinearity Mitigation in Optical Communication Links Using Phase-Sensitive Parametric Amplifiers

In this thesis a numerical and an experimental investigation of the nonlinearity (SPM - self-phase modulation) mitigation of a two-mode single-channel single-polarization phase-sensitive amplifier (PSA) amplified fiber-optic transmission link is demonstrated. PSAs are especially interesting due to their low noise amplification (quantum limited noise figure of 0 dB) and simultaneous nonlinearity mitigation capability. It can be highly beneficial as fiber-optic communication systems are fundamentally limited by the optical amplification noise and the transmission fiber nonlinearity. PSA noise properties have been already thoroughly investigated before, but until 2015, when this thesis work began, not much research were conducted on the nonlinearity mitigation aspects of PSAs. However, it was already evident from previous work that a single-span dispersion map configuration has an effect on the SPM (nonlinearity) mitigation capability.

In this thesis the first significant transmission reach extension (by a factor of 5.6) of a 10 GBaud PSA link is demonstrated, when PSAs are used instead of phase insensitive amplifiers (PIAs). However, if the symbol rate is increased, a different regime (the dispersion length becomes smaller than the span length) occurs, where the nonlinearity mitigation capability of a PSA is reduced. In this thesis, two methods are proposed and investigated experimentally and numerically to improve the nonlinearity (SPM) mitigation of a 28 GBaud PSA link.

The first method allows the use of different span dispersion maps in different spans of a PSA link, i.e. multi-span dispersion map optimization. This method shows great potential because the nonlinearity mitigation is improved significantly. However, the computational complexity and effort increases rapidly by a brute-force optimization, therefore the optimization is carried out only up to four-span dispersion map optimization.

The reliability of numerical simulations is confirmed experimentally for the two-span PSA link optimization case, while the dispersion map optimization experimental investigation for higher number of spans was not feasible to implement. However, the numerical simulations of four-span optimized PSA

link in a short-haul highly nonlinear regime show a significant 6 dB nonlinear distortion reduction in terms of the error vector magnitude (EVM) compared to the single-span optimized case. Long-haul transmission simulations show a 2.1 fold transmission reach increase at optimal launch powers, if four-span optimized dispersion maps are used instead of single-span optimized maps. The four-span dispersion map optimized PSA link yields in a significant 6.9 fold transmission reach improvement, if PSAs are used instead of PIAs.

A PSA amplified link is capable of nonlinearity mitigation similar to the phase-conjugated twin waves (PCTW) approach. According to the assumptions from theory, a symmetric span power map with an anti-symmetric dispersion map should be used to achieve the best nonlinearity mitigation performance. Therefore the second proposed method makes use of distributed Raman amplification by designing a PSA amplified span that consists of three backward Raman pumped spans in order to achieve more symmetric span power map. However, opposite to expectations, the Raman assisted PSA link did not provide, in this configuration, a better nonlinearity mitigation performance, while an ideal span symmetry cannot be achieved by backward pumped distributed Raman amplification. The transmission reach improvements measured in the conducted experiments at optimal launch powers, if PSAs were used instead of PIAs, are 2.9 fold increase for the Raman assisted case and 3.8 fold transmission reach improvement for the conventional lumped amplified PSA link case.

The Raman assisted PSA method seems to be not able to fulfill the power map symmetry condition that is suggested in theory. It can be concluded that the multi-span dispersion map optimization seems to provide a superior nonlinearity mitigation performance for high symbol rate PSA links if more spans are optimized, but a complete mathematical understanding has to be derived to further optimize more number of spans.

LÜHIKOKKUVÕTE
Edastusfiibri mittelineaarsete mõjutuste vähendamine optilistes sidesüsteemides faasitundlike parameetriliste võimendite abil

Käesolevas väitekirjas uuritakse fiiberoptilise ülekandeliini mittelineaarsete mõjutuste (eeskätt iseenesliku faasimodulatsiooni) vähendamise võimalusi faasitundlike optiliste võimendite abil. Selleks on teostatud mahukad numbrilised arvutused ja eksperimentaalsed katsed ühe kanali ja polarisatsiooniga kahe-moodiliselt faasitundlikult võimendatud fiiberoptilistes ülekandeliinides. Faasitundlikud optilised võimendid on huvipakkuvad nende väga madala müratseme (kvant-limiteeritud-mürategur 0 dB) ja samaaegse mittelineaarsete mõjutuste vähendamise võimekuse poolest. Need kaks omadust on kasulikud, sest fiiberoptilise sidesüsteemi edastuskvaliteet on fundametaalselt limiteeritud optiliste võimendite poolt lisatava müra ning edastusfiibri poolt põhjustatud mittelineaarsete moonutuste tõttu. Faasitundlike optiliste võimendite müra omadusi on põhjalikumalt uuritud, kuid enne 2015 aastat, kui käesoleva väitekirjaga seotud teadustöö algas, oli veel vähe uuritud faasitundlike optiliste võimendite mittelineaarsete mõjutuste vähendamise aspekte. Sellegipoolest oli teada, et erinevad dispersiooni kompenseerimise jaotused ühel faasitundlikult võimendatud edastusfiibri lõigul avaldavad erinevat mõju mittelineaarsete mõjutuste vähendamise võimekusele.

Selles väitekirjas on esitletud esimene märkimisväärne fiiberoptilise ülekandeliini edastuskauguse suurenemine (5.6 korda) 10 GBaudises edastussüsteemis juhul, kui faasitundlikke optilisi võimendeid kasutatakse tavapäraste faasi-mittetundlike võimendite asemel. Sümboli edastuskiiruse suurenemisel avaldub tööreziim, mille korral dispersiooni mõjupikkus muutub lühemaks kui liinilõigu pikkus ning faasitundlike optiliste võimendite mittelineaarsete mõjutuste vähendamise võimekus väheneb. Selles väitekirjas pakutakse välja ning uuritakse kahte võimalikku meetodit 28 GBaudise faasitundlikult võimendatud optilise sideliini mittelineaarsete mõjutuste vähendamise võimekuse tõstmiseks.

Esimese meetodi kohaselt võimaldatakse kasutada erinevates faasitundlikult võimendatud liinilõikudes erinevaid dispersiooni kompenseerimise jaotusi, mida nimetatakse väitekirjas mitme liinilõigu dispersiooni kompenseerimis

jaotuste optimeerimiseks. See meetod näitab numbriliste arvutuste põhjal märgatavat mittelineaarsete mõjutuste vähenemist. Kahjuks kasvab samaaegselt optimeerimise keerukus ja arvutusmaht kiiresti iga järgneva optimeerimisele lisanduva liinilõigu korral. Seda siis, kui kasutada nn. jõu-meetodil optimeerimist. Seetõttu on dispersiooni kompenseerimis jaotuste optimeerimine sooritatud kuni neljale liinilõigule.

Numbriliste arvutuste usaldusväärsus kinnitatakse eksperimentaalsete katsetega kahe liinilõigu dispersiooni kompenseerimis jaotuste optimeerimisel, sest eksperimentaalseid katseid ei olnud võimalik sooritada suurema liinilõikude arvu korral. Numbrilised arvutused näitavad tugevalt mittelineaarses režiimis töötava neljal lõigul optimeeritud faasitundliku lühimaa ülekandeliini erakordset 6 dB (mõõtühikuks EVM – „error vector magnitude" ehk vea vektori magnituud) võrra suurenenud mittelineaarsete mõjutuste vähendamise võimekuse kasvu. Pikamaa ülekandeliini numbrilised arvutused näitavad 2.1 kordset edastuskauguse suurenemist optimaalsel edasutsvõimsustel juhul, kui neljal lõigul optimeeritud dispersiooni kompenseerimis jaotused on kasutatud ühel lõigul optimeeritute asemel. Neljal lõigul optimeetitud faasitundlikult võimendatud ülekandeliin saavutab 6.9 kordselt suurema edastuskauguse juhul, kui faasitundlikke võimendeid kasutatakse faasi-mittetundlike võimendite asemel.

Faasitundlikult võimendatud optilises edastusliinis toimub mittelineaarsete mõjutuste vähendamine sarnaselt faasi-konjugeeritud kaksiklainete meetodile. Selle teoreetilise eelduse kohaselt tagab sümmeetriline liinilõigu võimsusprofiil koos anti-sümmeetrilise dispersiooni kompenseerimis jaotusega parima mittelineaarsete mõjutuste vähendamise võimekuse. Seetõttu väitekirjas esitletud teise meetodi korral kasutatakse ühes faasitundlikult võimendatud liinilõigus lisaks kolme tagasisuunal võimendavat Ramani võimendit. Ramani võimendite abil on võimalik fiiberoptilises kaablis saavutada ühtlasem võimsusprofiil. Vastupidiselt eeldustele, ei taga koos Ramani võimendusega töötav faasitundlikult võimendatud ülekandeliini lõik paremat mittelineaarsete mõjutuste vähendamise võimekust, sest liinilõigu võimsussümmeetria tingimus ei ole Ramani võimenditega saavutatav. Mõõdetud eksperimentaalne ülekande kauguse suurenemise määr oli 2.9 kordne juhul, kui faasitundlikke optilisi võimendeid kasutati faasi-mittetundlike võimendite asemel optimaalsel edastusvõimsusel ja Ramani võimendite kaaskasutuse korral ning 3.8 korda kui Ramani võimendid ei olnud kasutusel.

Ramani võimendite kaaskasutuse korral ei ole tagatud teoorias soovitatud liinilõigu võimsusprofiili sümmeetrilisus. Sellest tulenevalt pakub mitme liinilõigu dispersiooni kompenseerimis jaotuse optimeerimise meetod parimat saavutatavat mittelineaarsete mõjutuste vähendamise võimekust faasitundlikult võimendatud ülekandeliinides juhul, kui kasutusel on kõrgem sümboli edastuskiiruse töörežiim. Mittelineaarsete mõjutuste vähendamise

võimekus kasvab vastavalt optimeeritud lõikude arvule, kuid täielik analüütiline optimiseerimise eeskiri tuleks veel välja töötada. See võimaldaks sooritada optimeerimist suuremate liinilõikude arvu korral.

Part II

Included Publications

Paper A

Long-haul optical transmission link using low-noise phase-sensitive amplifiers

S. L. I. Olsson, H. Eliasson, E. Astra, M. Karlsson and P. A. Andrekson, Nature Communications, no. 9 (2018): 2513.

ARTICLE

Long-haul optical transmission link using low-noise phase-sensitive amplifiers

Samuel L.I. Olsson [1,3], Henrik Eliasson[1], Egon Astra [2], Magnus Karlsson [1] & Peter A. Andrekson [1]

The capacity and reach of long-haul fiber optical communication systems is limited by in-line amplifier noise and fiber nonlinearities. Phase-sensitive amplifiers add 6 dB less noise than conventional phase-insensitive amplifiers, such as erbium-doped fiber amplifiers, and they can provide nonlinearity mitigation after each span. Realizing a long-haul transmission link with in-line phase-sensitive amplifiers providing simultaneous low-noise amplification and nonlinearity mitigation is challenging and to date no such transmission link has been demonstrated. Here, we demonstrate a multi-channel-compatible and modulation-format-independent long-haul transmission link with in-line phase-sensitive amplifiers. Compared to a link amplified by conventional erbium-doped fiber amplifiers, we demonstrate a reach improvement of 5.6 times at optimal launch powers with the phase-sensitively amplified link operating at a total accumulated nonlinear phase shift of 6.2 rad. The phase-sensitively amplified link transmits two data-carrying waves, thus occupying twice the bandwidth and propagating twice the total power compared to the phase-insensitively amplified link.

---

[1] Department of Microtechnology and Nanoscience, Chalmers University of Technology, SE-412 96 Gothenburg, Sweden. [2] Thomas Johann Seebeck Department of Electronics, Tallinn University of Technology, Tallinn 19086, Estonia. [3] Present address: Nokia Bell Labs, 791 Holmdel Road, Holmdel, NJ 07733, USA. Correspondence and requests for materials should be addressed to S.L.I.O. (email: samuel.olsson@nokia-bell-labs.com)

The achievable transmission performance of fiber optical transmission systems is limited by amplifier noise and fiber nonlinearities degrading the signal[1–3]. Phase-sensitive amplifiers (PSAs) can provide low-noise amplification, because at high gains their noise figure (NF) is 3 dB lower than that of even ideal phase-insensitive amplifiers (PIAs)[4,5]. Using an alternative NF definition where only the signal power is accounted for (idler power is neglected), the NF difference between PSAs and PIAs increases to 6 dB[5]. PSAs are also capable of all-optical mitigation of nonlinear transmission distortions[6–8]. Using PSAs low-noise amplification and nonlinearity mitigation capabilities, PSAs can potentially improve the transmission performance of fiber optical transmission systems[9,10].

PSAs can be realized, for example using, parametric gain in $\chi^{(2)}$ nonlinear materials through three-wave mixing (TWM)[11], or $\chi^{(3)}$ nonlinear materials through four-wave mixing (FWM)[12]. Typically, two weak waves, called signal and idler, are amplified by one or two high-power waves, called pumps. Depending on how the frequencies of the interacting waves are chosen, different amplification schemes are possible. Two common schemes are the one-mode PSAs in which signal and idler are frequency degenerate and the two-mode PSAs in which signal and idler are frequency non-degenerate.

In one-mode PSAs, one quadrature is amplified while the other quadrature is deamplified, squeezing the signal phase along the direction of the amplified quadrature[4]. If the PSA is operated in unsaturated regime, phase noise in the squeezed quadrature will be converted into amplitude noise in the amplified quadrature. If, however, the PSA is operated in saturation both phase and amplitude noise can be suppressed thus making this scheme suitable for simultaneous phase and amplitude regeneration of binary phase-shift keying (BPSK) signals[13–15]. Using this scheme, a two times reach extension, originating from phase and amplitude regeneration, not low-noise amplification, has been demonstrated[16,17]. Two severe drawbacks of the one-mode PSA scheme is that it is inherently single-channel and that it is only suitable for BPSK signals. Using other PSA-based schemes, regeneration of more advanced modulation formats such as quadrature phase-shift keying (QPSK)[18,19], and star 8-quadrature amplitude modulation (QAM)[20], have been demonstrated as well as simultaneous regeneration of more than one channel[21,22].

Another way to benefit from PSAs is to utilize their capabilities of low-noise amplification and nonlinearity mitigation. This can be done using two-mode PSAs implemented with the so-called copier-PSA scheme[23]. Using the copier-PSA scheme, all signal phase states will experience low-noise amplification thus providing modulation-format transparency[24]. Moreover, two-mode PSAs are multi-channel compatible and can be used for amplification of wavelength division multiplexing (WDM) signals[25]. In ref.[26], it was shown that two-mode PSAs potentially can be combined with multi-channel amplitude regenerators for multi-channel regeneration of advanced modulation formats. For details on the requirements regarding the tracking and alignment of polarization in PSA links see ref.[27].

Mitigation of fiber nonlinearities to extend transmission reach is a vivid research area currently[28], and many different schemes have been proposed, e.g., phase conjugated twin waves[29] or conjugate data repetition[30], which are based on the idea that the signal and the conjugate signal are co-propagated through the same medium and coherently superposed to suppress the nonlinear-induced phase distortion. Cancellation of nonlinear distortion by digital signal processing[31] in the receiver[32] or transmitter[33] has also been demonstrated, as has optical phase conjugation (OPC)[34]. Typically, a doubling or at most a tripling of the system reach have been reported by these schemes, at the expense of spectral efficiency and/or complexity. A way to further

enhance performance could be to distribute the compensation, which is attractive for all-optical schemes such as PSAs or OPC, and for OPCs that was recently demonstrated[35,36], although relatively moderate Q-factor improvements over single OPCs were reported.

Here we present experimental evidence that in-line PSAs, can provide an unprecedented nonlinear tolerance and transmission reach extension[9,10]. In this demonstration of a recirculating loop (i.e., long-haul) transmission experiment with in-line PSAs, we benefit from the inherent simultaneous low-noise amplification and nonlinearity mitigation. This scheme, which is both modulation format-independent and multi-channel compatible[5], is shown experimentally to have a 5.6 times reach improvement compared to a transmission link using conventional in-line erbium-doped fiber amplifiers (EDFAs) when transmitting a 10 GBd QPSK signal. The accumulated nonlinear phase shift in the PSA link is 6.2 rad, which we believe is the highest nonlinear tolerance ever reported in a lumped-amplifier system. These results demonstrate not only the feasibility of realizing long-haul transmission links using low-noise PSAs but also significant improvement over conventional approaches. The concept of amplification using cascaded PSAs might also find applications in the field of quantum information science, where generation and processing of quantum states are of interest.

Results

Basic principle. The amplifier implementation we consider in this work is the degenerate pump, two-mode PSA. It consists of three waves, an intense pump surrounded by a signal and an idler. The input–output relation for the signal and idler is given by

$$\begin{pmatrix} u_{\mathrm{s}} \\ u_{\mathrm{i}}^{*} \end{pmatrix}_{\mathrm{out}} = \begin{pmatrix} \mu & \nu \\ \nu^{*} & \mu^{*} \end{pmatrix} \begin{pmatrix} u_{\mathrm{s}} + n_{\mathrm{s}} \\ u_{\mathrm{i}}^{*} + n_{\mathrm{i}}^{*} \end{pmatrix}_{\mathrm{in}} \qquad (1)$$

where $u_{\mathrm{s,i}}$ are the signal and idler wave amplitudes, $n_{\mathrm{s,i}}$ represents vacuum noise present at the input, and the amplifier is characterized via the scalar coefficients μ and ν, where $|\mu|^{2} - |\nu|^{2} = 1$ ensures photon-number conservation, i.e., two pump photons are converted into one signal and one idler photon. If the input idler wave is absent, $u_{\mathrm{i,in}} = 0$ then the output signal is amplified phase insensitively with gain $G_{\mathrm{PIA}} = |\mu|^{2} \approx |\nu|^{2}$, where the approximate equality holds in the limit of high gain.

In our experiment, we employ a sequence of these amplifiers with intermediate fiber losses that are compensated for by the provided gain. The first amplifier has $u_{\mathrm{i,in}} = 0$, so it copies the conjugate incoming signal to the output idler wave. The generated signal-idler pair then propagates through all subsequent amplifiers, while achieving a phase-sensitive gain G_{PSA} of approximately $4G_{\mathrm{PIA}}$ due to coherent addition of signal and idler conjugate.

In contrast to the signal, for which the gain is 6 dB higher in phase-sensitive (PS) mode than in phase-insensitive (PI) mode, the gain for the vacuum noise is always $2G_{\mathrm{PIA}}$ since the noise is uncorrelated between signal and idler and will thus not add coherently. By comparing PI- and PS-operation at the same signal gain the difference between PIA and PSA amplification can be stated as that a PSA will add 6 dB less noise than a PIA. The first 3 dB of this improvement comes from the phase-sensitive nature of the gain, which releases the PSA from being constrained by the 3 dB quantum limit on PIA NF[4], at the expense of using half of the available bandwidth for propagating the idler[37]. This NF improvement has been characterized in detail in refs.[38,39] The second 3 dB of the improvement comes from the fact that the data in the two-mode-PSA-amplified link are carried by two beams (signal and idler) of equal powers, which makes the effective total data-carrying power in the PSA link twice that of
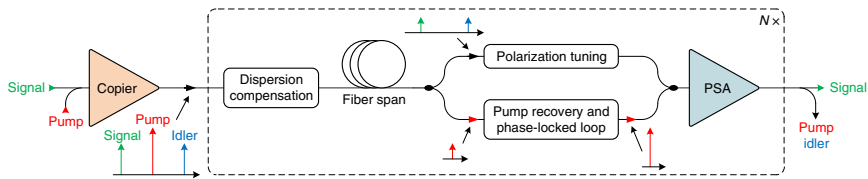
Fig. 1 Long-haul PSA-amplified link. Conceptual schematic of a long-haul PSA-amplified link implemented using the copier-PSA scheme
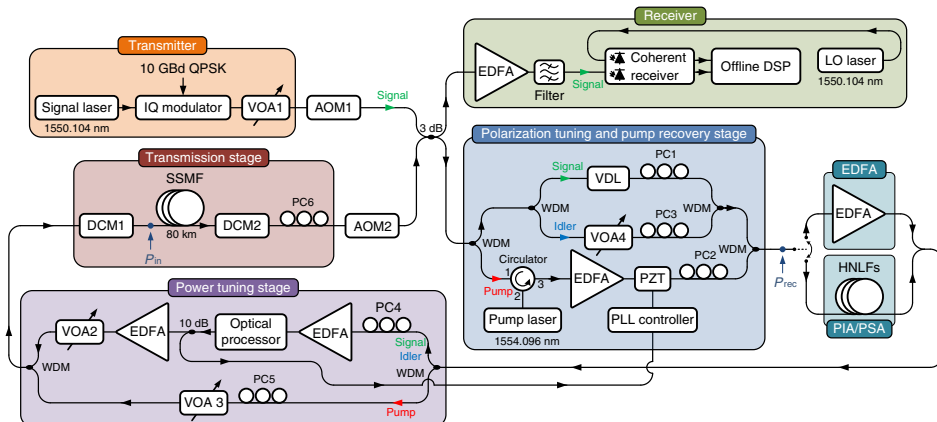

Fig. 2 Experimental set-up. Recirculating loop set-up used to demonstrate long-haul transmission with in-line PSA-based amplification. Option with in-line EDFA- and PIA-based amplification used for benchmarking is also shown. Colored arrows indicating waves represent PSA case for the second and the following round trips. IQ modulator in phase/quadrature modulator, AOM acousto-optic modulator, VDL variable delay line, PC polarization controller, HNLF highly nonlinear fiber, PLL phase-locked loop, DSP digital signal processing, LO local oscillator

the PIA link[37]. Described above is the so-called copier-PSA scheme, and its linear link properties were analyzed in refs.[40,41] and experimentally verified for a single-span link in refs.[5,42] A conceptual schematic of a multi-span implementation of the copier-PSA scheme is shown in Fig. 1.

Experimental set-up. The experimental set-up used to demonstrate long-haul transmission with in-line PSAs is illustrated in Fig. 2. A signal modulated with 10 GBd QPSK data were launched into a recirculating loop. During the first round trip ($N = 1$), only one wave, the signal, was present at the input of the polarization tuning and pump recovery stage and a pump wave was generated using a laser. After combining the signal with the pump using a WDM coupler, the two waves were launched into a fiber optical parametric amplifier (FOPA) where a conjugated copy of the signal, the idler, was generated. During the first round trip, the FOPA thus operated as a copier. The three waves were then passed through a power tuning stage where an optical processor (OP) was used to filter the signal and idler as well as adjust their powers. Following the OP, the signal and idler were passed through an EDFA followed by a variable optical attenuator (VOA) for launch power tuning. The pump was passed through a separate path and was attenuated using a VOA. The transmission link consisted of two tunable fiber Bragg-grating dispersion compensating modules (DCMs) and an 80 km standard single-mode fiber (SSMF) transmission span. The combined loss of the SSMF span and the second DCM was 21.5 dB.

During the second and the following round trips ($N \geq 2$), the pump was regenerated in the polarization tuning and pump recovery stage by injection-locking it to the pump laser and

subsequently amplifying it with an EDFA. The process of self-injection-locking enabled stable injection-locking over many circulations. The signal and idler were split into two separate paths and the delay between them introduced by the SSMF was compensated for. A phase-locked loop based on a piezoelectric transducer (PZT) fiber stretcher was used to compensate for any dynamic phase drifts between the arms introduced by temperature and acoustic influence. After the polarization tuning and pump recovery stage, the waves were launched into the FOPA, which now operated as a PSA with 22 dB net gain providing low-noise amplification and nonlinearity mitigation. To compensate for the fact that the copier operated as a PIA, 6 dB more noise to the signal than the following PSAs, the signal power launched into the loop was 6 dB higher than the power present at the point of the loop input after the first round trip. The received power was measured at point P_{rec} and the loss from point P_{in} to point P_{rec} was 39 dB. In each round trip, part of the light was coupled out of the recirculating loop and detected using a coherent receiver. A more detailed description of the experimental set-up is presented in the Methods section.

Constellation diagrams. To benchmark the performance of the PSA-amplified link, measurements were also performed on an EDFA-amplified link and a FOPA-PIA-amplified link. The FOPA-PIA-amplified link was obtained by blocking the idler in the OP and fully attenuating the pump in the power tuning stage. The EDFA link was obtained by replacing the FOPA with an EDFA and turning off the pump laser as well as the pump booster EDFA. The three cases were compared both by studying constellation diagrams and by measuring bit error rate (BER).
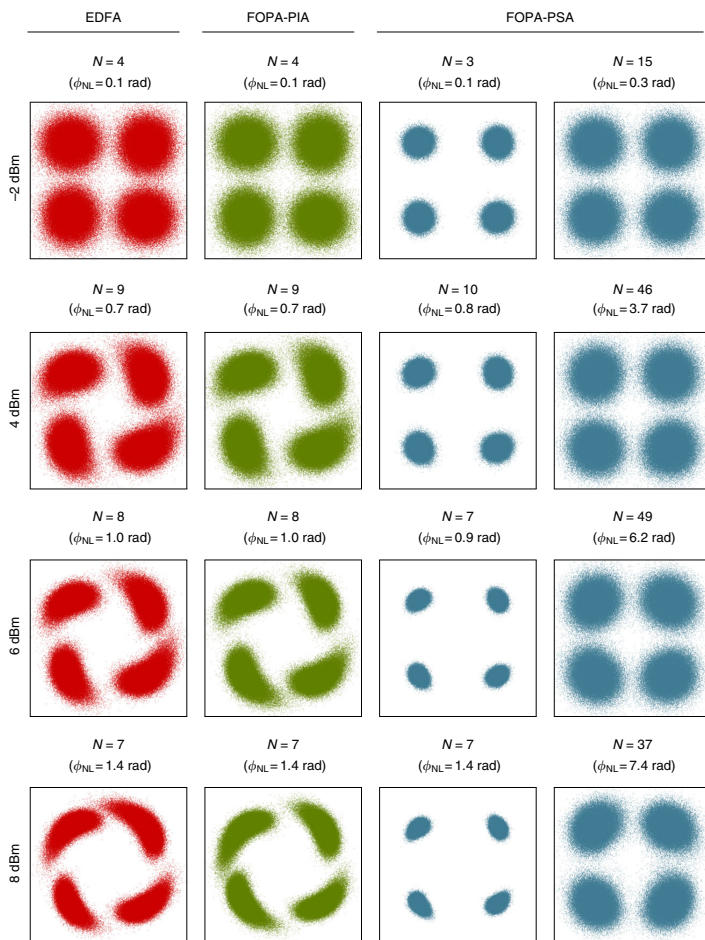
Fig. 3 Signal constellation diagrams. Constellation diagrams at various launch powers using EDFA-based amplification, FOPA-PIA-based amplification, and FOPA-PSA-based amplification. Constellations in column one, two, and four corresponds to a BER of 10^{-3}. The variable N indicates the number of round trips where each round trip include an 80 km dispersion compensated SSMF span and ϕ_{NL} denotes the accumulated nonlinear phase shift

Figure 3 shows constellation diagrams at various launch powers (measured at point P_{in}) for the three investigated amplification schemes. The constellations in columns one, two, and four correspond to a measured BER of 10^{-3} while the third column shows the constellations for the FOPA-PSA case at the closest available number of round trips to the EDFA case. The variable N indicates the number of round trips. The accumulated nonlinear phase shift was calculated using $\phi_{NL} = \gamma P_{in} L_{eff}$, where γ is the nonlinear coefficient, P_{in} is the launch power, and L_{eff} is the effective length defined as $L_{eff} = [1 - \exp(-\alpha L)]/\alpha$ with α being the fiber attenuation and L the link length, and is shown in parenthesis above each constellation. When calculating ϕ_{NL} we used $\gamma = 1.5\,\mathrm{W}^{-1}\,\mathrm{km}^{-1}$, $\alpha = 0.2\,\mathrm{dB\,km}^{-1}$, and $L = 80$ km.

It is clear from Fig. 3 that EDFA- and FOPA-PIA-based amplification provide similar performance from -2 dBm launch power, where the reach is limited by amplifier noise, up to 8 dBm launch power, where reach is limited by nonlinear distortions. We can also see that PSA-based amplification significantly reduces the accumulated amplifier noise as well as the impact of fiber nonlinearities, thus allowing for improved reach at all launch powers.

Bit error rate measurements. Measured BER versus number of round trips and transmission distance at various launch powers is presented in Fig. 4a. It can be seen that the EDFA case and FOPA-PIA case are close to indistinguishable while the PSA case shows significantly improved reach. The reach improvement as well as the maximum number of round trips (for a BER of 10^{-3}) versus launch power is presented in Fig. 4b. From the figure we note that the optimal launch power for the PSA case is 6 dBm while the optimal launch power in the EDFA- and FOPA-PIA cases is 4 dBm. At 6 dBm launch power, the reach improvement using PSA-based amplification is about six times while if the comparison is made at optimal launch powers, the reach improvement is 5.6 times.

Discussion

Our demonstration of long-haul PSA-amplified transmission was performed using a signal with 10 GBd QPSK data. However, in principle any modulation format and symbol rate can be used with the copier-PSA scheme. Increasing the symbol rate will make it more challenging to achieve good enough temporal
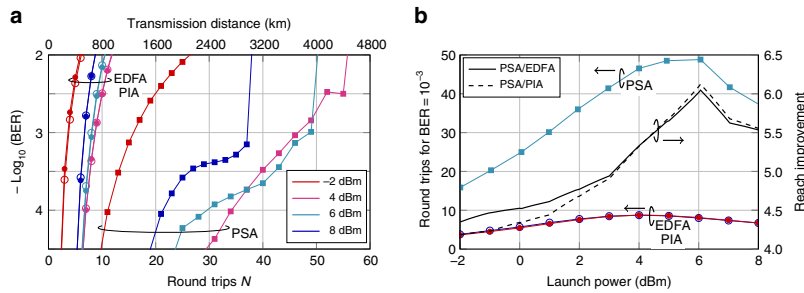
Fig. 4 BER characterization. **a** BER curves at various launch powers using in-line EDFA- (filled circles), FOPA-PIA- (open circles), and FOPA-PSA-based (filled squares) amplification. **b** Number of round trips giving a BER of 10^{-3} versus launch power and reach improvement comparing EDFA- (filled circles) and FOPA-PIA-based (open circles) amplification to PSA-based (filled squares) amplification

alignment of the waves but by using high precision delay lines this should be possible. The copier-PSA performance in linear regime is not expected to depend on either symbol rate or modulation format. However, the ability to mitigate nonlinearities might depend on both symbol rate and modulation format and will require further investigation. Approaches that have been suggested as means to improve nonlinearity mitigation at, e.g., higher symbol rates in PSA-amplified links are addition of distributed Raman amplification[43] or multi-span dispersion map optimization[44]. In our demonstration, we transmitted a single channel but with the copier-PSA scheme multi-channel transmission is possible although with increased complexity due to required polarization, delay, and phase alignment of each channel.

Using a recirculating loop to demonstrate long-haul PSA-amplified transmission is a good approach to demonstrate the possible performance improvements that can be gained using in-line PSAs. However, using a recirculating loop simplifies certain aspects of the implementation and in order to realize a real transmission link with in-line PSAs a few challenges remain to be solved. One such challenge is the pump recovery. The injection-locking-based pump recovery is sensitive to frequency differences between the incoming pump wave and the free-running pump laser frequency. In our recirculating loop set-up, this frequency difference could be kept small since it is dictated by the pump laser wavelength drift during the measurement time which was 24 ms for 60 round trips. In a real transmission link, a feedback system would be required to tune the frequency of the slave lasers to match the frequency of the incoming pump wave. Another aspect that will be more challenging in a real transmission link is the polarization alignment of the involved waves. In our recirculating loop set-up, this alignment could be done manually. However, in a real transmission-link polarization tracking would be required to align the waves and to keep them aligned over time.

We have demonstrated the possibilities and potential of using cascaded PSAs in the context of high-speed optical communications. However, our results might also find applications in quantum informatics and related fields where generation and processing of quantum states are of interest.

Methods

Recirculating loop experiment. A continuous wave (CW) laser (Keysight N7711A) at 1550.104 nm with <100 kHz linewidth, -145 dB Hz^{-1} relative intensity noise (RIN), and 30 mW output power was modulated with 10 GBd QPSK data (pseudorandom bit sequence (PRBS) of length $2^{15}-1$) using a LiNbO$_3$-based single polarization I/Q modulator. The electrical signals driving the I/Q modulator were generated using a bit pattern generator (SHF 12103A) followed by electrical amplifiers (SHF 804 TL). After passing a VOA, VOA1, for loop launch power tuning the signal was passed into a recirculating loop that was controlled using a

loop controller (Brimrose AMM-55-8-70-C-RLS(nfs)-RM) containing two acousto-optic modulators (AOMs).

During the first round trip only the signal was present at the input of the polarization tuning and pump recovery stage and a CW pump wave at 1554.096 nm was generated using a distributed feedback (DFB) laser without isolator (EM4 AA1406-192900-100) with <1 MHz linewidth, -150 dB Hz^{-1} RIN, and 100 mW output power. The pump wave was subsequently amplified using a 3 W fanless high-power EDFA (IPG EUA-3K-C-CHM) and attenuated to obtain 1 W at the FOPA input. The signal was combined with the pump before the FOPA using a WDM coupler and the signal and pump state of polarizations (SOPs) were aligned using PC1 and PC2 for maximum FOPA gain. With only signal and pump present at the FOPA input, the FOPA operated as a PIA with 16 dB net gain. The FOPA consisted of four cascaded spools of strained highly nonlinear fiber (HNLF) (OFS HNLF-SPINE with zerodispersion wavelength (ZDW) at 1543 nm) of lengths 101, 124, 156, and 205 m, with in-line isolators placed between the individual spools for stimulated Brillouin scattering (SBS) suppression[45]. During the first round trip, the FOPA generated a conjugated copy of the signal, frequency- and phase-locked to the signal and pump, at the idler wavelength through FWM.

After the in-line amplifier, the waves were led to a power tuning stage where the high-power pump was separated from the signal and idler waves. The signal and idler were amplified using an EDFA (Nortel) and then passed into an OP (Finisar WaveShaper 1000S) for filtering (0.4 nm bandpass filters) and power tuning such that they were balanced in power at point P_{in}, just before the transmission fiber. The two waves were then led into a custom built EDFA with 3.1 dB NF and 25 dBm output power followed by VOA2 for launch power tuning. PC4 was tuned so that the polarization dependent loss (PDL) experienced by the signal over the transmission stage was minimized. The pump was attenuated using VOA3 to obtain -5 dBm at point P_{in} and PC5 was tuned so that the SOP of the pump launched into the pump laser in the second round trip was aligned with the free-running pump laser SOP.

The transmission link constituted of two 100 GHz channel grid tunable fiber Bragg-grating DCMs (TeraXion TDCMX-C100-(-80 km/+5 km)), DCM1 for dispersion pre-compensation and DCM2 for post-compensation, and an 80 km SSMF transmission span. The dispersion map was experimentally optimized for longest reach in a strongly nonlinear regime (6 dBm launch power). In the PSA case, the optimum dispersion map was 289 ps nm^{-1} pre-compensation and 986 ps nm^{-1} post-compensation. In both the EDFA- and the FOPA-PIA case, the optimum dispersion map was 68 ps nm^{-1} pre-compensation and 1207 ps nm^{-1} post-compensation. The amount of per span residual dispersion was experimentally optimized for longest reach in a nonlinear transmission regime for the PSA case and was <35 ps nm^{-1}. This amount of residual dispersion had a negligible impact on the performance in linear transmission regime both for the PSA and PIA cases as well as for the PIA cases in nonlinear transmission regime due to the low symbol rate and few round trips. The launch power was measured as signal power at point P_{in}. PC6 was adjusted so that the signal SOP at the beginning of the second round trip was the same as the SOP of the signal launched into the transmission loop. The round trip time was 0.4 ms.

During the second and the following round trips both signal, idler, and pump were present at the input of the polarization tuning and pump recovery stage. The pump was separated from the signal and idler and injection-locked to the pump laser. This process of self-injection-locking enabled stable locking over many circulations. The signal and idler were also separated, and the delay between them introduced by the transmission fiber was compensated for using a variable delay line (VDL) with a 1 dB insertion loss. The idler was attenuated such that the signal and idler had equal power going into the FOPA and their SOPs were aligned using PC1 and PC3 so that the FOPA gain was maximized. A phase-locked loop (PLL) based on a PZT fiber stretcher was used to compensate for any dynamic phase drifts between the arms introduced by temperature and acoustic influence. The FOPA-PSA net gain was 22 dB. For simplicity the PSA-amplified link was implemented such that the same FOPA was used both for the copier and the PSA.

As a consequence of this, the first and last in-line amplifiers in the PSA-amplified link were PIAs. In order to compensate for the extra signal degradation caused by the first in-line PIA, the signal power launched into the loop was 6 dB higher than the power present at the point of the loop input after the first round trip. The absence of nonlinearity mitigation in the last in-line amplifier in the link was not compensated for. Due to the placement of the loop output coupler, the loss of the final span was lower than the other spans by ~2 dB. For the EDFA case and the FOPA-PIA case, this resulted in slightly better performance compared to what would have been achieved in a link in which all spans had the same loss. For the PSA case, the performance was still worse then it would have been if the last amplifier in the link was a PSA. Note, however that the impact of having slightly lower loss in the last span is negligible after many circulations.

In each round trip, part of the light was coupled out of the recirculating loop and amplified by an EDFA (JDS Uniphase OAB optical amplifier) followed by an optical filter (OTF-30M-12S2) with a 3 dB bandwidth of 0.9 nm centered at the signal wavelength. The amplified and filtered signal was then coupled into a coherent receiver (NeoPhotonics Integrated PBS ICR) along with a local oscillator wave generated by a CW laser (IDPhotonics CBDX1-1-C-H01-FA) at the signal wavelength with <100 kHz linewidth, −145 dB Hz^{-1} RIN, and 40 mW output power. The signal was sampled at 50 GS s^{-1} using a real-time sampling oscilloscope (Tektronix DPO73304SX) with 33 GHz analog bandwidth. For each round trip, 2.5×10^6 samples (corresponding to 50 μs at 50 GS s^{-1}) were taken in the middle of the 0.4 ms long burst and then post processed off-line using conventional DD-LMS-based digital signal processing (DSP). The back-to-back signal-to-noise ratio (SNR) penalty of the transmitter and receiver was 0.5 dB at a BER of 10^{-3}.

For the EDFA case, the pump laser was turned off and the FOPA was substituted with a custom built EDFA with 3.1 dB NF and 25 dBm output power followed by a VOA tuned such that the net gain of the EDFA and VOA was 22 dB. For the FOPA-PIA case, the idler was blocked in the OP and the pump was fully attenuated before the transmission stage using VOA3. The in-line FOPA-PIA net gain was 16 dB.

Data availability. The data that support the findings of this study are available from the corresponding author upon reasonable request.

References

1. Essiambre, R.-J., Kramer, G., Winzer, P. J., Foschini, G. J. & Goebel, B. Capacity limits of optical fiber networks. *J. Lightwave Technol.* **28**, 662–701 (2010).
2. Ellis, A. D., Zhao, J. & Cotter, D. Approaching the non-linear shannon limit. *J. Lightwave Technol.* **28**, 423–433 (2010).
3. Agrell, E. Nonlinear fiber capacity. In *European Conference and Exhibition on Optical Communication (ECOC)*, London, England, 2013, paper We.4.D.3.
4. Caves, C. M. Quantum limits on noise in linear amplifiers. *Phys. Rev. D.* **26**, 1817–1839 (1982).
5. Tong, Z. et al. Towards ultrasensitive optical links enabled by low-noise phase-sensitive amplifiers. *Nat. Photonics* **5**, 430–436 (2011).
6. Olsson, S. L. I. et al. Phase-sensitive amplified optical link operating in the nonlinear transmission regime. In *European Conference and Exhibition on Optical Communication (ECOC)*, Amsterdam, The Netherlands, 2012, paper Th.2.F.1
7. Olsson, S. L. I. et al. Phase-sensitive amplified transmission links for improved sensitivity and nonlinearity tolerance. *J. Lightwave Technol.* **33**, 710–721 (2015).
8. Olsson, S. L. I, Karlsson, M. & Andrekson, P. A. Nonlinear phase noise mitigation in phase-sensitive amplified transmission systems. *Opt. Express* **23**, 11 724–11 740 (2015).
9. Olsson, S. L. I., Lundstrom, C., Karlsson, M. & Andrekson, P. Long-haul (3465 km) transmission of a 10 GBd QPSK signal with low noise phase-sensitive in-line amplification. In *European Conference and Exhibition on Optical Communication (ECOC)*, Cannes, France, 2014, paper PD.2.2.
10. Olsson, S. L. I., Karlsson, M. & Andrekson, P. Long-haul optical transmission of 16-QAM signal with in-line phase-sensitive amplifiers. In *European Conference and Exhibition on Optical Communication (ECOC)*, Gothenburg, Sweden, 2017, paper W.3.B.3.
11. Lovering, D. J., Levenson, J. A., Vidakovic, P., Webjorn, J. & Russell, P. S. J. Noiseless optical amplification in quasi-phase-matched bulk lithium niobate. *Opt. Lett.* **21**, 1439–1441 (1996).
12. Tong, Z., Lundstrom, C., Andrekson, P. A., Karlsson, M. & Bogris, A. Ultralow noise, broadband phase-sensitive optical amplifiers, and their applications. *IEEE J. of Selected Top. Quantum Electron.* **18**, 1016–1032 (2012).
13. Croussore, K. & Li, G. Phase and amplitude regeneration of differential phase-shift keyed signals using phase-sensitive amplification. *IEEE J. Selected Top. Quantum Electron.* **14**, 648–658 (2008).
14. Slavik, R. et al. All-optical phase and amplitude regenerator for next-generation telecommunications systems. *Nat. Photonics* **4**, 690–695 (2010).
15. Umeki, T., Asobe, M. & Takenouchi, H. In-line phase sensitive amplifier based on PPLN waveguides. *Opt. Express* **21**, 12077–12084 (2013).
16. Slavik, R. et al. Field-trial of an all-optical PSK regenerator multicaster in a 40 Gbit/s, 38 channel DWDM transmission experiment. *J. Lightwave Technol.* **30**, 512–520 (2012).
17. Umeki, T., Asobe, M., Takara, H., Miyamoto, Y. & Takenouchi, H. Multi-span transmission using phase and amplitude regeneration in PPLN-based PSA. *Opt. Express* **21**, 18170–18177 (2013).
18. Kakande, J. et al. Multilevel quantization of optical phase in a novel coherent parametric mixer architecture. *Nat. Photonics* **5**, 748–752 (2011).
19. Kakande, J. et al. QPSK phase and amplitude regeneration at 56 Gbaud in a novel idler-free non-degenerate phase sensitive amplifier. In *Optical Fiber Communication Conference (OFC)*, Los Angeles, CA, 2011, paper OMT4.
20. Richter, T., Elschner, R. & Schubert, C. QAM phase-regeneration in a phase-sensitive fiber-amplifier. In *European Conference and Exhibition on Optical Communication (ECOC)*, London, England, 2013, paper We.3.A.2
21. Sygletos, S., Frascella, P., Garcia Gunning, F. C. & Ellis, A. D. Multi-wavelength regeneration of phase encoded signals based on phase sensitive amplifiers. In *International Conference on Transparent Optical Networks (ICTON)*, Coventry, England, 2012, paper We.B1.4.
22. Guan, P. et al. 16 channel WDM regeneration in a single phase-sensitive amplifier through optical fourier transformation. In *European Conference and Exhibition on Optical Communication (ECOC)*, Dusseldorf, Germany, 2016, paper Th.3.B.3.
23. Tang, R. et al. Gain characteristics of a frequency nondegenerate phase-sensitive fiber optic parametric amplifier with phase self-stabilized input. *Opt. Express* **13**, 10483–10493 (2005).
24. McKinstrie, C. J., Karlsson, M. & Tong, Z. Field-quadrature and photon-number correlations produced by parametric processes. *Opt. Express* **18**, 19792–19 823 (2010).
25. Tang, R., Devgan, P. S., Grigoryan, V. S., Kumar, P. & Vasilyev, M. In-line phase-sensitive amplification of multi-channel CW signals based on frequency nondegenerate four-wave-mixing in fiber. *Opt. Express* **16**, 9046–9053 (2008).
26. Li, L. et al. All-optical regenerator of multichannel signals. *Nat. Commun.* **8**, 884 (2017).
27. Lorences-Riesgo, A., Andrekson, P. A. & Karlsson, M. Polarization-independent phase-sensitive amplification. *J. Lightwave Technol.* **34**, 3171–3180 (2016).
28. Karlsson, M., Alic, N., Chandrsekhar, S. & Mecozzi, A. Feature issue introduction: nonlinearity mitigation for coherent transmission systems. *Opt. Express* **25**, 4552–4553 (2017).
29. Liu, X., Chraplyvy, A. R., Winzer, P. J., Tkach, R. W. & Chandrasekhar, S. Phase-conjugated twin waves for communication beyond the Kerr nonlinearity limit. *Nat. Photonics* **7**, 560–568 (2013).
30. Eliasson, H., Johannisson, P., Karlsson, M. & Andrekson, P. A. Mitigation of nonlinearities using conjugate data repetition. *Opt. Express* **23**, 2392–2402 (2015).
31. Temprana, E. et al. Overcoming Kerr-induced capacity limit in optical fiber transmission. *Science* **348**, 1445–1448 (2015).
32. Maher, R. et al. Spectrally shaped DP-16QAM super-channel transmission with multi-channel digital back-propagation. *Sci. Rep.* **5**, 8214 (2015).
33. Alic, N., Myslivets, E., Temprana, E., Kuo, B.-P. & Radic, S. Non-linearity cancellation in fiber optic links based on frequency referenced carriers. *J. Lightwave Technol.* **32**, 26902698 (2014).
34. Yoshima, S. et al. Mitigation of nonlinear effects on WDM QAM signals enabled by optical phase conjugation with efficient bandwidth utilization. *J. Lightwave Technol.* **35**, 971–978 (2017).
35. Ellis, A. D. et al. 4 Tb/s transmission reach enhancement using 10 × 400 Gb/s super-channels and polarization insensitive dual band optical phase conjugation. *J. Lightwave Technol.* **34**, 1717–1723 (2016).
36. Hu, H., Jopson, R. M., Gnauck, A. H., Randel, S. & Chandrasekhar, S. Fiber nonlinearity mitigation of WDM-PDM QPSK/16-QAM signals using fiber-optic parametric amplifiers based multiple optical phase conjugations. *Opt. Express* **25**, 1618–1628 (2017).
37. Vasilyev, M. Distributed phase-sensitive amplification. *Opt. Express* **13**, 7563–7571 (2005).
38. Tong, Z. et al. Modeling and measurement of the noise figure of a cascaded non-degenerate phase-sensitive parametric amplifier. *Opt. Express* **18**, 14 820–14 835 (2010).
39. Tong, Z., Lundstrm, C., Karlsson, M., Vasilyev, M. & Andrekson, P. A. Noise performance of a frequency nondegenerate phase-sensitive amplifier with unequalized inputs. *Opt. Lett.* **36**, 722–724 (2011).
40. Tong, Z., McKinstrie, C. J., Lundstrom, C., Karlsson, M. & Andrekson, P. A. Noise performance of optical fiber transmission links that use non-degenerate cascaded phase-sensitive amplifiers. *Opt. Express* **18**, 15 426–15 439 (2010).

41. McKinstrie, C. J., Alic, N., Karlsson, M. & Tong, Z. Higher-capacity communication links based on two-mode phase-sensitive amplifiers. *Opt. Express* **19**, 11 977–11 991 (2011).

42. Corcoran, B., Olsson, S. L. I., Lundstrom, C., Karlsson, M. & Andrekson, P. A. Phase-sensitive optical pre-amplifier implemented in an 80 km DQPSK link. In *Optical Fiber Communication Conference (OFC)*, Los Angeles, CA, 2012, paper PDP5A.4.

43. Eliasson, H., Olsson, S. L. I., Karlsson, M. & Andrekson, P. A. Mitigation of nonlinear distortion in hybrid raman/phase-sensitive amplifier links. *Opt. Express* **24**, 888–900 (2016).

44. Astra, E., Olsson, S. L. I., Eliasson, H. & Andrekson, P. A. Dispersion management for nonlinearity mitigation in two-span 28 GBaud QPSK phase-sensitive amplifier links. *Opt. Express* **25**, 13 163–13 173 (2017).

45. Lundstrom, C. et al. Fiber optic parametric amplifier with 10-dB net gain without pump dithering. *IEEE Photonics Technol. Lett.* **25**, 234–237 (2013).

Acknowledgements

Author contributions

S.L.I.O., H.E., and E.A. designed and built the set-up. S.L.I.O. and H.E. carried out the experiment and data analysis. P.A.A. and M.K. provided overall technical leadership and supervision. S.L.I.O., M.K., and P.A.A. jointly wrote the paper.

Additional information

Competing interests: The authors declare no competing interests.

Reprints and permission information is available online at http://npg.nature.com/reprintsandpermissions/

Publisher's note: Springer Nature remains neutral with regard to jurisdictional claims in published maps and institutional affiliations.

Paper B

Dispersion management for nonlinearity mitigation in two-span 28 GBaud QPSK phase-sensitive amplifier links

Dispersion management for nonlinearity mitigation in two-span 28 GBaud QPSK phase-sensitive amplifier links

EGON ASTRA,[1,*] SAMUEL L. I. OLSSON,[2,3] HENRIK ELIASSON,[2] AND PETER A. ANDREKSON[1,2]

[1] *Thomas Johann Seebeck Department of Electronics, Tallinn University of Technology, Tallinn, Estonia*
[2] *Department of Microtechnology and Nanoscience, Photonics Laboratory, Chalmers University of Technology, Göteborg, Sweden*
[3] *Now at: Nokia Bell Labs, 791 Holmdel Road, Holmdel, NJ 07733, USA*
[*] *egon.astra@ttu.ee*

Abstract: We present an investigation of dispersion map optimization for two-span single-channel 28 GBaud QPSK transmission systems with phase-sensitive amplifiers (PSAs). In experiments, when the PSA link is operated in a highly nonlinear regime, a 1.4 dB error vector magnitude (EVM) improvement is achieved compared to a one-span optimized dispersion map link due to improved nonlinearity mitigation. The two-span optimized dispersion map of a PSA link differs from the optimized dispersion map of a dispersion managed phase-insensitive amplifier (PIA) link. Simulations show that the performance of the two-span dispersion map optimized PSA link does not improve by residual dispersion optimization. Further, by using the two-span optimized dispersion maps repeatedly in a long-haul PSA link instead of one-span optimized maps, the maximum transmission reach can be improved 1.5 times.

© 2017 Optical Society of America

OCIS codes: (060.2320) Fiber optics amplifiers and oscillators; (070.4340) Nonlinear optical signal processing; (190.4380) Nonlinear optics, four-wave mixing.

References and links

1. Z. Tong, C. Lundström, P. A. Andrekson, C. J. McKinstrie, M. Karlsson, D. J. Blessing, E. Tipsuwannakul, B. J. Puttnam, H. Toda, and L. Grüner-Nielsen, "Towards ultrasensitive optical links enabled by low-noise phase-sensitive amplifiers," Nat. Photonics **5**(7), 430–436 (2011).
2. S. L. I. Olsson, B. Corcoran, C. Lundström, T. A. Eriksson, M. Karlsson, and P. A. Andrekson, "Phase-Sensitive Amplified Transmission Links for Improved Sensitivity and Nonlinearity Tolerance," J. Lightwave Technol. **33**(3), 710–721 (2015).
3. S. L. I. Olsson, C. Lundström, M. Karlsson, and P. A. Andrekson, "Long-Haul (3465 km) Transmission of a 10 GBd QPSK Signal with Low Noise Phase-Sensitive In-Line Amplification," in Proc. European Conference on Optical Communications (ECOC, 2014), paper PD.2.2.
4. X. Liu, A. R. Chraplyvy, P. J. Winzer, R. W. Tkach, and S. Chandrasekhar, "Phase-Conjugated Twin Waves for Communication Beyond the Kerr Nonlinearity Limit," Nat. Photonics **7**(7), 560–568 (2013).
5. W. Forysiak, J. H. B. Nijhof, and N. J. Doran, "Dispersion Managed Solitons: The Key to Terabit Per Second Optical Fiber Communication Systems," Opt. Photon. News **11**(5), 35–39 (2000).
6. C. Peucheret, N. Hanik, R. Freund, L. Molle, and P. Jeppesen, "Optimization of pre- and post-dispersion compensation schemes for 10-Gbits/s NRZ links using standard and dispersion compensating fibers," Photon. Technol. Lett. **12**(8), 992–994 (2000).
7. Y. Frignac and S. Bigo, "Numerical optimization of residual dispersion in dispersion-managed systems at 40 Gbit/s," in Proc. Optical Fiber Communications Conference and Exhibition (OFC, 2000), paper TuD3-1.
8. M. Malach, C.-A. Bunge, and K. Petermann, "Fibre-Independent Optimum Dispersion Mapping for SPM and XPM Suppression in 10 Gbit/s WDM NRZ Optical Transmission Systems," in Proc. European Conference on Optical Communications (ECOC, 2006), paper We3.P.130.
9. J. K. Fischer, C.-A. Bunge, and K. Petermann, "Equivalent Single-Span Model for Dispersion-Managed Fiber-Optic Transmission Systems," J. Lightwave Technol. **27**(16), 3425–3432 (2009).
10. A. Cartaxo, N. Costa, and D. Fonseca, "Analysis of optimum dispersion maps for DQPSK systems," in Proc. International Conference on Transparent Optical Networks (ICTON, 2010), paper Mo.D1.1.
11. Y. Frignac and P. Ramantanis, "Average Optical Phase Shift as an Indicator of the Dispersion Management Optimization in PSK-Modulated Transmission Systems," Photon. Technol. Lett. **22**(20), 1488–1490 (2010).

12. B. Corcoran, S. L. I. Olsson, C. Lundström, M. Karlsson, and P. A. Andrekson, "Mitigation of Nonlinear Impairments on QPSK Data in Phase-Sensitive Amplified Links," in Proc. European Conference on Optical Communications (ECOC, 2013), paper We.3.A.1.
13. H. Eliasson, S. L. I. Olsson, M. Karlsson, and P. A. Andrekson, "Mitigation of nonlinear distortion in hybrid Raman/phase-sensitive amplifier links," Opt. Express **24**(2), 888–900 (2016).
14. E. Astra, S. L. I. Olsson, H. Eliasson, T. Laadung, and P. A. Andrekson, "Dispersion Map Optimization for Nonlinearity Mitigation in Two-Span Phase-Sensitive Amplifier Links," in Proc. European Conference on Optical Communications (ECOC, 2016), paper Th.1.A.3.
15. S. L. I. Olsson, B. Corcoran, C. Lundström, E. Tipsuwannakul, S. Sygletos, A. D. Ellis, Z. Tong, M. Karlsson, and P. A. Andrekson , "Injection locking-based pump recovery for phase-sensitive amplified links," Opt. Express **21**(12), 14512-14529 (2013).
16. H. Eliasson, S. L. I. Olsson. M. Karlsson, and P. A. Andrekson, "Comparison between coherent superposition in DSP and PSA for mitigation of nonlinearities in a single-span link," in Proc. European Conference on Optical Communications (ECOC, 2014), paper Mo.3.5.2.

1. Introduction

Phase-sensitive amplifiers (PSAs) are implemented by making use of the four-wave mixing (FWM) process of signal, idler and pump waves in a nonlinear medium e.g. a highly nonlinear fiber (HNLF). If PSAs are used as in-line amplifiers in a fiber-optic communication link instead of phase-insensitive amplifiers (PIAs), a signal quality improvement is possible due to the PSA's ability to provide simultaneously low-noise amplification and nonlinearity mitigation [1–3].

In single-channel two-mode PSA-amplified links, the signal wave is co-propagated with an idler wave that is a conjugated copy of the signal wave, located at a different wavelength. The nonlinearity mitigation in such links is the result of correlated nonlinear distortion on signal and idler and the all-optical coherent superposition (CS) of signal and the conjugate of the idler in the PSA [2]. A similar approach for nonlinearity mitigation is the phase-conjugated twin waves (PCTW) scheme, where a phase-conjugated copy of the signal is co-propagated on the orthogonal polarization and the CS is performed electronically after coherent detection in digital signal processing (DSP) [4].

It is well known that the link dispersion map plays an important role in the interaction of group velocity dispersion (GVD) and nonlinear effects [5, 6]. It has been found that for non-return-to-zero (NRZ) and return-to-zero on-off-keying (RZ-OOK) modulation formats, non-zero residual dispersion per span can reduce the impact of nonlinear impairments [7–9] and the same holds for quadrature phase-shift keying (QPSK) [10]. It has also been shown that the optimization of link dispersion map minimizes the average nonlinear phase-shift introduced by the interplay of GVD and nonlinearities [11].

The optimum amount of dispersion pre- and post-compensation for PSA-amplified links has been thoroughly investigated for the single-span scenario [2, 12] and such a single-span optimized dispersion map has been used in multi-span PSA links [3, 13]. Also the temporal walk-off induced by different dispersion values between signal and idler waves at their wavelengths in the standard single mode fiber (SSMF) were compensated for before coherent interaction of signal and idler in the PSA. Thus, only fully dispersion compensated spans in PSA links has been studied to date [1–3, 12–14].

In [14] we showed numerically and experimentally that using the single-span optimized dispersion map for both spans in a two-span PSA link is not optimal and allowing different span dispersion maps in the two spans can improve the nonlinearity mitigation performance. In this paper we expand our results on dispersion map optimization of two-span single-channel 28 GBaud QPSK PSA links by including more details, investigate the effects of residual dispersion in a simulation study and compare the found optimal dispersion map configurations in long-haul PSA link simulations.

2. Numerical investigation

2.1. Two-span simulation model

The simulation model of the two-span PSA link in Fig. 1 consists of a transmitter, two in-line dispersion compensated transmission spans amplified by PSAs and receiver DSP. In the transmitter, a single-channel and single-polarization 28 GBaud QPSK signal was generated and separated into signal and idler channels. In the idler channel, the signal was conjugated to generate the idler, fulfilling $I_1 = S_1^*$. The launch powers P_{in} were set equal for the signal and idler at the span input for both spans. The effects of polarization, higher-order dispersion and laser phase noise were neglected. The dispersion pre- and post-compensation performed in the dispersion compensating modules (DCMs) was linear and lossless. Also amplifier noise was neglected in the two-span simulations, assuming that signal-noise interaction is negligible. These simplifications were made to highlight the impact of the dispersion map on the efficiency of the mitigation of self-phase modulation (SPM) induced nonlinear distortion.

Both spans were dispersion pre- and post-compensated in DCMs before and after the 80 km of SSMF. The dispersion pre-compensation values $D_{pre,1}$ of span 1 and $D_{pre,2}$ of span 2 show the percentage of dispersion pre-compensation applied in the DCMs before the SSMF. Each span was fully dispersion compensated, but the span dispersion maps were chosen independently. The dispersion post-compensation values for the DCMs after the SSMFs can be found by subtracting the span pre-compensation values from 100%. The SSMF parameters were loss $\alpha = 0.2$ dB/km, dispersion parameter $D = 17$ ps/nm/km and nonlinear coefficient $\gamma = 1.27$ W^{-1}km^{-1}. The light propagation in SSMF was modelled using a split-step Fourier method (SSFM) solution of the nonlinear Schrödinger equation (NLSE). Two separate single-polarization NLSE solvers with the same propagation parameters were used for signal and idler propagation, as the signal and idler were separated by 8 nm (signal 1549.74 nm and idler 1558.60 nm) in experiment. Therefore it was assumed that the nonlinear cross-talk between signal and idler waves in the SSMF was negligible compared to SPM.

The PSA gain was set to compensate for the transmission span loss. The two-mode PSA amplification process was modeled as in [2]. It was assumed that the PSA was working in high-gain regime and therefore a simplified PSA model was used. In the first PSA, S_1' from the signal channel and I_1' from the idler channel were separated and conjugated using the conjugate operator. After conjugation the constellations were aligned by introducing a necessary phase rotation in the constellation alignment (CA) module, so that the optical power was maximized
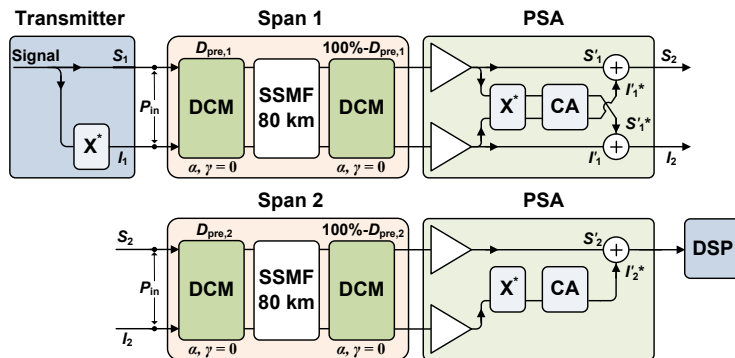

Fig. 1. Simulation model of the two-span PSA link. Acronyms are explained in the text.

after the coherent addition of signal and idler waves. After CS the signal channel output is given by $S_2 = S'_1 + I'^*_1$ and for the idler channel $I_2 = S'^*_1 + I'_1$. In the second PSA, after span 2, the idler channel output was not used in the DSP input and therefore the coherent addition in the idler channel was dropped for simplicity. Conventional receiver DSP was used for QPSK signal post-processing consisting of a linear channel equalizer, phase recovery and error vector magnitude (EVM) value calculation with hard decision thresholds.

2.2. Simulation results

The EVM value as a function of dispersion pre-compensation values for span 1 (y-axis) and span 2 (x-axis) at 12 dBm signal launch power, meaning 15 dBm total power of signal and idler, are shown in Fig. 2(a) for a PSA amplified link. The dispersion compensation ratio between pre- and post-compensation was changed from 0% to 100% in steps of 5% in each span, resulting in 441 different dispersion map configurations. Figure 2(a) shows that there exists two optima that have different amounts of applied dispersion pre-compensation values for both spans, 5% for span 1 and 35% for span 2 (5%, 35%) with EVM = -11.2 dB or the other way around (35%, 5%) with EVM = -11.1 dB. These optima are positioned symmetrically around the diagonal. The one span dispersion map optimized PSA link in two-span configuration with 15 % dispersion pre-compensation value for both spans (15%, 15%) has EVM = -8.9 dB. The EVM improvement using the two-span optimized dispersion map (5%, 35%) PSA link compared to the one span dispersion map optimized PSA link (15%, 15%) is thus 2.3 dB. These relatively high launch powers in simulations were needed to determine whether it is possible to observe and confirm any nonlinearity mitigation improvement effects experimentally that were predicted by simulations.

The two-span dispersion map optimization simulations were also compared and evaluated with a more realistic propagation model (not presented in this paper), where the third-order dispersion (TOD) effects were included, meaning that the dispersion value for signal and idler was different $D_s \neq D_i$. At signal wavelength 1550 nm the dispersion value $D_s = 17$ ps/nm/km and at idler wavelength 1558 nm the dispersion value $D_i = 17.5$ ps/nm/km were applied. Also ideal dispersion compensation and time delay alignment for signal and idler were assumed. No
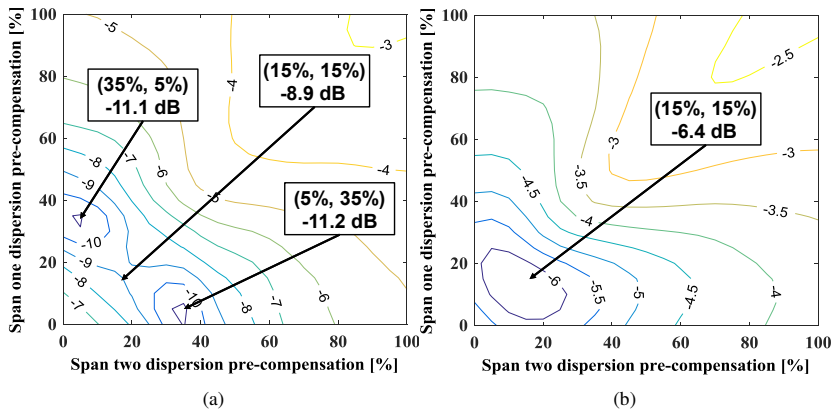

Fig. 2. Simulation results of EVM at 12 dBm signal launch power, meaning 15 dBm total power of signal and idler, of the two-span (a) PSA amplified and (b) PIA amplified link; The y- and x-axis show the percentages of applied dispersion pre-compensation in span 1 and span 2 respectively.

significant differences in the simulation results were observed when third-order dispersion was included. For simplicity and to achieve a better understanding of the fundamental role of the dispersion management in two-span PSA amplified systems, the effects of higher-order dispersion were not included in the simulation results presented here.

In Fig. 2(b) the EVM as a function of the dispersion pre-compensation values for span 1 and span 2 at 12 dBm signal launch power are shown for a two-span PIA amplified link. The PIA link simulation model is similar to the PSA link model shown in Fig. 1 with the difference that the idler and its channel are not present in the model. Instead of PSA module is phase-insensitive amplifier that amplifies only signal wave. Therefore only signal is transmitted and in-line amplified. The optimal dispersion pre-compensation values for the PIA link are 15% for span 1 and 15% for span 2 (15%, 15%) with EVM value of -6.4 dB. The overall performance in terms of nonlinearity mitigation of a dispersion managed two-span PIA link can be improved by 2.5 dB by making use of PSA amplification and 4.8 dB in total, if PSAs and two-span dispersion map optimization are applied for improved nonlinearity mitigation. It is however clear from the comparison, that the optimized dispersion map for the PSA link is different from the optimized dispersion map for the PIA link and the mechanism for mitigating nonlinear distortion by the right choice of dispersion map for the PIA links is different than for the PSA link.

In Figs. 3(a) and 3(b) the optimal dispersion pre-compensation values of a two-span PSA link are shown as a function of loss parameter α at 12 dBm signal launch power and as a function of signal launch power at loss $\alpha = 0.2$ dB/km with the dispersion parameter $D = 17$ ps/nm/km and nonlinear coefficient $\gamma = 1.27$ W^{-1}km^{-1}. The dispersion compensation ratio in these simulations was also swept with a step size of 5%. Figure 3(a) shows that the optimum dispersion map configuration varies significantly with the loss parameter α. Figure 3(b) shows, that the optimum dispersion map does not depend on signal launch power. Simulations were also performed with sweeped dispersion parameter D in the range from 4 to 34 ps/nm/km and the nonlinear coefficient γ from 0.1 to 2.3 W^{-1}km^{-1} at 12 dBm signal launch power with loss $\alpha = 0.2$ dB/km, but no significant change in the two-span optimum dispersion map configuration was noticed. It follows that the dispersion length $L_{\rm D}$ and nonlinear length $L_{\rm NL}$ do not have a strong influence compared to the effective length $L_{\rm eff}$ of the SSMF on the optimal dispersion map configuration at least for
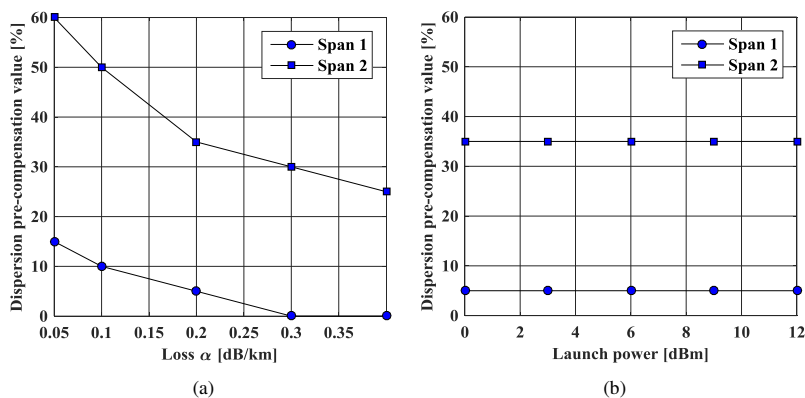

(a) (b)

Fig. 3. Simulation results of a two-span PSA amplified link showing optimal dispersion pre-compensation values for both spans as a function of (a) loss α at 12 dBm launch power and (b) signal launch power at loss $\alpha = 0.2$ dB/km.

the modulation format and symbol rate studied here.

Simulations with similar parameters and parameter sweep-ranges were also performed for a dispersion managed two-span PIA link. The results from these simulations (not presented here) show that the optimum dispersion map configuration for a two-span PIA link is not significantly dependent on the effective length L_{eff} of the SSMF as it was observed for the PSA link. Also no significant change by dispersion length L_D and nonlinear length L_{NL} on the optimum dispersion map configuration of the SSMF for the two-span PIA link was noticed.

3. Experimental investigation

3.1. Experimental setup

Figure 4 shows the setup used for the experimental investigation. A 28 GBaud QPSK signal was generated at 1549.74 nm and combined with a high-power continuous wave (CW) pump at 1554.16 nm using a wavelength division multiplexing (WDM) coupler. Before the signal and pump were combined and launched into a fiber optical parametric amplifier (FOPA), the copier, the signal and pump polarizations were controlled using polarization controllers (PCs). In the copier, a phase-conjugated copy of the signal, the idler, at 1558.60 nm was generated. After the copier, the signal and idler were separated from the pump for power balancing using an optical processor (OP), dispersion pre-compensation using a tunable dispersion compensating module (TDCM1) and amplification using an erbium doped fiber amplifier (EDFA). After power adjustment using variable optical attenuators (VOAs), the signal, idler and pump were recombined and launched into span 1 consisting of 80 km of SSMF.

After span 1, the signal, idler and pump were separated from each other. A variable delay line was used to compensate for the different propagation delays experienced by the signal and idler in span 1. A VOA in the idler path was used for equalizing the signal and idler powers at the input of the PSA. The three PCs were used to align the signal, idler and pump state-of-polarizations (SOPs) before the PSA. The signal and idler were combined and subsequently dispersion post-compensated in TDCM2. The received signal and idler powers were kept constant using a VOA
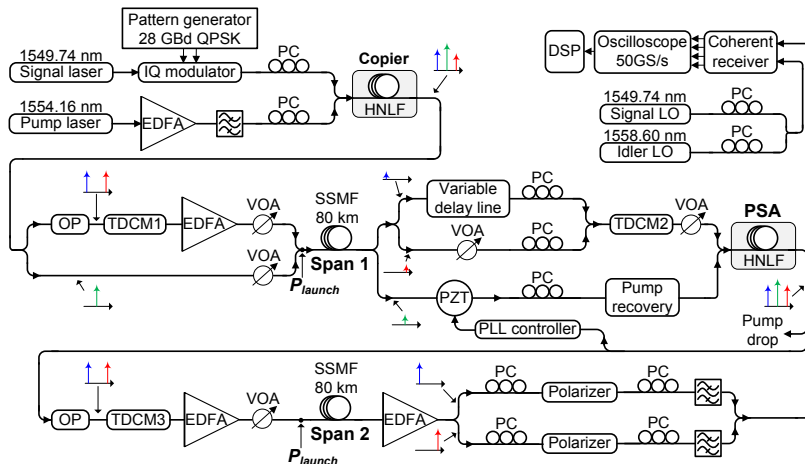

Fig. 4. The experimental setup used for two-span PSA link measurements. Acronyms are explained in the text.

to ensure a fixed OSNR after the PSA. A piezoelectric transducer (PZT) and a phase-locked loop (PLL) controller was used to dynamically adjust the relative phase between signal, idler and pump so that the PSA gain was maximized. A pump recovery stage was used to regenerate and amplify the pump using optical injection-locking [15]. The pump, signal and idler were recombined and launched into the PSA. The PSA on-off gain was 20 dB.

After the PSA, the pump was dropped and the signal and idler were passed through an OP for power adjustments, so that the signal and idler powers launched into span 2 were equal. TDCM3 was used for dispersion pre-compensation of span 2 and an EDFA followed by a VOA was used for setting the signal and idler powers launched into span 2, that consisted of 80 km SSMF. The launch powers P_{launch} of signal and idler were set equal before both spans. After span 2, the signal and idler were amplified using an EDFA and split into two separated paths. Polarization controllers (PCs), polarizers and filters were used before the receiver for the removal of non-co-polarized amplifier noise and to adjust the SOPs of signal and idler so that they were orthogonal. After recombining the signal and idler, they were coherently detected using a dual-polarization hybrid in the receiver and sampled at 50 GS/s before being processed in DSP. Span 2 dispersion post-compensation and coherent superposition was performed electronically in DSP. It has been demonstrated that SPM mitigation in a single-span link is performed equally well all-optically using a PSA and electronically in DSP [16].

3.2. Experimental results

The two-span optimized (5%, 35%) and one-span optimized (15%, 15%) dispersion map configurations were compared. It should be noted that the used dispersion maps were not optimized experimentally and the selection was based on the simulation results, limited in accuracy mainly by the dispersion compensation step size of 5% and the chosen loss parameter α. In Fig. 5(a) the experimentally measured EVM values as a function of signal launch power for the two different dispersion map scenarios are shown. The two-span optimized dispersion map configuration (5%, 35%) outperforms the one-span optimized dispersion map configuration (15%, 15%) case. The highest EVM performance improvement, 1.4 dB, is observed at 13 dBm signal launch power. This lower EVM improvement compared to the simulation results, where an EVM improvement of 2.3 dB was predicted, is attributed to amplifier noise that was present in the system and the fact that the optimum dispersion map was not experimentally optimized.
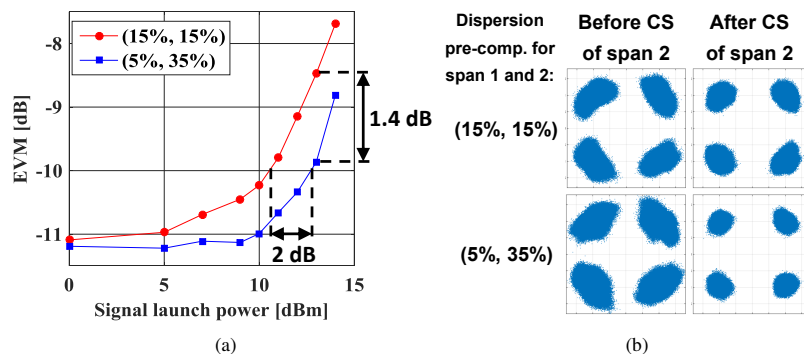

Fig. 5. Measured (a) EVM versus signal launch power for two dispersion map configurations, (b) constellation diagrams showing the signal before and after CS of span 2 at 13 dBm signal launch power.

In Fig. 5(a), we also see that the two-span optimized dispersion map configuration shows 2 dB higher launch power tolerance at an EVM of -10 dB. The calculated nonlinear phase shift is 1.1 radians at 13 dBm signal launch power.

Figure 5(b) shows constellation diagrams for the two dispersion map scenarios before and after CS of span 2 at 13 dBm launch power. Before CS of span 2, the constellations are more severely distorted for the (5%, 35%) dispersion map configuration than for the (15%, 15%) dispersion map configuration. However the opposite is true after CS of span 2, where the (5%, 35%) dispersion map configuration shows less distorted constellations. This confirms the simulation results and shows that the optimal dispersion map does not minimize the interplay between GVD and SPM effects which is the case in ordinary dispersion managed single-channel QPSK PIA transmission links [11]. However, in the two-span dispersion map optimized PSA link, the nonlinear distortions on the signal and idler are correlated to a higher degree compared to the one-span dispersion map optimized case, resulting in a more efficient mitigation of nonlinear distortions by the CS of span 2.

4. The impact of residual dispersion in PSA

Simulations of one-span and two-span PSA links were conducted where, in addition, residual dispersion per span was allowed to be non-zero. The same simulation model as illustrated in Fig. 1 was used, but with the difference that the dispersion post-compensation was performed to under- or overcompensate the dispersion by given values. In the one-span PSA link, the DSP processing and EVM calculation was done after the first PSA. Figure 6 shows EVM performance as a function of total dispersion compensation and dispersion pre-compensation for a one-span PSA link. Dispersion compensation values were swept with a step size of 5%. Figure 6 shows that without residual dispersion the best EVM performance of -11.8 dB is achieved at a dispersion pre-compensation value of 15%. However, the EVM can be enhanced 0.8 dB by setting the dispersion pre-compensation value to 20% and introducing 10% residual dispersion, meaning 90% total dispersion compensation before CS in a one-span PSA link.

Figures 7(a) and 7(b) show the EVM performance assuming that the total dispersion compensation value in both spans of a two-span PSA link are varied. In Fig. 7(a) the one-span optimized dispersion map with 15% dispersion pre-compensation applied in both spans (15%, 15%) is
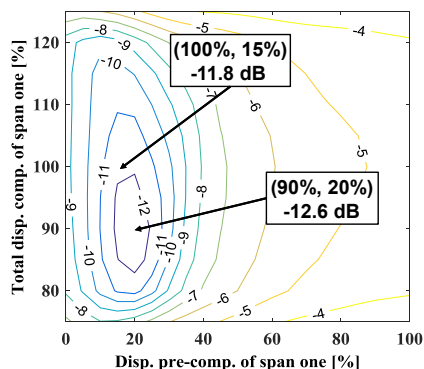

Fig. 6. Simulation results showing EVM of a one-span PSA amplified link at 12 dBm signal launch power where the span total dispersion compensation percentage is indicated on the y-axis and dispersion pre-compensation values on the x-axis.
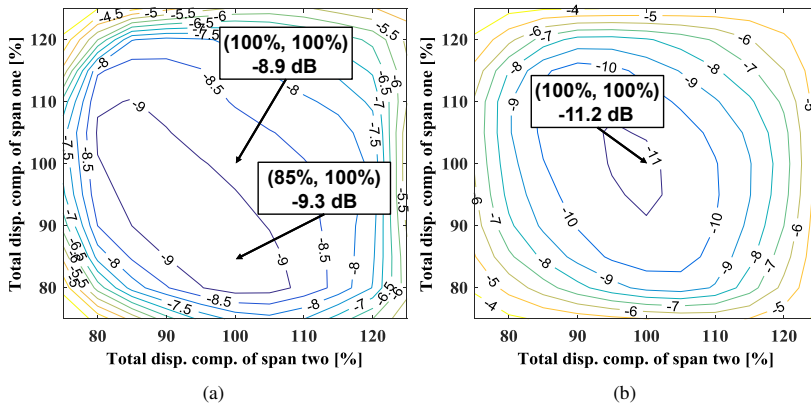
Fig. 7. Two-span PSA amplified link simulation results at 12 dBm signal launch power showing the EVM performance as a function of total dispersion compensation applied before CS of span 1 and 2 with (a) one span optimized (15%, 15%) and (b) two-span optimized (5%, 35%) dispersion map configurations.

shown. By allowing extra degrees of freedom by different total dispersion compensation values in both spans, the EVM performance can be improved by 0.4 dB, if 15% residual dispersion in span 1 is applied compared to the fully dispersion compensated spans case. In Fig. 7(b) the two-span optimized dispersion map configuration (5%, 35%) is shown with varied total dispersion compensation values. As can be seen, allowing for residual dispersion in the two-span optimized dispersion map case does not improve the EVM performance further. The two-span PSA link with optimized dispersion map shows, however, 1.9 dB better EVM performance than one-span optimized two-span PSA link with residual dispersion in both spans allowed.

5. Long-haul simulations

The optimized two-span PSA link dispersion map (5%, 35%) was applied repeatedly in long-haul transmission simulations and compared with the one-span optimized dispersion map, where the same 15% dispersion pre-compensation was applied in every span. In Fig. 8(a), EVM as a function of transmission distance for two dispersion map scenarios are shown at 9 dBm signal launch power. The two-span optimized case shows 2.1 fold increase in the transmission distance (23 spans) compared to the one-span optimum case (11 spans) at an EVM level of -5 dB. The two-span optimized dispersion map outperforms one-span optimized case after the first span. During the first decade of spans, the EVM fluctuations after the even number of transmitted spans for the two-span optimized case are well observable.

A long-haul transmission comparison at optimal launch power in the presence of amplifier noise with a PSA noise figure of 1 dB [1] is shown in Fig. 8(b). The optimal launch power for the two-span optimized case is 2 dB higher than in the one-span optimized case and the reach increase is 1.5 times, 289 spans compared to 197 spans with single-span optimized case at an EVM level of -5 dB. The results of Figs. 8(a) and 8(b) were also verified with bit error ratio (BER) simulations that show approximately the same distance improvement factors at BER = 10^{-3} for both cases.

Figure 9 shows the constellation diagrams as a comparison of the two dispersion map optimized cases illustrated in Fig. 8(a) at 9 dBm signal launch power and in Fig. 8(b) at optimal signal
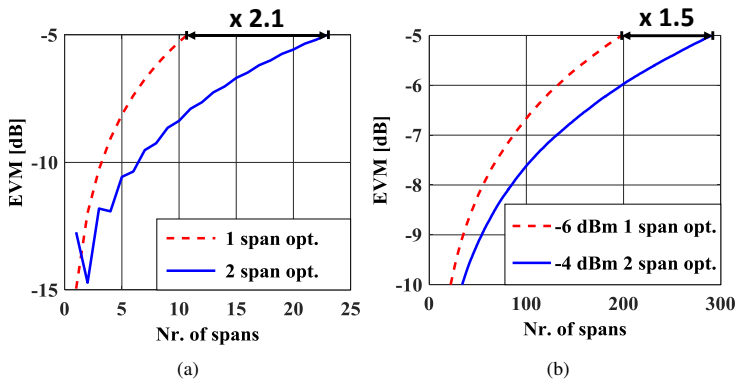
Fig. 8. Simulation results for long-haul transmission showing EVM as a function of propagated distance in spans, comparing one-span optimized and two-span optimized dispersion maps (a) at 9 dBm signal launch power and (b) at optimal launch power in the presence of amplifier noise.
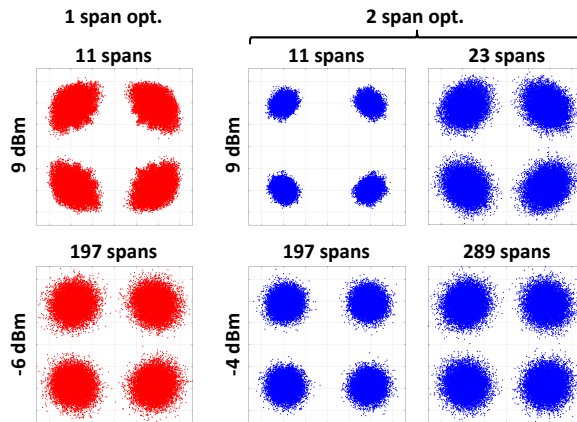

Fig. 9. Constellation diagrams of long-haul PSA transmission link simulations comparing one-span and two-span optimized dispersion maps at 9 dBm signal launch power and at optimal launch powers.

launch powers. The constellations of two optimized dispersion maps in Fig. 9 are compared at transmission reach, where the EVM level is -5 dB. These constellations show similarly that at the same transmission reach, the constellations are less distorted using two-span optimized dispersion map and the reach can be extended up to 2.1 times at 9 dBm signal launch power and up to 1.5 times at optimal signal launch powers to achieve equally distorted contellations compared to the one-span optimized dispersion map in a long-haul transmission link.

6.   Conclusion

The optimized dispersion map configuration for a two-span single-channel 28 GBaud QPSK PSA amplified link was investigated in simulations and verified by an experimental study. Using the same amount of dispersion pre- and post-compensation values for both spans is suboptimal with respect to the efficiency of mitigating nonlinear distortions by span-wise CS. Also the means to optimize dispersion map of a conventional dispersion managed PIA transmission link, do not apply for the dispersion map optimization of the two-span PSA link. Allowing residual dispersion per span does not improve the performance of two-span dispersion map optimized PSA links. Simulation results show that applying two-span optimized dispersion map repeatedly in a long-haul transmission can improve the maximum transmission reach by a factor of 1.5 compared to the one-span dispersion map optimized long-haul PSA amplified transmission.

Funding

Paper C

Four-span dispersion map optimization for improved nonlinearity mitigation in phase-sensitive amplifier links

E. Astra, H. Eliasson and P. A. Andrekson, in Proc. European Conference on Optical Communication (ECOC), Gothenburg, Sweden (2017): paper P2.SC6.14.

Four-Span Dispersion Map Optimization for Improved Nonlinearity Mitigation in Phase-Sensitive Amplifier Links

Egon Astra[1], Henrik Eliasson[2], Peter A. Andrekson[1,2]

[1] Thomas Johann Seebeck Department of Electronics, Tallinn University of Technology, Tallinn, Estonia, egon.astra@ttu.ee

[2] Photonics Laboratory, Department of Microtechnology and Nanoscience, Chalmers University of Technology, Gothenburg, Sweden.

Abstract *The first investigation of a four-span dispersion map optimization for PSA links is presented. We show numerically, that the maximum transmission reach improves 2.1 times, if four-span optimized dispersion maps are used repeatedly instead of single-span optimized maps.*

Introduction

Phase-sensitive amplifiers (PSAs) are an interesting research topic for long-haul fiber-optic transmission systems due to their ultra-low noise amplification property as well as their ability to mitigate nonlinear distortion. The quantum-limited noise figure (NF) of a PSA is 0 dB, in practice a NF of 1.1 dB has been reported[1]. A recent experimental study for a single-channel PSA link showed that the maximum transmission reach can be extended up to three times[2], if PSAs are used as inline amplifiers instead of phase-insensitive amplifiers (PIAs) in a dispersion-managed link.

The nonlinearity cancellation in a two-mode PSA link is possible due to correlated nonlinear distortion on the signal and its phase conjugate - the idler. A PSA that operates in a high-gain regime performs coherent superposition (CS) of the signal and idler waves during the phase-sensitive amplification process[4]. In the case of pure self-phase modulation (SPM) rotation, correlated distortions on the signal and idler will convert into amplitude distortions[3,4].

The dispersion management profile of a fiber-optic transmission system plays an important role for the overall link performance degradation due to nonlinearities[5]. The dispersion map optimization of a PSA link has been investigated for single-span PSA links[3,4] and a single-span optimized dispersion map has been used for multi-span PSA links[2,6], i.e. applying the same span dispersion map in every span of a PSA link.

In[7], it was shown that the nonlinearity mitigation performance of a two-span PSA link can be improved by allowing different span dispersion maps in the two spans. In this paper, we show in numerical simulations that the nonlinearity mit-

igation performance can be improved further by optimizing the dispersion map over three or four spans in a PSA link.

Simulation model

A simplified schematic of the simulation model for the PSA-amplified transmission link is shown in Fig. 1. The model consists of a transmitter, N PSA-amplified dispersion-managed transmission spans and a receiver. At the transmitter, a 28 GBd QPSK signal S and idler I were generated. The idler was generated as a conjugated copy of the signal I=S*. Before and after each standard single mode fiber (SSMF) span, dispersion pre- and post-compensation was applied in dispersion compensating modules (DCMs) by values $D_{pre,n}$ and $100\% - D_{pre,n}$ meaning that each span was fully dispersion compensated. The index n shows the span number and n=1...N, where N is the total number of spans in the transmission link. The DCMs were considered linear and lossless.

Before the SSMF, the signal and idler launch powers P_{in} were adjusted to be equal in every transmission span. The launch power was given per channel, meaning that the total power of signal and idler was 3 dB higher. The SSMF parameters were length L = 80 km, loss α = 0.2 dB/km, dispersion parameter D = 17 ps/nm/km and nonlinear coefficient γ = 1.27 W^{-1}km^{-1}. The propagation of light in the SSMF was modeled using a split-step Fourier method (SSFM) solution of the nonlinear Schrödinger equation (NLSE). It was assumed that the cross-phase modulation (XPM) between the signal and idler was negligible compared to SPM due to their wavelength separation of 8 nm, therefore the waves were co-propagated using two separate NLSEs with the same propagation parameters.
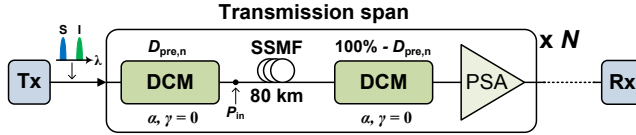
The phase-sensitive amplification process was

Fig. 1: The simulation model for a PSA-amplified transmission link. Acronyms are explained in the text.

modeled using a simplified model[4,8] under the assumptions that the PSAs were operating in a high-gain regime with low signal input powers. The total gain of the PSAs was adjusted to compensate for the span loss. After N transmission spans, the signal was detected in the receiver for error vector magnitude (EVM) or bit error ratio (BER) calculations.

In the long-haul simulations, amplifier noise was added with a PSA NF of 1.1 dB[1] to the signal and idler. In the simulations at 9 dBm launch power, no amplifier noise was added in order to avoid unwanted nonlinear phase noise (NLPN) effects. Also the effects of laser phase noise, polarization and higher order dispersion were neglected in all simulations to only observe the impact of the dispersion map on the efficiency of the mitigation of SPM induced nonlinear distortions.

Dispersion map optimization

Dispersion maps were optimized for one, two, three and four-span PSA links at 9 dBm launch power. The dispersion pre-compensation values were varied in steps of 5% for all the four cases. For the one- and two-span links, the dispersion pre-compensation sweep-ranges were -20% to 80%, resulting in 21 dispersion maps for the one-span link and 441 dispersion maps for the two-span link. For three-span optimization, the total number of link dispersion maps would be 9261, which requires a significant computational effort. Therefore the optimization for three- and four-span links was done using smaller sweep ranges. Due to the 5% accuracy in dispersion compensation step size, we expect that the results shown below can be improved somewhat further. It is also possible that the sensitivity of the EVM due to dispersion compensation step size increases with optimization over more spans. We also note that since we restrict the ranges of the dispersion pre-compensation for optimization over three and four spans, we can not claim for certain that we have actually found the global optimum. It is possible that the best four-span dispersion map found is a local optimum.

The results of the dispersion map optimization of one, two, three and four-span PSA links are
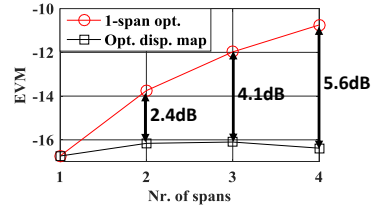

Fig. 2: EVM vs. number of spans showing the performance of the one-span and one to four-span dispersion map optimized PSA links.
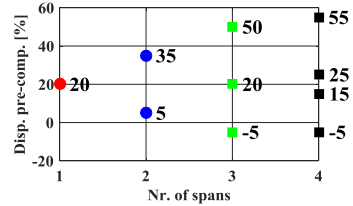

Fig. 3: The found optimum dispersion pre-compensation values for dispersion map optimized PSA links.

shown in Figs. 2 and 3. Figure 2 shows that the EVM improvement increases with increasing number of optimized spans compared to the one-span optimized link. The EVM improvement achieved from the four-span dispersion map optimization in a four span link is 5.6 dB compared to the one-span optimized link.

The optimized dispersion map values are shown in Fig. 3. The optimized values starting from two spans are evolving symmetrically around the one-span optimum 20% value as the number of spans is increased to four spans. No significant EVM difference was noticed, if the ordering of dispersion pre-compensation values was altered. For example, the dispersion pre-compensation values (50%, 20%, -5%) from the first to the third span in a three span link resulted approximately the same EVM values as (-5%, 20%, 50%) or (50%, -5%, 20%) dispersion maps. In the following simulations, a decreasing order of the dispersion pre-compensation values for repeatedly applied optimized dispersion map configurations has been used.

Highly nonlinear transmission regime

The signal EVM during propagation in a transmission link up to 12 spans using the four optimized dispersion map cases repeatedly in a highly non-
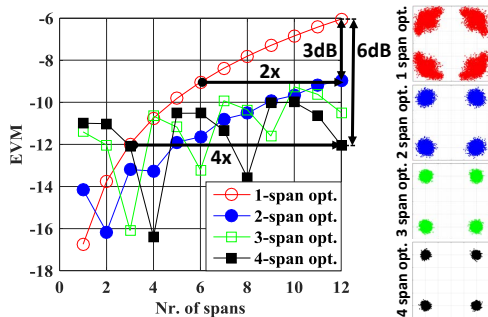
Fig. 4: The simulation results up to 12 spans showing the propagation of one to four-span dispersion map optimized PSA links and constellations in a highly nonlinear regime.

linear regime at 9 dBm launch powers is shown in Fig. 4. After 12 spans, the PSA link with the two-span optimized dispersion map provides 3 dB better EVM and the four-span optimized link offers 6 dB better EVM compared to the one-span dispersion map optimized PSA link. Also the reach extensions compared to the one-span optimized link are two times higher at EVM = -9 dB for the two-span optimized and four times higher at EVM = -12 dB for the four-span dispersion map optimized PSA link.

On the right side of Fig. 4 are shown constellation diagrams after propagation of 12 spans for the four dispersion map cases. The constellations show that in a highly nonlinear regime, the right choice of PSA link dispersion map can lead to a significant improvement of the nonlinearity mitigation performance for a 28 GBaud QPSK signal.

Long-haul simulations

Long-haul simulations were performed for one, two and four-span dispersion map optimized PSA links at optimum launch powers. The maximum transmission reaches, shown in Fig. 5 for the one, two and four-span optimized dispersion map cases, are 316, 430 and 652 spans respectively at BER = 10^{-3}. The transmission reach improvements are approximately 1.4 times for the two-span optimized case and 2.1 times for the four-span optimized case compared to the one-span optimized case. Also the constellations shown in Fig. 5 at BER = 10^{-3} have visibly nonlinearly distorted characteristics for the one-span optimized case. We expect that the maximum transmission reach can be extended further if the dispersion map is optimized over more than four spans.

Conclusions

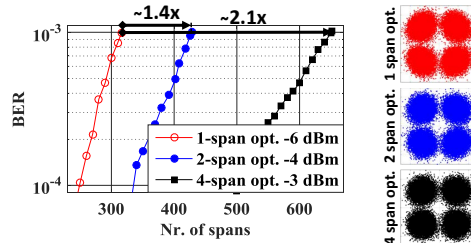A dispersion map optimization for one- to four-span dispersion map optimized PSA links was

Fig. 5: Long-haul simulation results showing the BER vs. number of propagated spans and constellation diagrams at BER = 10^{-3} for one-, two- and four-span dispersion map optimized PSA links at optimum launch power.

carried out numerically. A significant EVM improvement of 6 dB due to improved nonlinearity mitigation was observed when comparing one- and four-span optimized links in a highly nonlinear regime. At optimum launch powers, a transmission reach improvement of approximately 2.1 times for the four-span optimized link compared to the one-span dispersion map optimized PSA link was achieved. The results show that it is possible to increase the transmission reach of a PSA link substantially by optimizing the dispersion map over an increasing number of spans.

Acknowledgements

References

[1] Z. Tong et al., "Towards ultrasensitive optical links enabled by low-noise phase-sensitive amplifiers," Nat. Photonics, Vol. **5**, no. 7, p. 430 (2011).

[2] S. L. I. Olsson et al., "Long-Haul (3465 km) Transmission of a 10 GBd QPSK Signal with Low Noise Phase-Sensitive In-Line Amplification," Proc. ECOC, PD.2.2, (2014).

[3] B. Corcoran et al., "Mitigation of Nonlinear Impairments on QPSK Data in Phase-Sensitive Amplified Links," Proc. ECOC, We.3.A.1, (2013).

[4] S. L. I. Olsson et al., "Phase-Sensitive Amplified Transmission Links for Improved Sensitivity and Nonlinearity Tolerance," J. Lightwave Technol., Vol. **33**, no. 3, p. 710 (2015).

[5] Y. Frignac et al., "Average Optical Phase Shift as an Indicator of the Dispersion Management Optimization in PSK-Modulated Transmission Systems," Photon. Technol. Lett., Vol. **22**, no. 20, p. 1488 (2010).

[6] H. Eliasson et al., "Mitigation of nonlinear distortion in hybrid Raman/phase-sensitive amplifier links," Opt. Express, Vol. **24**, no. 2, p. 888 (2016).

[7] E. Astra et al., "Dispersion Map Optimization for Nonlinearity Mitigation in Two-Span Phase-Sensitive Amplifier Links," Proc. ECOC, Th.1.A.3, (2016).

[8] S. L. I. Olsson et al., "Nonlinear phase noise mitigation in phase-sensitive amplified transmission systems," Opt. Express, Vol. **23**, no. 9, p. 11724 (2015).

Improved mitigation of self-phase modulation induced impairments in 28 GBaud phase-sensitive amplified links

Improved mitigation of self-phase modulation induced impairments in 28 GBaud phase-sensitive amplified links

Egon Astra,[1,*] Henrik Eliasson,[2] Toomas Ruuben,[1] and Peter A. Andrekson[2]

[1]*Thomas Johann Seebeck Department of Electronics, Tallinn University of Technology, Tallinn, Estonia*
[2]*Department of Microtechnology and Nanoscience, Photonics Laboratory, Chalmers University of Technology, Göteborg, Sweden*
*egon.astra@ttu.ee

Abstract: The improved mitigation of self-phase modulation (SPM) induced nonlinear impairments by the use of a multi-span dispersion map optimization in 28 GBaud phase-sensitive amplifier (PSA) links is numerically investigated. We show that a four-span dispersion map optimized PSA link provides 2.1 times reach improvement over a single-span optimized PSA link with a total nonlinear phase shift tolerance increase from 2.1 radians to 8.8 radians. Furthermore, the optimized PSA link increases the maximum transmission reach by 6.9 times compared to a single-span optimized in-line dispersion managed phase-insensitive amplifier (PIA) link and 4.3 times reach extension is achieved compared to a dispersion unmanaged PIA link.

1. Introduction

Phase-sensitive amplifiers (PSAs) are known for their ability to increase transmission system performance [1, 2], mainly limited by amplifier noise and fiber nonlinearities in fiber-optic links [3–5]. This is possible due to the combined ultra-low noise amplification and nonlinearity mitigation capability of PSAs [2, 6]. PSAs quantum-limited noise figure (NF) is 0 dB [7, 8] and a NF of 1.1 dB has been reported in experiments [9, 10]. In contrast, conventional phase-insensitive amplifiers (PIAs) have a quantum-limited NF of 3 dB [7]. A recent experimental study showed 5.6 times transmission reach improvement by using PSAs instead of PIAs such as erbium-doped fiber amplifiers (EDFAs) in an in-line dispersion managed 10 GBaud fiber-optic link that could tolerate a total accumulated nonlinear phase shift of 6.2 radians [11].

The nonlinearity mitigation effect in a frequency non-degenerate two-mode (signal and it's phase conjugated wave, called the idler, at different wavelengths [12]) PSA link is similar to the nonlinearity mitigation of a phase-conjugated twin-wave (PCTW) approach, where signal and idler waves can be transmitted on different polarizations, wavelengths or time-slots [13–15]. Signal and idler waves are both co-propagated through a nonlinear transmission medium, where they experience nonlinear distortions during propagation. The nonlinearity mitigation is performed in a coherent superposition (CS) process where a signal wave and an idler wave, that is phase conjugated again during the process, are coherently superposed. In a PSA link, the CS is performed during a parametric phase-sensitive amplification process by a PSA, where correlated phase distortions on signal and idler waves are converted into smaller amplitude distortions, resulting in a phase-to-amplitude distortion conversion and a self-phase modulation (SPM) mitigation [2].

After the introduction of electronic dispersion compensation (EDC), coherent fiber optic links with in-line dispersion compensation were outperformed by EDC links without in-line dispersion management [16, 17]. However, PSA links need in-line dispersion management to fulfill the phase-matching criteria for a phase-sensitive amplification process [2]. Much work

regarding the dispersion map optimization for in-line dispersion compensated PIA links has been carried out [18–20], but these principles are not directly applicable to PSA links, since the effectiveness of the nonlinearity mitigation in PSA links is highly dependent on correlation properties of propagated signal and idler waves. It has been shown previously that the dispersion management for a single-span dispersion map optimized PSA link [2, 11, 21] and for a two-span dispersion map optimized PSA link [22] plays an important role for the nonlinearity mitigation performance. The importance of dispersion map optimization for twin-waves was first noted in [13], where according to the first-order perturbation theory, a symmetric span power map with an anti-symmetric dispersion map should be used for the best nonlinearity mitigation performance for the PCTW approach. In [23] it was experimentally shown that 50% dispersion pre- and post-compensation for a Raman assisted PSA link with almost power-symmetric fiber spans results in an increased nonlinearity mitigation performance. However, in our study, PSA links with lumped amplification are under investigation and therefore different dispersion map optimization assumptions have to be used.

In [24], it was shown numerically that the nonlinearity mitigation performance of a 28 GBaud PSA link can be significantly increased by allowing different span dispersion maps to be used in a multi-span dispersion map optimization. A dispersion map was optimized up to four spans with a dispersion compensation value step precision of 5% that resulted in 2.1 times PSA transmission system maximum reach increase compared to a single-span optimized PSA link. In this paper, we investigate by numerical simulations a 28 GBaud PSA link dispersion map optimization up to four spans with an optimization step precision of 1% and compare these results with 5% optimization precision results in a long-haul transmission. Furthermore, the dispersion map optimized PSA link maximum long-haul transmission reaches are compared with conventional EDFA long-haul transmission link maximum reaches with dispersion in-line compensated and in-line uncompensated EDC links. The SPM mitigation is also investigated for a wavelength-division multiplexing (WDM) system scenario where the wavelength separation between signal and idler waves increases with the increasing number of channels, therefore resulting in increasingly different dispersion parameter values for signal and idler wavelengths.

2. General simulation model

The simulation model that was used is shown in Fig. 1. The model consists of a transmitter, N PSA or PIA amplified and dispersion-managed transmission spans and a receiver. At the transmitter, a 10 GBaud or 28 Gbaud quadrature phase-shift keying (QPSK) modulated signal S was generated. The generated signal waveform was a non-return-to-zero (NRZ) signal oversampled to 32 samples per symbol and filtered with a 5th order Bessel filter characteristic with 75% full width half maximum (FWHM) bandwidth of the used symbol rate. In all simulations single-channel and single-polarization signals were used. After the signal waveform generation, the signal was divided between upper and lower path, where the latter was used to generate the idler I through an ideal conjugation of the signal I=S* if a PSA implementation was desired. No wavelength conversion in the conjugation process was made, as signal and idler waves were separately propagated assuming a 8 nm wavelength separation. Separate propagation was used to neglect inter-channel nonlinear effects between signal and idler channels and to focus only on the PSA performance of mitigating the SPM effects. The launch powers P_{in} of signal and idler were set by an ideal and noiseless amplification before they were launched into the transmission span. The launch power is given per signal and per idler, resulting in a 3 dB higher total launch power.

After the waveforms were launched into the transmission span, they were dispersion pre-compensated before and post-compensated after each standard single mode fiber (SSMF) in the dispersion compensating modules (DCMs) by values $D_{pre,n}$ and $100\% - D_{pre,n}$ meaning that each span was fully dispersion compensated. The simulated DCMs were ideal (linear and lossless). The index n shows span number, where N is the total number of spans in the
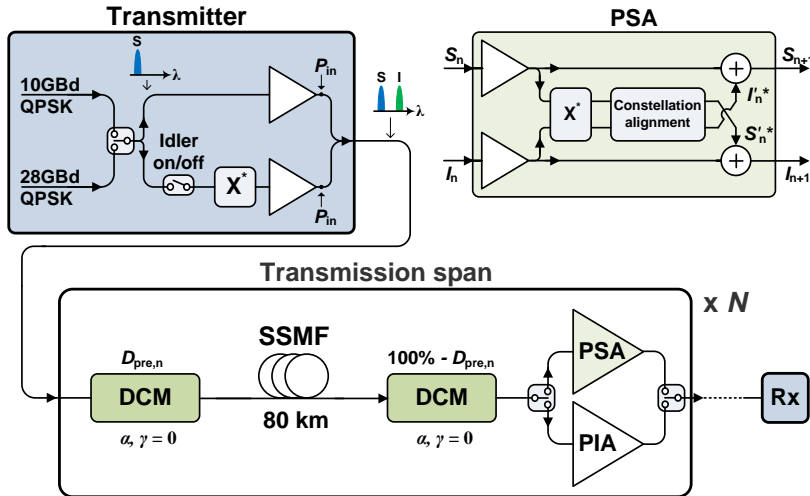
Fig. 1. The simulation model for a PSA or a PIA amplified transmission link. Acronyms are explained in the text.

transmission link and n=1...N. The simulated SSMF length was 80 km. The SSMF parameters were loss α = 0.2 dB/km, dispersion parameter D = 17 ps/nm/km and nonlinear coefficient γ = 1.27 $W^{-1}km^{-1}$. The propagation of light in the SSMF was modeled by using two separate (for signal and idler waveform) split-step Fourier method (SSFM) solutions of the nonlinear Schrödinger equation (NLSE). For simplicity and better understanding, the used group velocity dispersion (GVD) parameter β_2 was same for signal and idler waves, if not stated otherwise. In [2] and [22] it is noted that different GVD parameter value for a 8 nm wavelength separation does not have significant impact on the SPM induced nonlinearity mitigation performance of a PSA link.

At the end of each transmission span, the loss of the transmission span was compensated by PSA or PIA amplification. The in-line amplifiers used in the simulations were ideal and noiseless, unless it is stated otherwise by the given NFs. The phase-sensitive amplification process was modeled using a simplified model, shown in Fig. 1, under the assumptions that the PSA was operating in a high-gain regime with low signal input powers [2, 6]. The signal S_n and idler I_n are both amplified by the gain necessary to compensate the span loss and then separated for conjugation and constellation alignment processes. As a result of the constellation alignment process, constellations of the conjugated signal S_{n*} and idler I_{n*} are rotated by introducing the necessary phase-shift to maximize the power after coherent addition of signal S_n and conjugated and rotated idler I'_{n*} in the upper arm and coherent addition of idler I_n and conjugated and rotated signal S'_{n*} in the lower arm resulting in a phase-sensitively amplified signal S_{n+1} and idler I_{n+1} waveforms. The transmission span amplifier noise was added only in the long-haul simulations with a PSA NF=1.1 dB [9] to signal and idler and a 3 dB higher NF=4.1 dB was used for PIA case [7, 8]. In the PSA simulation model, the uncorrelated additive Gaussian noises were added to signal and idler waves in the amplification stage at the PSA model input shown in Fig. 1, by following a general output noise formula of a PSA that is based on semi-classical theory of quantum mechanical system under the high-photon-number assumption described in [25]. For

all of the other simulations, no amplifier noise was added in order to avoid unwanted nonlinear phase noise (NLPN) effects. It should be noted that also the effects of laser phase noise and polarization were neglected in all simulations to only observe the impact of the dispersion map on the efficiency of the mitigation of SPM induced nonlinear distortions.

After N transmission spans, the signal waveform was detected in the receiver Rx for error vector magnitude (EVM) [26] or bit error ratio (BER) estimation. A conventional receiver for detecting QPSK signals was used, consisting of a down-sampler to 2 samples per symbol, a channel equalizer deploying constant modulus algorithm (CMA) and the Viterbi-Viterbi phase recovery algorithm to align constellation for EVM or BER calculations.

3. 28 GBaud QPSK PSA link dispersion map optimization

3.1. Dispersion map optimization procedure

The dispersion map optimization was carried out for one, two, three and four-span 28 GBaud QPSK PSA links. In this paper, the optimized dispersion pre-compensation values were found with a precision of 1% and compared with values from a 5% optimization precision procedure that was presented in [24]. For the optimization procedure, PSA links with different dispersion map configurations were simulated. The dispersion map configuration is determined here by the dispersion pre-compensation value, that is swept and the post-compensation value is automatically adjusted assuming that transmission span is 100% dispersion compensated. As a result of the simulation, an EVM metric was calculated and the dispersion map configuration of a PSA link with the lowest EVM value was selected as an optimal solution. The signal launch power was set to 9 dBm for all cases to assure a sufficient EVM level for comparison.

For the one-span PSA link optimization procedure, the dispersion pre-compensation value was swept from -20% to 80% resulting in 101 dispersion map scenarios with an optimization step accuracy of 1%. For a two-span PSA link, the dispersion pre-compensation value for the span one was swept from -40% to 40% and for the span two from 0% to 80%, resulting in 6561 dispersion map scenarios. For the three-span case, coarse sweeps with a precision of 2% were performed over total range of -40% to 100% to estimate the best regions for fine sweeps. The final sweep with 1% precision was performed from -20% to 0% for the span one, 10% to 30% for the span two and 42% to 62% for the span three, resulting in 9261 dispersion maps. Also for the four-span optimization, coarse sweeps with a precision of 5% and 2% were first performed over total range of -40% to 100% to find the best sweep regions for fine sweeps. Also the fine sweeps with 1% precision were performed over multiple sweep ranges where a sweep for a span consisted of 11 points resulting in 14641 dispersion maps for one optimization sweep run of four-span optimization.

It should be noted that it is possible that the found optima for three and four-span optimization are local optima and we cannot claim for certain that we have found the global optimum, since sweep ranges of a dispersion map optimization are restricted. However, by brute forcing simulations for three and four-span PSA link dispersion map optimization over large sweep areas for every span leads to an unrealistic computational effort. For example a four-span optimization with a 1% precision over a range of -20% to 80% for all the four spans, results in over 104 million different dispersion map configurations.

3.2. Dispersion map optimization results

The comparison between 5% and 1% optimization step precision of one to four-span dispersion map optimization at a signal launch power of 9 dBm is shown in Fig. 2(a). The 1% precision optimized dispersion maps compared to the 5% optimized maps show clear EVM improvement with every number of dispersion map optimized spans. In fact the 1% optimization precision for the four-span dispersion map optimized case is 0.3 dB better in terms of EVM than in 5%
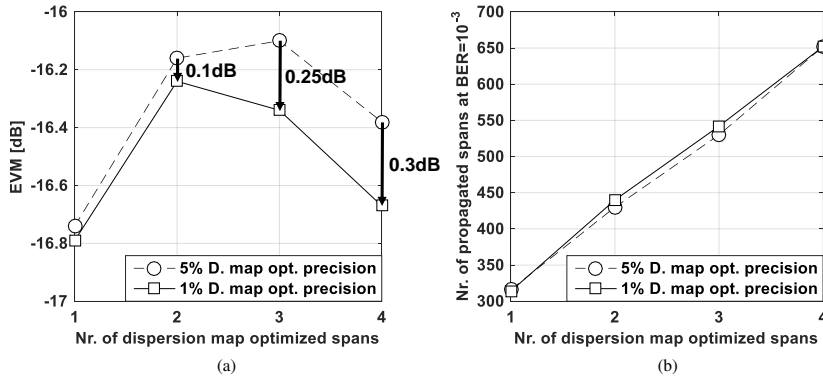
Fig. 2. Simulation results showing (a) EVM performance comparison of 5% and 1% optimization precision at a signal launch power of 9 dBm and (b) maximum number of propagated spans at BER = 10^{-3} at optimal launch power comparison between PSA dispersion map optimization precision steps of 5% and 1% as a function of number of dispersion map optimized spans.

steps optimized dispersion map case. Furthermore the four-span optimized dispersion map case with an optimization precision of 1% results in a significant nonlinearity mitigation performance where the signal quality in terms of EVM after a propagation of four spans is only 0.15 dB worse than the best scenario for single-span PSA link. It means that the PSA link reach can be fourfold increased for a fixed launch power in a highly nonlinear regime if four-span optimized dispersion maps are used.

Despite the short-haul links with a 1% optimization precision step up to four span optimization show improved results, it turns out that in long-haul propagation studies (see simulation details in section 4), these dispersion map optimized links show no significant improvement with the higher optimization precision. Figure 2(b), where dispersion map optimized spans for 1% and 5% optimization precision are used repeatedly at optimal launch powers, shows that a 1% precision in a dispersion map optimization does not increase the maximal PSA link reach with four-span optimized case. The maximum number of propagated spans with a four-span optimization at BER = 10^{-3} is 652 spans for the both optimization precision cases. However, a slight improvement less than 2.3% for a 1% optimization precision can be seen for the two and three-span optimization cases. The two-span case propagation distance is increased from 430 spans to 440 spans and for the three-span optimization case increase is from 531 spans to 543 spans. It is possible that the nature of the EVM metric can hinder the optimization procedure since nonlinear distortions are not Gaussian distributed. An optimization procedure has also been performed (not shown here) by using the EVM measure only in phase or only in amplitude dimension, but no better optima were found. The usage of the EVM in phase dimension led to the same optimization results as the standard EVM measure. Secondly, the chosen launch power for the optimization was high compared to optimal launch powers that could cause an offset as the dispersion map optimum is slightly power dependent. However the launch power was kept at 9 dBm to ensure the reliability of the EVM metric.

In Fig. 3(a) with a 5% optimization precision and in Fig. 3(b) with a 1% optimization precision dispersion pre-compensation values are shown for the one to four-span optimized dispersion
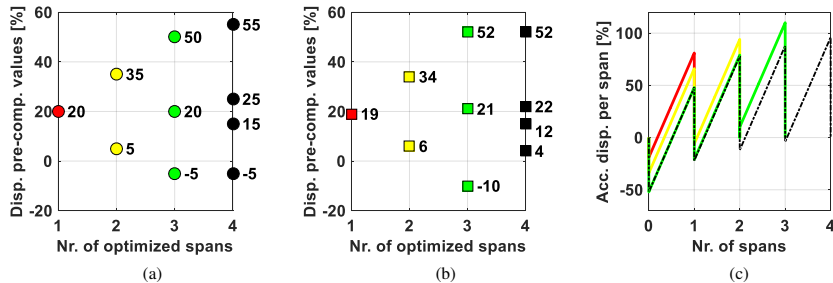
Fig. 3. Dispersion pre-compensation values for one to four-span dispersion map optimized PSA links in (a) 5% and (b) 1% optimization step precision, (c) dispersion maps corresponding to 1% optimization precision for one (red line), two (yellow line), three (green line) and four-span (black dashed line) dispersion map optimized PSA links.

map cases. Figure 3(b) shows that for the one to three-span optimized dispersion map cases with a 1% optimization precision, the dispersion pre-compensation values are expanding more symmetrically than for the 5% optimized case in Fig. 3(a). The opposite is true for the four-span optimized case where the 1% precision case loses its symmetrical and expanding trend compared to the 5% optimized case. However, the 5% and 1% optimized cases perform equally well based on the long-haul transmission simulation results, which show us that multiple dispersion map solutions are available for four-span optimized cases that can have an equal performance. That is not true for one to three-span optimizations where only the one optimum with given dispersion pre-compensation values in Fig. 3(b) is available regardless of the chosen order of dispersion pre-compensation values. It must be noted, that we have not observed (results not shown here) any significant performance difference of short-haul and long-haul simulations if the ordering of dispersion pre-compensation values is altered. Figure 3(c) shows the accumulated dispersion as a function of propagated distance in spans for all the four dispersion map optimization cases with 1% optimization step precision.

This non-improvement of the four-span optimization with a higher optimization step accuracy can lead to a false conclusion that arbitrary values can be chosen for four-span dispersion maps without losing link performance. Figure 4(a) shows an example of the dispersion pre-compensation values for the four-span dispersion map (gray boxes), chosen by following the symmetric and expanding nature of the one to three-span dispersion map optimized values. Figure 4(b) shows the long-haul simulation results comparing the link performances of the chosen dispersion map to the dispersion map optimized PSA link case at BER = 10^{-3}. The long-haul results in Fig. 4(b) show that the performance of the chosen dispersion map drops significantly compared to the optimized case, resulting in a maximum transmission distance of 546 spans that has approximately only the same reach as a three-span optimized long-haul PSA link at BER = 10^{-3}.

4.　Long-haul 28 GBaud transmission comparison of dispersion map optimized PSA and PIA links

Long-haul simulations were performed to compare the maximum transmission distances at BER = 10^{-3} with optimum launch powers for one, two, three and four-span dispersion map optimized PSA links, an in-line dispersion compensated PIA link and a dispersion unmanaged PIA link with EDC as benchmarks. The dispersion unmanaged PIA link with EDC means
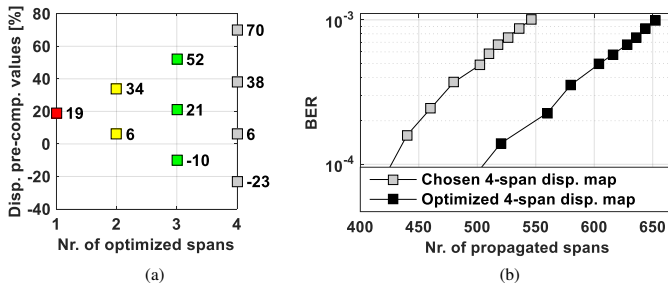
Fig. 4. (a) Dispersion pre-compensation values up to four-span dispersion map optimized PSA links where the dispersion pre-compensation values for the four-span dispersion map case (gray boxes) are chosen by following the symmetric and expanding nature of the one to three-span dispersion map optimized values and (b) BER simulations comparing the long-haul performance of optimized and chosen PSA four-span dispersion map cases.

that the dispersion compensation is unmanaged inside the transmission link, but the dispersion pre-compensation is applied before the link in the transmitter and the post-compensation after the link in the receiver. We chose a NF of the PIA of 4.1 dB, which is about 1 dB larger than what is achievable in practice (quantum limit being 3 dB), while a NF of 1.1 dB was chosen for the PSA. In this way our simulations reflect the 3 dB NF difference in the quantum limit [7, 9], while at the same time reducing the computational effort. We expect that the relative differences between PIA and PSA will still be very similar, compared with a case of using 3 dB and 0 dB NFs, respectively. The dispersion pre-compensation values for an in-line dispersion compensated PIA link have been chosen according to the single-span dispersion map optimized PIA link, that is 15% dispersion pre-compensation and 85% post-compensation in every span. For the EDC PIA case, 50% of all the link accumulated dispersion was pre-compensated before a fiber transmission and 50% of accumulated dispersion was post-compensated after the last span [27, 28].

In Fig. 5 the maximum transmission reaches are shown for PSA and PIA links. The maximum transmission distances of PSA links for one, two, three and four-span dispersion map optimized cases are 316, 440, 543 and 652 spans respectively and for the in-line dispersion compensated PIA link 94 spans and for the PIA EDC link 150 spans at BER = 10^{-3}. The transmission reach of a PSA link can be improved approximately 2.1 times if four-span optimized dispersion maps are used repeatedly instead of a single-span optimized dispersion management throughout the transmission link. It is estimated up to four-span optimization that the improvement factor from multi-span dispersion map optimization is approximately equal to the square-root of the optimized span number, because the increase factors are 1.4, 1.7 and 2.1 for two-, three- and four-span optimized cases respectively compared to single-span optimized PSA case.

A significant transmission distance improvement of approximately 6.9 times is achieved by using a four-span optimized PSA link instead of a single-span optimized and dispersion in-line managed PIA link. However, the latter comparison is not entirely fair as PIA links without in-line dispersion management using EDC are more resilient to nonlinear impairments as can be seen in Fig. 5. That results in 4.3 times maximum transmission distance improvement if a four-span dispersion map optimized PSA link is used instead of a PIA EDC link. It must be noted that we have used ideal DCMs in our simulations for PSA links, but in reality DCMs will add loss and cause additional penalties e.g. due to nonlinearities and non-ideal phase response [29, 30]. Furthermore dispersion unmanaged PIA links with EDC do not require DCMs at all. However, we expect that the maximum transmission reach of a PSA link can be extended further if the
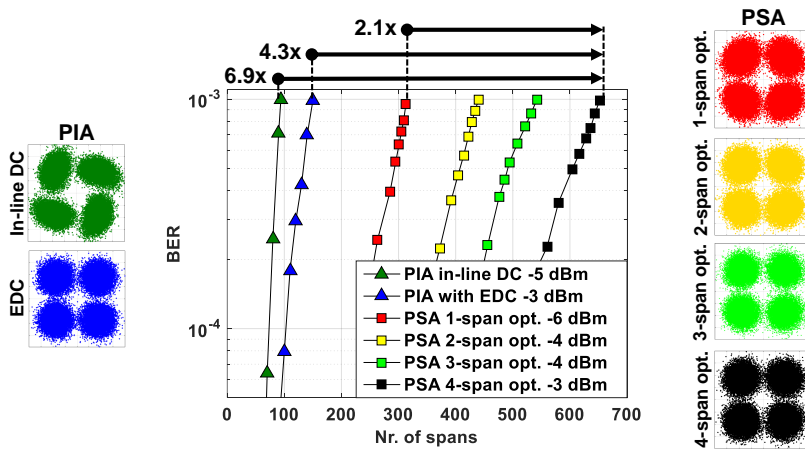
Fig. 5. Long-haul simulation results showing the BER vs. number of propagated spans and constellation diagrams at BER = 10^{-3} for one to four-span dispersion map optimized PSA links and EDFA links with and without an in-line dispersion compensation at optimum launch powers.

dispersion map over more than four spans is optimized.

The constellations are also shown in Fig. 5 for corresponding PSA and PIA links at BER = 10^{-3} level. The in-line dispersion compensated PIA link constellation is the most nonlinearly distorted. Nonlinear characteristics are also more visibly distinguishable for the one-span dispersion map optimized PSA link case than for the four-span optimized case. The four-span dispersion map optimized PSA link constellation is similar to constellation of PIA EDC link without any observable nonlinear characteristics. Using a four-span dispersion map optimized PSA link instead of a single-span optimized link, results in a maximum nonlinear phase shift tolerance fourfold increase from 2.1 radians to 8.8 radians or compared to a two-span optimized link, a maximum nonlinear phase shift tolerance increase from 4.7 radians to 8.8 radians.

5. Necessity of multi-span dispersion map optimization

It has been experimentally shown that a single-channel and single polarization two-mode PSA link at lower transmission speeds, such as 10 GBaud, can result in a remarkable transmission distance improvement of 5.6 times if a PSA link is used instead of an in-line dispersion managed PIA link [11]. However, our simulation study shows that at higher transmission speeds, such as 28 GBaud, a PSA ability to provide a significantly better transmission performance compared to a PIA link in a single-span transmission scenario, does appear to not hold anymore. Figure 6 shows 10 GBaud and 28 GBaud single-span transmission link performance improvements in terms of EVM, if a single-span PSA link is used instead of a single-span PIA link. The single-span optimized dispersion pre-compensation values were used 22% for a PIA and 24% for a PSA case at 10 GBaud and 16% for a PIA and 19% for a PSA case at 28 GBaud. At a symbol rate of 10 GBaud, where the dispersion length is much longer than the span length ($L_D \gg L_{span}$), a PSA link provides approximately 12 dB better EVM performance than a PIA link at 6 dBm signal launch powers. At 28 GBaud, when $L_D < L_{span}$, the improvement by using PSA link instead of a PIA link has diminished by 9.4 dB to a level of 3 dB. This improvement degradation at
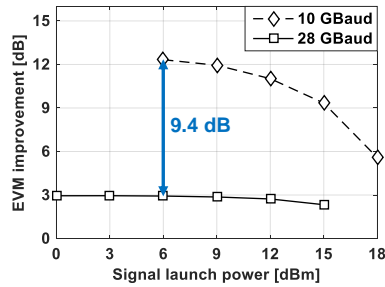
Fig. 6. EVM improvement as a function of signal launch power showing the improvement of using a single-span dispersion map optimized PSA link instead of a PIA link in terms of EVM for 10 GBaud and 28 GBaud single-span transmission links.
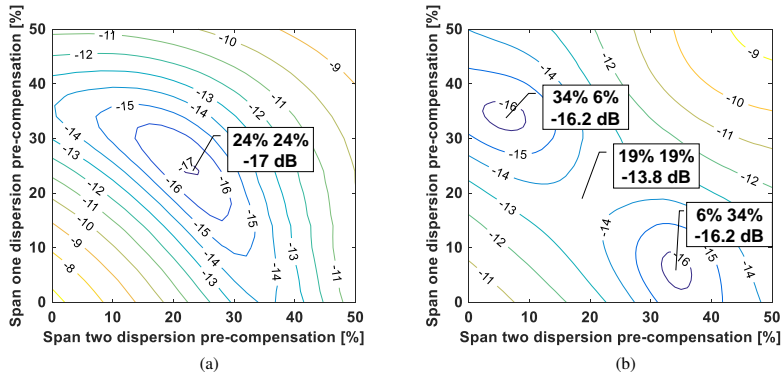

Fig. 7. Two-span dispersion map optimization simulation results showing EVM as a function of dispersion pre-compensation values for span one and span two for (a) 10 GBaud PSA link at 15 dBm launch power and (b) 28 GBaud PSA link at 9 dBm launch power.

higher symbol rate was also observed in [31], where distributed Raman amplified PSA and PIA links were experimentally compared. The improvement in Fig. 6 also degrades at higher launch powers where nonlinear distortions on signal and idler waves become less correlated.

Furthermore, in Figs. 7(a) and 7(b) are shown two-span dispersion map optimization results for 10 GBaud PSA link at 15 dBm launch power and 28 GBaud PSA link at 9 dBm launch power respectively. Figure 7(a) shows that there is an optimal solution by using the same dispersion pre-compensation value 24% for each span of a two-span 10 GBaud PSA link. The opposite is true for a two-span 28 GBaud PSA link where an optimal solution is to use a 6% dispersion pre-compensation in the first span and a 34% dispersion pre-compensation in the second span or vice versa. The improvement of using a two-span optimized case (6%, 34%) instead of using the same dispersion pre-compensation values in each span (19%, 19%) is 2.4 dB in terms of EVM. Therefore the multi-span dispersion map optimization for PSA links in condition where $L_D < L_{span}$ is of practical interest to fully utilize the PSA nonlinearity mitigation ability.
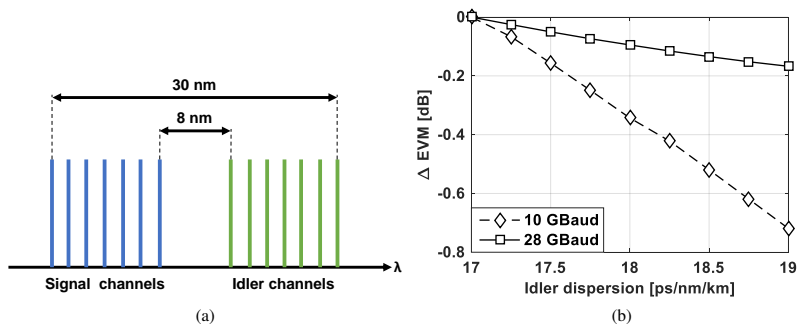
Fig. 8. (a) An example of allocation of wavelengths between signal and idler channels in a WDM PSA system and (b) EVM change as a function of the idler dispersion parameter value showing the EVM difference if an idler dispersion parameter value is swept from 17 ps/nm/km and a signal dispersion parameter value is kept fixed at 17 ps/nm/km for 10 GBaud and 28 GBaud single-span PSA links at 9 dBm launch power.

6.   Effect of third-order dispersion on SPM mitigation

In [2] and [22] it was claimed that the third-order dispersion effects do not play a significant role in a PSA nonlinearity mitigation performance and a simplification can be made to use the same GVD parameter for signal and idler waves. Therefore in our previous simulations this simplification was applied, although the signal and idler wavelengths are assumed to be 8 nm separated resulting in dispersion parameter values of $D = 17$ ps/nm/km for a signal and $D = 17.56$ ps/nm/km for an idler with a dispersion slope parameter approximately $S = 0.07$ ps/nm^2/km.

Nevertheless no exact indication or measure was given about the third-order dispersion effects. However, simulation results from section 5 showed that the dispersion length L_D plays a significant role in the SPM induced nonlinearity mitigation in a PSA link. Therefore we are interested also to benchmark the influence of signal and idler wavelength separation for 10 GBaud and 28 GBaud single-span PSA links as a function of a dispersion parameter change for an idler wave. Furthermore, in WDM PSA systems where signal and idler wavelengths are spaced more far apart with every added WDM channel, shown in Fig. 8(a), SPM mitigation is also of practical interest, since PSA amplification is WDM compatible [32–34].

Simulations were performed where the third-order dispersion effects were included and the PSA link SPM mitigation performance regarding the idler wavelength separation up to 30 nm were investigated. The signal dispersion parameter value was kept fixed at $D = 17$ ps/nm/km and the idler dispersion parameter value was swept from $D = 17$ ps/nm/km to $D = 19$ ps/nm/km corresponding to a wavelength separation of signal and idler waves from 0 nm to 30 nm. Due to different accumulated dispersion values on signal and idler waves, the dispersion compensators used in these simulations were capable of compensating for the dispersion slope as well. The results are shown in Fig. 8(b), where the measure of influence is conveyed in terms of EVM difference taken from the EVM value where the signal and idler waves have 0 nm wavelength separation.

Figure 8(b) shows that a 28 GBaud single-span PSA link is more resilient to third-order dispersion effects than a 10 GBaud PSA link. In fact, the used 8 nm wavelength separation, where the idler dispersion parameter value is $D = 17.56$ ps/nm/km, has a very small offset of approximately 0.05 dB in terms of EVM for the 28 GBaud PSA link, but more significant
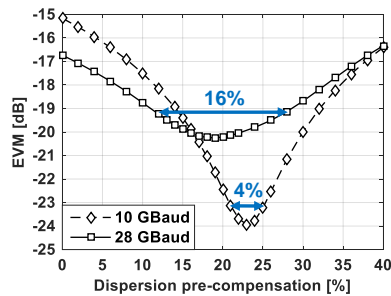
Fig. 9. EVM as a function of applied dispersion pre-compensation showing the chosen dispersion map dependence on a link performance for 10 GBaud at 12 dBm launch power and 28 GBaud at 6 dBm launch power single-span PSA links.

difference nearly 0.2 dB for the 10 GBaud single-span PSA link. If the signal and idler separation is 30 nm for the 10 GBaud PSA link, then the PSA's SPM mitigation results in an approximately 0.7 dB worse EVM performance.

The resiliency of the 28 GBaud PSA link can be related to the fact that in a condition where $L_D < L_{span}$, the dispersion itself plays major role reducing the twin-wave nonlinearity mitigation efficiency. It was shown in Fig. 6 that the single-span 28 GBaud link EVM improvement using a PSA instead of a PIA has dropped 9.4 dB compared to the single-span 10 GBaud case. Additionally Fig. 9 shows that the dispersion map optimum peak for the single-span 10 GBaud PSA case is much sharper than the 28 GBaud PSA case. For example the 10 GBaud case can tolerate only 2% offset from the optimum dispersion pre-compensation value if 1 dB worse EVM performance is allowed, while the 28 GBaud case can tolerate up to 8% offset. We expect that PSA links with an efficient nonlinearity mitigation performance require a precise dispersion management configuration, while also the third-order dispersion effects increase sensitivity towards the SPM mitigation performance if signal and idler waves are widely spaced.

7. Conclusion

We have presented a numerical dispersion map optimization for one- to four-span dispersion map optimized 28 GBaud PSA links for improved SPM mitigation and compared PSA links with PIA links, such as EDFA amplified links in long-haul transmission simulations at BER = 10^{-3}. The maximum reach of a 28 GBaud PSA link can be extended further by 2.1 times tolerating a total accumulated nonlinear phase shift of 8.8 radians, if four-span optimized dispersion maps are used repeatedly instead of single-span optimized dispersion maps. A significant reach improvement of 6.9 times can be achieved if a four-span optimized PSA link is used instead of an in-line dispersion managed PIA link. However, a reach extension of 4.3 times for a four-span optimized PSA link can be achieved compared to a dispersion unmanaged PIA link with EDC. The multi-span dispersion map optimization for PSA links is beneficial at higher symbol rates where the dispersion length is smaller than a span length $L_D < L_{span}$ and in such conditions a single-span dispersion map optimized PSA link does not provide the best SPM induced nonlinearity mitigation performance anymore. In a WDM PSA system, it is also important to notice the decrease of a SPM mitigation efficiency if the signal and idler waves are separated widely.

Funding

Acknowledgments

References

1. Z. Tong, C. Lundström, P. A. Andrekson, M. Karlsson, and A. Bogris, "Ultralow noise, broadband phase-sensitive optical amplifiers, and their applications," IEEE J. Sel. Topics Quantum Electron. **18**, 1016–1032 (2012).
2. S. L. I. Olsson, B. Corcoran, C. Lundström, T. A. Eriksson, M. Karlsson, and P. A. Andrekson, "Phase-sensitive amplified transmission links for improved sensitivity and nonlinearity tolerance," J. Light. Technol. **33**(3), 710–721 (2015).
3. A. D. Ellis, J. Zhao, and D. Cotter, "Approaching the non-linear Shannon limit," J. Light. Technol. **28**(4), 423–433 (2010).
4. R.-J. Essiambre, G. Kramer, P. J. Winzer, G. J. Foschini, and B. Goebel, "Capacity limits of optical fiber networks," J. Light. Technol. **28**(4), 662–701 (2010).
5. E. Agrell, M. Karlsson, A. R. Chraplyvy, D. J. Richardson, P. M. Krummrich, P. Winzer, K. Roberts, J. K. Fischer, S. J. Savory, B. J. Eggleton, M. Secondini, F. R. Kschischang, A. Lord, J. Prat, I. Tomkos, J. E. Bowers, S. Srinivasan, M. Brandt-Pearce, and N. Gisin, "Roadmap of optical communications," J. Opt., **18**(6), 063002 (2016).
6. S. L. I. Olsson, M. Karlsson, and P. A. Andrekson, "Nonlinear phase noise mitigation in phase-sensitive amplified transmission systems," Opt. Express **23**(9), 11724–11740 (2015).
7. C. M. Caves, "Quantum limits on noise in linear amplifiers," Phys. Rev. D **26**, 1817–1839 (1982).
8. M. Vasilyev, "Distributed phase-sensitive amplification," Opt. Express **13**(19), 7563–7571 (2005).
9. Z. Tong, C. Lundström, P. A. Andrekson, C. J. McKinstrie, M. Karlsson, D. J. Blessing, E. Tipsuwannakul, B. J. Puttnam, H. Toda, and L. Grüner-Nielsen, "Towards ultrasensitive optical links enabled by low-noise phase-sensitive amplifiers," Nat. Photonics **5**(7), 430–436 (2011).
10. M. E. Marhic, P. A. Andrekson, P. Petropoulos, S. Radic, C. Peucheret, and M. Jazayerifar, "Fiber optical parametric amplifiers in optical communication systems," Laser photonics reviews **9**(1), 50–74 (2015).
11. S. L. I. Olsson, H. Eliasson, E. Astra, M. Karlsson, and P. A. Andrekson, "Long-haul optical transmission link using low-noise phase-sensitive amplifiers," Nat. Commun. **9**:2513 (2018).
12. Z. Tong, and S. Radic, "Low-noise optical amplification and signal processing in parametric devices," Adv. Opt. Photonics, **5**(3), 318–384 (2013).
13. X. Liu, A. R. Chraplyvy, P. J. Winzer, R. W. Tkach, and S. Chandrasekhar, "Phase-conjugated twin waves for communication beyond the Kerr nonlinearity limit," Nat. Photonics **7**(7), 560–568 (2013).
14. H. Eliasson, S. L. I. Olsson. M. Karlsson, and P. A. Andrekson, "Comparison between coherent superposition in DSP and PSA for mitigation of nonlinearities in a single-span link," in Proc. European Conference on Optical Communications (ECOC, 2014), paper Mo.3.5.2.
15. H. Eliasson, P. Johannisson, M. Karlsson, and P. A. Andrekson, "Mitigation of nonlinearities using conjugate data repetition," Opt. Express **23**(3), 2392–2402 (2015).
16. S. J. Savory, G. Gavioli, R. I. Killey, and P. Bayvel, "Electronic compensation of chromatic dispersion using a digital coherent receiver," Opt. Express **15**(5), 2120–2126 (2007).
17. V. Curri, P. Poggiolini, A. Carena, and F. Forghieri, "Dispersion compensation and mitigation of nonlinear effects in 111-Gb/s WDM coherent PM-QPSK systems," Photonics Technol. Lett. **20**(17), 1473–1475 (2008).
18. J. K. Fischer, C.-A. Bunge, and K. Petermann, "Equivalent single-span model for dispersion-managed fiber-optic transmission systems," J. Light. Technol. **27**(16), 3425–3432 (2009).
19. A. Cartaxo, N. Costa, and D. Fonseca, "Analysis of optimum dispersion maps for DQPSK systems," in Proc. International Conference on Transparent Optical Networks (ICTON, 2010), paper Mo.D1.1.
20. Y. Frignac and P. Ramantanis, "Average optical phase shift as an indicator of the dispersion management optimization in PSK-modulated transmission systems," Photonics Technol. Lett. **22**(20), 1488–1490 (2010).
21. H. Eliasson, S. L. I. Olsson, M. Karlsson, and P. A. Andrekson, "Mitigation of nonlinear distortion in hybrid Raman/phase-sensitive amplifier links," Opt. Express **24**(2), 888–900 (2016).
22. E. Astra, S. L. I. Olsson, H. Eliasson, and P. A. Andrekson, "Dispersion management for nonlinearity mitigation in two-span 28 GBaud QPSK phase-sensitive amplifier links," Opt. Express **25**(12), 13163–13173 (2017).
23. H. Eliasson, K. Vijayan, B. Foo, S. L. I. Olsson, E. Astra, M. Karlsson, and P. A. Andrekson, "Phase-sensitive amplifier link with distributed Raman amplification," Opt. Express **26**(16), 19854–19863 (2018).
24. E. Astra, H. Eliasson, and P. A. Andrekson, "Four-span dispersion map optimization for improved nonlinearity mitigation in phase-sensitive amplifier links," in Proc. European Conference on Optical Communications (ECOC, 2017), paper P2.SC6.14.
25. Z. Tong, A. Bogris, C. Lundström, C. J. McKinstrie, M. Vasilyev, M. Karlsson, and P. A. Andrekson , "Modeling and measurement of the noise figure of a cascaded non-degenerate phase-sensitive parametric amplifier," Opt. Express **18**(14), 14820–14835 (2010).

26. R. A. Shafik, S. Rahman, and R. Islam, "On the extended relationships among EVM, BER and SNR as performance metrics," in Proc. 4th International Conference on Electrical and Computer Engineering (ICECE, 2006).
27. A. J. Lowery, "Fiber nonlinearity pre- and post-compensation for long-haul optical links using OFDM," Opt. Express **15**(20), 12965–12970 (2007).
28. R. Sinha, A. K. Garg, and S. Tyagi, "Dispersion compensation techniques: a comprehensive review," Int. J. Electron., Electrical and Computational System **6**(4), 57–61 (2017).
29. L. Gruner-Nielsen, M. Wandel, P. Kristensen, C. Jorgensen, L. V. Jorgensen, B. Edvold, B. Palsdottir, and D. Jakobsen, "Dispersion-compensating fibers," J. Light. Technol. **23**(11), 3566–3579 (2005).
30. F. Ramos, and J. Marti, "Influence of non-ideal chirped fibre grating characteristics on dispersion-compensated analogue optical links in presence of fibre-induced SPM," Electron. Lett. **39**(4), 353–355 (2003).
31. K. Vijayan, H. Eliasson, B. Foo, S. L. I. Olsson, M. Karlsson, and P. A. Andrekson, "Optical bandwidth dependency of nonlinearity mitigation in phase-sensitive amplifier links," in Proc. European Conference on Optical Communications (ECOC, 2018), paper We2.44.
32. R. Tang, P. S. Devgan, V. S. Grigoryan, P. Kumar, and M. Vasilyev , "In-line phase-sensitive amplification of multi-channel CW signals based on frequency nondegenerate four-wave-mixing in fiber," Opt. Express **16**(12), 9046–9053 (2008).
33. K. Vijayan, B. Foo, H. Eliasson, and P. A. Andrekson, "Cross-phase modulation mitigation in WDM transmission systems using phase-sensitive amplifiers," in Proc. European Conference on Optical Communications (ECOC, 2018), paper We3H.4.
34. Z. Tong, C. Lundström, E. Tipsuwannakul, M. Karlsson, and P. A. Andrekson, "Phase-sensitive amplified DWDM DQPSK signals using free-running lasers with 6-dB link SNR improvement over EDFA-based systems," in Proc. European Conference and Exhibition on Optical Communication (ECOC, 2010), paper PDP1.3.

Phase-sensitive amplifier link with distributed Raman amplification

H. Eliasson, K. Vijayan, B.Foo, S.L.I. Olsson, E. Astra, M. Karlsson and P. A. Andrekson, Optics Express, 26, no. 16 (2018): 19854–19863.

Phase-sensitive amplifier link with distributed Raman amplification

Henrik Eliasson,[1] Kovendhan Vijayan,[1] Benjamin Foo,[1]
Samuel L. I. Olsson,[1,2] Egon Astra,[3] Magnus Karlsson,[1]
and Peter A. Andrekson[1,*]

[1]*Photonics Laboratory, Department of Microtechnology and Nanoscience, Chalmers University of Technology, SE-412 96, Gothenburg, Sweden*
[2]*Now at: Nokia Bell Labs, 791 Holmdel Road, Holmdel, NJ 07733, USA*
[3]*Thomas Johann Seebeck Department of Electronics, Tallinn University of Technology, Tallinn, Estonia*
[*]*peter.andrekson@chalmers.se*

Abstract: We demonstrate long-haul transmission using a hybrid amplifier approach combining distributed Raman amplification and lumped phase-sensitive amplification. Aside from the well-known resulting SNR improvement, distributed Raman amplification is included in an effort to improve the nonlinearity mitigation capability of the phase-sensitive amplifiers. When changing from phase-insensitive operation to phase-sensitive operation in a link employing distributed Raman amplification, the transmission reach at BER = 10^{-3} is increased from 15 to 44 spans of length 81 km while simultaneously increasing the optimal launch power by 2 dB.

References and links

1. J. Cartledge, F. Guiomar, F. Kschischang, G. Liga, and M. Yankov, "Digital signal processing for fiber nonlinearities," Opt. Express **25**(3), 1916–1936 (2017).
2. R. A. Fisher, B. R. Suydam, and D. Yevick, "Optical phase conjugation for time-domain undoing of dispersive self-phase-modulation effects," Opt. Lett. **8**(12), 611–613 (1983).
3. H. Hu, R. M. Jopson, A. H. Gnauck, S. Randel, and S. Chandrasekhar, "Fiber nonlinearity mitigation of WDM-PDM QPSK/16-QAM signals using fiber-optic parametric amplifiers based multiple optical phase conjugations," Opt. Express **25**(3), 1618–1628 (2017).
4. T. Umeki, T. Kazama, A. Sano, K. Shibahara, K. Suzuki, M. Abe, H. Takenouchi, and Y. Miyamoto, "Simultaneous nonlinearity mitigation in 92 × 180-Gbit/s PDM-16QAM transmission over 3840 km using PPLN-based guard-band-less optical phase conjugation," Opt. Express **24**(15), 16945–16951 (2016).
5. A. Ellis, M. McCarthy, M. Al-Khateeb, and S. Sygletos, "Capacity limits of systems employing multiple optical phase conjugators," Opt. Express **23**(16), 20381–20393 (2015).
6. L. Li, P. G. Patki, Y. B. Kwon, V. Stelmakh, B. D. Campbell, M. Annamalai, T. I. Lakoba and M. Vasilyev, "All-optical regenerator of multi-channel signals," Nat. Commun. **8**(1), 884 (2017).
7. D. Rafique, "Fiber nonlinearity compensation: Commercial applications and complexity analysis," J. Lightw. Technol. **34**(2), 544–553 (2016).
8. P. Rosa, S. T. Le, G. Rizzelli, M. Tan, and J. Ania-Castañón, "Signal power asymmetry optimisation for optical phase conjugation using Raman amplification," Opt. Express **23**(25), 31772–31778 (2015).
9. R. Tang, J. Lasri, P. Devgan, V. Grigoryan, P. Kumar, and M. Vasilyev, "Gain characteristics of a frequency nondegenerate phase-sensitive fiber-optic parametric amplifier with phase self-stabilized input," Opt. Express **13**(26), 10483–10493 (2005).
10. S. L. I. Olsson, B. Corcoran, C. Lundström, T. Eriksson, M. Karlsson, and P. A. Andrekson, "Phase-sensitive amplified transmission links for improved sensitivity and nonlinearity tolerance," J. Lightw. Technol. **33**(3), 710–721 (2015).
11. S. L. I. Olsson, H. Eliasson, E. Astra, M. Karlsson, and P. A. Andrekson, "Long-haul optical transmission link using low-noise phase-sensitive amplifiers," Nat. Commun. 9, 2513 (2018).
12. X. Liu, A. R. Chraplyvy, P. J. Winzer, R. W. Tkach and S. Chandrasekhar, "Phase-conjugated twin waves for communication beyond the Kerr nonlinearity limit," Nat. Photon. **7**(7), 560–568 (2013).
13. Z. Tong, C. Lundström, P. A. Andrekson, C. J. McKinstrie, M. Karlsson, D. J. Blessing, and L. Grüner-Nielsen, "Towards ultrasensitive optical links enabled by low-noise phase-sensitive amplifiers," Nat. Photon. **5**(7), 430–436 (2011).

14. H. Eliasson, S. L. I. Olsson, M. Karlsson, and P. A. Andrekson, "Mitigation of nonlinear distortion in hybrid Raman/phase-sensitive amplifier links," Opt. Express **24**(2), 888–900 (2016).
15. H. Eliasson, S. L. I. Olsson, M. Karlsson and P. A. Andrekson, "Experimental investigation of nonlinearity mitigation properties of a hybrid distributed Raman/phase-sensitive amplifier link," in Optical Fiber Communication Conference (OFC), Los Angeles, USA, paper Th3J.4. (2017).
16. C. Lundström, R. Malik, L. Grüner-Nielsen, B. Corcoran, S. L. I. Olsson, M. Karlsson, and P. A. Andrekson, "Fiber optic parametric amplifier with 10-dB net gain without pump dithering," IEEE Photon. Technol. Lett. **25**(3), 234–237 (2013).
17. X. Liu, S. Chandrasekhar, P. Winzer, B. Maheux-L, G. Brochu, and F. Trepanier, "Efficient fiber nonlinearity mitigation in 50-GHz-DWDM transmission of 256-Gb/s PDM-16QAM signals by folded digital-back-propagation and channelized FBG-DCMs," in Optical Fiber Communication Conference (OFC), San Fransisco, USA, paper Tu3A.8. (2014).
18. G. Rizzelli, P. Rosa, P. Corredera, and J. Ania-Castañón, "Transmission span optimization in fiber systems with cavity and random distributed feedback ultralong Raman laser amplification," J. Lightw. Technol. **35**(22), 4967–4972 (2017).
19. J. C. Bouteiller, K. Brar and C. Headley, "Quasi-constant signal power transmission," in European Conference on Optical Communication (ECOC), Copenhagen, Denmark, paper S3.04 (2002).
20. M. Vasilyev, B. Szalabofka, S. Tsuda, J. M. Grochocinski and A. F. Evans, "Reduction of Raman MPI and noise figure in dispersion-managed fibre," Electron. Lett. **38**(6), 271–272 (2002).
21. M. Vasilyev, "Raman-assisted transmission: Toward ideal distributed amplification," in Optical Fiber Communication Conference (OFC), Atlanta, USA, paper WB1 (2003).
22. S. L. I. Olsson, B. Corcoran, C. Lundström, E. Tipsuwannakul, S. Sygletos, A. Ellis, Z. Tong, M. Karlsson, and P. A. Andrekson, "Injection locking-based pump recovery for phase-sensitive amplified links," Opt. Express **21**(12), 14512–14529 (2013).
23. R. J. Essiambre, P. Winzer, J. Bromage and C. H. Kim, "Design of bidirectionally pumped fiber amplifiers generating double Rayleigh backscattering," IEEE Photon. Technol. Lett. **14**(7), 914–916 (2002).

1. Introduction

The main limiting factors to the transmission distance or data throughput of modern coherent long-haul fiber-optic communication links are the nonlinear distortion in the single-mode fiber (SMF) due to the Kerr effect and amplified stimulated emission (ASE) noise from inline optical amplifiers. One way of extending the limits imposed by fiber nonlinearities is to actively reverse or undo the nonlinear distortion which is to a large part deterministic in nature. One approach for mitigating the negative impact of nonlinearities is to use digital methods like digital back-propagation (DBP), digital pre-compensation (DPC), perturbation based compensation or nonlinear Fourier transforms (NLFTs) [1]. One advantage of digital approaches, with the possible exception of NLFT, is that the transmission link itself does not have to be modified, limiting the increased complexity to the transceiver hardware. This makes digital approaches easier to implement in existing infrastructure. Another group of methods for mitigation of nonlinear distortion is all-optical approaches, relying on all-optical signal processing to compensate the nonlinear distortion. The most common all-optical approach is to use optical phase conjugation (OPC), placing one or more phase conjugation devices inline in a serial manner along the link [2–5]. An advantage of all-optical approaches is the potential to mitigate nonlinear distortion over large optical bandwidths or multiple channels [6] compared to digital approaches which are bandwidth-limited by the transceiver electrical bandwidth as well as computational complexity which can be prohibitively large already for compensation of one channel [7]. The span power map is an important parameter in optimizing the efficiency of the nonlinearity mitigation in OPC links and can be manipulated using distributed Raman amplification (DRA) [8]. Another all-optical approach for mitigation of nonlinear distortion is to use the copier-phase-sensitive amplifier (PSA) scheme [9]. In this scheme, a copier is used at the transmitter to generate a phase-conjugated copy (or idler) from the signal. Both waves are then transmitted and propagated in parallel followed by coherent superposition in the PSAs enabling nonlinearity mitigation [10, 11]. This scheme has many similarities to the phase-conjugated twin waves (PCTWs) concept where the signal and its phase-conjugated copy are transmitted on orthogonal polarization states followed by coherent superposition in receiver digital signal processing (DSP) [12]. Thus in the case of PCTW

periodic nonlinearity mitigation is not possible. An inherent disadvantage to both the copier-PSA and PCTW scheme is that 50 % spectral efficiency is sacrificed due to the co-propagation of a phase-conjugated copy alongside the signal. In addition to allowing for nonlinearity mitigation, the copier-PSA scheme also enables a 0 dB quantum-limited amplifier noise figure [13] compared to 3 dB for an Erbium-doped fiber amplifier (EDFA) or any other phase-insensitive amplifier (PIA).

A first-order perturbation analysis suggests that a flat or symmetric span power map in a PCTW link could lead to efficient nonlinearity mitigation [12]. This conclusion holds for copier-PSA links as well assuming that the signal and idler are separated in wavelength sufficiently for cross-phase modulation (XPM) to be negligible in comparison to self-phase modulation (SPM). Thus it is reasonable to believe that a flat or symmetric span power map could benefit the nonlinearity mitigation performance in PSA links in a similar manner as in OPC links [5]. We previously investigated this in simulations of a hybrid PSA-DRA link showing the potential for gains beyond what is predicted by the span noise figure (NF) improvement due to DRA [14]. Previously, we also reported on a small subset of the experimental results that we now will present [15].

In this paper, we present an experimental investigation of a hybrid approach where we combine DRA and PSAs. We provide experimental comparisons of 28 GBaud quadrature phase-shift keying (QPSK) long-haul transmission links using four different amplifier configurations. The investigated amplifier configurations are PIA, PSA, hybrid PIA-DRA and hybrid PSA-DRA. In [14] it was found that the impact of the span power map is larger at symbol rates where the dispersive length is on the order of, or shorter than the effective length which is why we use a 28 GBaud signal. In all cases we apply inline dispersion compensation since this is required in the PSA scenarios. For each of the amplifier configurations we optimize the ratio between dispersion pre- and post-compensation for maximizing the transmission reach in a nonlinear transmission regime. Using the optimal dispersion maps we then perform long-haul transmission experiments. When comparing the PIA-DRA case to the PSA-DRA case in long-haul transmission we observe a 2 dB increase in optimal launch power for the PSA-DRA case that is not present in the comparison between the PIA and the PSA case. We attribute this mainly to improved nonlinearity mitigation but also due to that the difference in equivalent span NF between the PIA-DRA and PSA-DRA case is smaller than the difference between the PIA and PSA case because of the noise contribution from DRA.

2. Experiment

A recirculating loop experiment was carried out to investigate if it is possible to improve the efficiency of the PSA nonlinearity compensation with the addition of DRA. The experimental setup is illustrated in Fig. 1. Light from a 100 kHz linewidth laser at 1550.1 nm was modulated at 28 GBaud using a IQ-modulator and pseudorandom binary sequences (PRBS) of length $2^{15} - 1$. The signal was then coupled into a recirculating loop using an acousto-optic modulator (AOM) where it was combined with a free-running high-power pump wave at 1554.1 nm and inserted into the FOPA acting as a copier with 14.2 dB net gain. The FOPA consisted of a cascade of four pieces of highly nonlinear fiber (HNLF) with isolators in between in order to suppress stimulated Brillouin scattering (SBS), more details on the FOPA implementation can be found in [16]. The generated idler wave was located at 1558.1 nm. The signal and idler waves were then separated from the pump in the launch power balancing stage where the launch powers of the signal and idler into the transmission span were balanced using a wavelength selective switch (WSS). After balancing, the launch powers were boosted by an EDFA and adjusted using a variable optical attenuator (VOA). When the link was operated in PIA mode, the idler wave was blocked by the WSS so that only the signal wave was transmitted. The pump wave was split up from the signal and idler balancing path and the pump launch power adjusted using a VOA. Since the pump recovery stage was based on injection locking, the pump wave was also transmitted alongside the
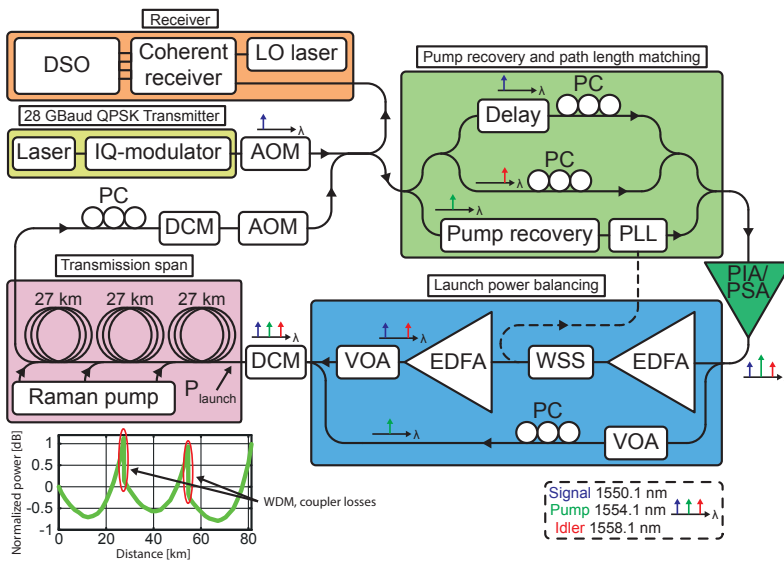
Fig. 1. Sketch of the experimental setup used to demonstrate hybrid PSA-DRA transmission. The same fiber-optic parametric amplifier (FOPA) acts as either PIA or PSA. The color coding used for illustrating the signal/idler/pump paths is shown in the bottom right. The results from an OTDR measurement of the span power map with DRA is shown in the bottom left.

signal and idler.

In order to achieve phase-sensitive amplification in the FOPA, the transmission span needs to be fully dispersion-compensated. This was achieved using tunable channelized fiber Bragg grating (FBG)-based dispersion compensating modules (DCMs) before and after the transmission span [17]. The ratio between dispersion pre- and post-compensation was optimized for each amplifier configuration in order to maximize the transmission reach in a nonlinear transmission regime. In order to achieve the flattest possible span power map with DRA, the span was divided into three 27 km segments that were individually backwards Raman pumped using a 1450 nm Raman fiber laser. In between each span segment was a wavelength division multiplexing (WDM) coupler for inserting the Raman pump as well as a monitor tap for measuring the signal launch power into each segment. The Raman pump powers into each segment were adjusted so that the signal launch power into each segment was the same, i.e. full transparency accounting for the losses of the WDM couplers and monitor taps in between each segment. A optical time-domain reflectometer (OTDR) operating at 1554 nm was used to measure the span power map with DRA. The results from these measurements are shown in the bottom left of Fig. 1 where we also note the impact of the WDM and coupler losses on the span power map. The loss of the segmented transmission span was 18 dB. It is clear that this implementation of DRA is not practical to use in real systems but we would like to point out that there are more practical DRA schemes that achieve similar levels of power map flatness without using remote optical pumping or placing active optical components inside each transmission span [18–21].

Before the FOPA on the second circulation the signal and idler waves were split up using a WDM coupler and path length matched so that they were synchronized into the FOPA on the
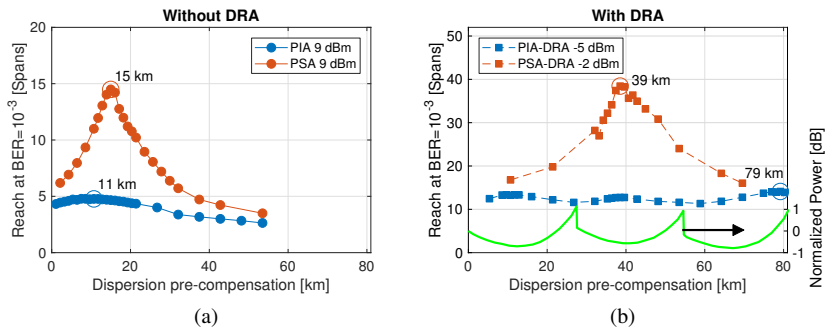
Fig. 2. Optimization of the span dispersion map for the four different amplifier configurations. For each case, the optimum point has been encircled. (a) Transmission reach at BER = 10^{-3} as a function of dispersion pre-compensation for the PIA and PSA link. (b) Same for the PIA-DRA and PSA-DRA link. Referenced to the right axis is the measured span power map.

second passthrough. The pump recovery stage was based on an injection locked laser followed by a high-power EDFA and a phase-locked loop (PLL). The PLL operated by applying a 40 kHz phase dithering tone on the pump using a piezoelectric fiber stretcher and maximizing the PSA gain by keeping the relative phase between signal, idler and pump constant, more details on the PLL implementation can be found in [22]. Thus, the FOPA acted as a PSA on the second and all subsequent round trips in the loop. The PSA gain was 19.8 dB giving a gain difference of 5.6 dB when comparing PIA and PSA operation. The total loss between the point where launch power was measured and the PSA input was 36.6 dB.

After each circulation the signal was coupled out from the loop and detected using a coherent receiver with a free-running 100 kHz linewidth local oscillator (LO) laser at 1550.1 nm. The radio frequency (RF) signals from the coherent receivers balanced photodetectors were sampled using a 50 GS/s digital sampling oscilloscope (DSO) followed by offline DSP. The offline DSP consisted of dynamic equalization based on the constant modulus algorithm (CMA) using 141 T/2-spaced taps and phase tracking using the Viterbi-Viterbi algorithm followed by bit error rate (BER) counting. The large number of equalizer taps was needed because of the group delay ripple (GDR) in the DCMs. For each measurement point, ten 2.5 MSample batches were stored down for offline processing and the BER was found by averaging over the three best batches. This was done to reduce the impact of the batches where e.g. the injection locking or the PLL failed at many roundtrips.

3. Experimental results

The experimental results are presented in two parts. First, we present results from the optimization of the span dispersion map for the different amplifier configurations. Second, the optimal span dispersion maps found will be used in long haul transmission to estimate the transmission reach.

3.1. Dispersion map optimization

The dispersion map was swept by changing the ratio between dispersion pre- and post-compensation. The fact that we used tunable DCMs for dispersion compensation enabled this sweep to be performed experimentally. The residual dispersion was set to zero for all cases.

For each of the amplifier configurations, the transmission reach at BER = 10^{-3} was measured with different dispersion maps at a launch power approximately 3 dB above optimal launch power. This choice was made in order to enhance the nonlinear distortion, making it easier to distinguish the optimum point. Note that the differences in reach for different dispersion maps is dictated by nonlinear distortion, i.e. in a linear transmission regime the dispersion map does not impact performance. The results from these measurements are presented in Fig. 2 where the transmission distance at BER = 10^{-3} is shown as a function of the dispersion pre-compensation for the four different amplifier configurations. The dispersion map sweeps for the PIA and PSA links are shown in Fig. 2(a) and for the PIA-DRA and PSA-DRA links in Fig. 2(b). In the cases without DRA we see that the dispersion pre-compensation optimum shifts from 11 km to 15 km when enabling phase-sensitive amplification by transmission of both signal and idler waves. For the cases with DRA, the difference between the characteristics of the PIA and PSA curve is more pronounced and the optimum shifts from 79 km to 39 km when enabling phase-sensitive amplification. The ripple behavior observed in the PIA-DRA case is due to the three individually Raman pumped span segments causing a periodic power map within one transmission span.

On the one hand, the fact that we observe sharp peaks in the PSA and PSA-DRA cases shows that the PSAs are in fact compensating for the nonlinear phase shift. On the other hand, the sharp optima could pose an issue in practical systems due to the required precision of the ratio between dispersion pre- and post-compensation.

3.2. Long-haul transmission

Using the optimal dispersion maps, a launch power sweep was performed, measuring the transmission reach at BER = 10^{-3} for different signal launch powers. In Figs. 3(a) and 3(b), the transmission reach is shown as a function of signal launch power for the four amplifier configurations. The launch power is defined as the optical power of the signal wave only, not taking into account the power of the idler wave. The transmission reach as a function of signal launch power for the PIA and PSA link is shown in Fig. 3(a). We see that the optimal launch power is 6 dBm for the PIA case and 5 dBm for the PSA case. The transmission reach is approximately 6 roundtrips for the PIA link and 23 roundtrips for the PSA link. This gives a transmission reach increase by a factor of 3.8 when comparing the PSA link to the PIA link and a total accumulated nonlinear phase shift of 2.0 radians for the PSA link at 23 roundtrips and 5 dBm launch power. The total accumulated nonlinear phase shift of the PIA link at 6 round trips and 6 dBm launch power was 0.7 radians. The transmission reach as a function of signal launch power for the PIA and PSA link with DRA is shown in Fig. 3(b). We see that the optimal launch power of the PIA link with DRA is -8 dBm while the PSA link with DRA has an optimal launch power of -6 dBm. The transmission reach for the PIA-DRA case is 15 roundtrips and 44 roundtrips for the PSA-DRA case. The total accumulated nonlinear phase shift for the PSA-DRA link at 44 roundtrips and -6 dBm launch power was 1.1 radians. The total accumulated nonlinear phase shift of the PIA-DRA link at 15 round trips and -8 dBm launch power was 0.2 radians. In Figs. 3(c) and (d) we show the reach increase factor as a function of launch power when comparing PIA to PSA and PIA-DRA to PSA-DRA, respectively. We note that for the cases without DRA that the reach increase factor decreases when the launch power is increased while the opposite is true for the cases with DRA. In the DRA cases the reach increase factor improves significantly when moving beyond optimal launch power. At very high launch powers the reach increase factors even exceed above the 4x factor that is expected [13] in a linear transmission regime dominated by ASE from the FOPA.

4. Numerical analysis

Simulations were performed to estimate the performance of the PSA-DRA link in Fig. 1 and compare to experimental results. In the simulations, a signal and idler wave modulated with 28 GBaud QPSK was propagated using independent split-step Fourier method (SSFM) solvers taking
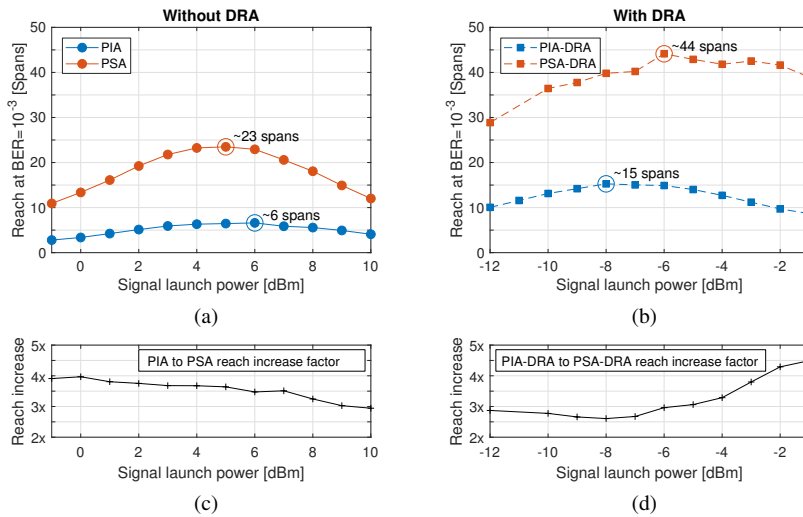
Fig. 3. Transmission reaches and reach increase factors as a function of signal launch power. For each case the point with the longest transmission reach have been encircled. (a) Reach at BER = 10^{-3} as a function of signal launch power for the PIA and PSA link. (b) Reach at BER = 10^{-3} as a function of signal launch power for the PIA-DRA and PSA-DRA link. (c) Reach increase factor when going from PIA to PSA as a function of launch power. (d) Reach increase factor when going from PIA-DRA to PSA-DRA as a function of launch power.

into account backwards Raman pumping in the segmented span. Noise from DRA was added in each split-step. The segmented span was modeled with a 1 dB lumped loss in between each segment giving a span power map similar to the measurement shown in Fig. 1. The Raman pump power was set so that each span segment was transparent accounting for the loss between segments. The excess loss of 18.6 dB after the transmission span due to dispersion post-compensation, loop components and the path length matching stage was also taken into account. The PSA noise figure was set to 1.4 dB. The amount of dispersion pre- and post-compensation was optimized for the PSA-DRA case and the optimal dispersion map used to simulate long haul transmission. The PSA after each span was modeled using a simplified matrix formulation in the same way as described in [14]. The same receiver DSP as in the experiments was used to process the received waveforms. The fiber parameters were L_{span} = 80 km, α_{signal} = 0.2 dB/km, $\alpha_{Raman\ pump}$ = 0.25 dB/km, D = 17 ps nm^{-1}km^{-1}, γ = 1.3 W^{-1}km^{-1}. In order to investigate the penalty from the FBG-based DCMs we made simulations both with and without taking the GDR and passband characteristic of the DCMs into account. The amplitude response and GDR of the simulated DCMs are shown in Fig. 4(b). Since the signal passed through the same two DCMs repeatedly in the recirculating loop experiment, the GDR was modelled by adding up the GDR of two passbands. This was done independently for the signal and idler, i.e. the signal experienced the summation of the ripple labeled signal phase A and B in Fig. 4(b) and the idler experiences the summation of idler phase A and B. It should however be noted that the GDR ripple used in simulations were not from the exact same units that were used in the experiments. Statistical fluctuations in GDR between specific units will cause differences in performance, this was however not studied. The results
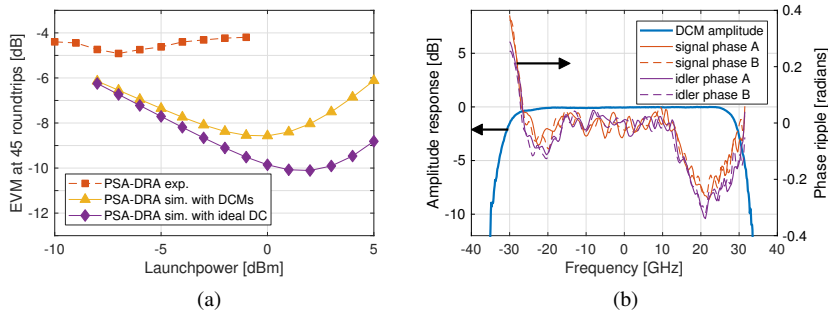
Fig. 4. Results from the simulations in comparison to experimental results. (a) The EVM at 45 roundtrips as a function of launch power for three cases, experimental, simulated with realistic modelling of the DCMs and simulated with ideal dispersion compensation. (b) The amplitude and phase responses of the simulated DCMs.

from the simulations are presented in Fig. 4(a) where the error vector magnitude (EVM) is shown as a function of launch power at 45 roundtrips and compared to the experimental results. As one might expect, the passband characteristics and GDR of the DCMs imposes a EVM penalty on the nonlinearity mitigation, reducing the optimal launch power in simulations by 2-3 dB. However it is also clear that the penalties from the GDR and passband characteristics of the DCMs is not sufficient to explain the experimental results fully since the optimum launch power in the experiments was 6 dB lower than in the simulations with DCMs. A longer discussion on this will follow in Section 5.

5. Discussion

In order for the PSAs to compensate nonlinear distortion efficiently it is important to chose a proper span dispersion map. We performed this optimization experimentally using tunable DCMs. The results from these measurements were shown in Fig. 2. When we studied the dispersion map sweep results for the PSA-DRA case, we observed a peak centered around 39 km. This is close to the 50 % dispersion pre-compensation predicted for the case with a perfectly flat or symmetric span power map [14]. Considering the shift in the optimum dispersion map between the PIA-DRA case and the PSA-DRA case, this indicates that the nonlinearity compensation through coherent superposition in the PSAs is working and that this effect is dominating over other interactions between dispersive and nonlinear effects.

Another important issue to discuss is the impact of DRA on the equivalent span NF. Assuming the span and excess losses measured in the experiment, ideal DRA, a 1 dB PSA NF and a 4 dB PIA NF one can obtain simple analytical estimates of the linear span NF for each of the different amplifier configurations. The equivalent span NF of a 81 km span with ideal DRA is 9.3 dB. The equivalent span NF for the four different amplifier configurations can be found using Friis formula. The equivalent span NF for the PIA case is 40.6 dB, for the PSA case 37.6 dB, for the PIA-DRA case 22.8 dB and for the PSA-DRA case 19.9 dB. This tells us that even in the cases with DRA the signal-to-noise ratio (SNR) degradation from the FOPA is larger than that from the DRA. Using the numerical simulations presented in Section 4 it was estimated that the nonlinear phase shift at a given launch power was increased by 5.7 dB when turning on the DRA.

Examining the launch power sweeps presented in Fig. 3 we need to discuss a few important

features. First of all we note that for the cases without DRA, the optimal launch power stays essentially unchanged when comparing the PIA and PSA case. If we instead look at the cases with DRA we note that the optimal launch power is increased by 2 dB when going from PIA-DRA to PSA-DRA. We interpret this as mainly being due to improved nonlinearity mitigation even though it is important to note that the difference in equivalent span NF between the PIA and PSA case will affect the optimum launch power difference between the two cases. Second, we discuss the transmission reach in the PSA-DRA case. When comparing experiments to simulations it becomes clear that the transmission reach in the PSA-DRA is shorter than what is predicted by the simulations. More importantly it is clear that the optimal launch power is lower in the experiments than in simulations by a margin of approximately 6 dB. This leads us to believe that there are significant penalties impacting the efficiency of the nonlinearity mitigation due to various nonidealities beyond our control in the presented experiment. One important feature of the experiment is that we are using channelized tunable DCMs based on FBG technology [17]. The advantage of using these is that we can perform the dispersion map optimization experimentally and do not need to rely on numerical simulations for finding the optimal dispersion map. The disadvantage is that the DCMs have a limited optical bandwidth and group delay ripple. It is reasonable to believe that the GDR will cause penalties both in terms of the signal and idler waves into the PSA not fulfilling phase-matching conditions as well as reducing the efficiency of the nonlinearity mitigation. Both the GDR and passband characteristic penalties are made worse by the fact that we propagate through the same DCMs in every roundtrip. This causes the group delay ripple to accumulate in a correlated manner as we pass through the DCMs repeatedly. It was also confirmed in the simulations that there is a significant penalty due to the DCM characteristics.

Other reasons for having a significant penalty compared to the simulations is that we use injection locking and noise accumulates on the pump as we propagate. We also have non-idealities regarding the span power map symmetry between signal and idler which will reduce the efficiency of the nonlinearity mitigation. Since we are using a single backwards Raman pump, the gain spectrum of the DRA is not perfectly flat over the 8 nm spanned by the signal and idler wave. This will cause penalties relative to the ideal scenario in the simulations where it was assumed that the signal and idler propagate with the same span power map. Another effect that was not taken into account in the simulations was double Rayleigh backscattering which will cause an effective SNR degradation at high launch powers in spans with transparency or high DRA gain [23]. The effects of polarization mode dispersion (PMD) and third-order dispersion were also neglected in the numerical modelling as well as XPM from signal and idler onto the co-propagating pump wave.

6. Conclusion

We have for the first time demonstrated long-haul transmission with a hybrid amplifier approach combining the copier-PSA scheme with DRA. This hybrid amplifier approach was implemented in a recirculating loop experiment to examine the nonlinearity mitigation properties of the PSAs and to investigate whether it was possible to improve the PSA nonlinearity compensation with the addition of DRA. For the study we performed measurements using four different amplifier configurations, PIA, PSA, hybrid PIA-DRA and hybrid PSA-DRA. By looking solely at the increase in transmission reach when comparing the PSA case to the PSA-DRA case it was not possible to draw the conclusion that the nonlinearity compensation was improved since the total accumulated nonlinear phase shift at a distance corresponding to e.g. BER = 10^{-3} at optimal launch power was lower in the PSA-DRA case (1.1 radians) compared to the PSA case (2.0 radians). This can be explained by penalties at long distances as well as nonidealities reducing the efficiency of the nonlinearity mitigation. We believe that an important contributing factor to these penalties was nonidealities in the inline dispersion compensation and this was also confirmed in simulations. A 2 dB increase in optimal launch power was, however, observed when comparing the PIA-DRA case to the PSA-DRA case, indicating improved nonlinearity compensation. When

going from PIA to PSA, the transmission reach increase factor at optimal launch powers was 3.8 while from PIA-DRA to PSA-DRA, the reach improved by a factor of 2.9.

Part III

Curriculum Vitae

CURRICULUM VITAE

Personal data

Name:	Egon Astra
Date of birth:	February 7, 1989
Place of birth:	Valga, Estonia
Citizenship:	Estonian

Contact data

Address:	Ehitajate tee 5, 19086, Tallinn University of Technology, Estonia
E-mail:	egon.astra@gmail.com

Education

2014 –	Tallinn University of Technology, School of Information Technologies, Thomas Johann Seebeck Department of Electronics, PhD studies
2011 – 2013	Tallinn University of Technology, Faculty of Information Technology, Telecommunications Engineering, MSc *cum laude*
2008 – 2011	Tallinn University of Technology, Faculty of Information Technology, Telecommunications Engineering, BSc *cum laude*

Language competence

Estonian:	Native speaker
English:	Fluent
German:	Basic

Professional employment

2018 –	SideBeam OÜ, Board member
2013 – 2014	The Estonian Patent Office, Head of the SME Support Division
2011 – 2013	The Estonian Patent Office, Senior Examiner
2010 – 2011	Estonian Public Broadcasting, AV Technician

Supervised theses

2016	*"The nonlinear limitation on achievable transmission distance in fiber-optical communication systems,"* Taavi Laadung, Tallinn University of Technology

ELULOOKIRJELDUS

Isikuandmed

Nimi: Egon Astra
Sünniaeg: 7. veebruar 1989
Sünnikoht: Valga, Estonia
Kodakondsus: Eesti

Kontaktandmed

Aadress: Ehitajate tee 5, 19086, Tallinn University of Technology, Estonia
E-post: egon.astra@gmail.com

Hariduskäik

2014 –	Tallinna Tehnikaülikool, doktoriõpe
2011 – 2013	Tallinna Tehnikaülikool, telekommunikatsioon, magistriõpe *cum laude*
2008 – 2011	Tallinna Tehnikaülikool, telekommunikatsioon, bakalaureuseõpe *cum laude*

Keelteoskus

Eesti keel: emakeel
Inglise keel: kõrgtase
Saksa keel: algtase

Teenistuskäik

2018 –	SideBeam OÜ, juhatuse liige
2013 – 2014	Patendiamet, väikeettevõtjate nõustamise talituse juhataja
2011 – 2013	Patendiamet, füüsika ja elektri ekspertiisi talituse vanemekspert
2010 – 2011	Eesti Rahvusringhääling, audio-visuaaltehnik

Juhendatud lõputööd

2016	*"Mittelineaarsustest tulenev piirang maksimaalsele edastuskaugusele fiiberoptilises sidesüsteemis,"* Taavi Laadung, Tallinna Tehnikaülikool